National Bureau of Standards
Library, N.W. Bldg
OCT 8 1964

NBS MONOGRAPH 85

A Study of Lunar Surface Radio Communication

U.S. DEPARTMENT OF COMMERCE
NATIONAL BUREAU OF STANDARDS

THE NATIONAL BUREAU OF STANDARDS

The National Bureau of Standards is a principal focal point in the Federal Government for assuring maximum application of the physical and engineering sciences to the advancement of technology in industry and commerce. Its responsibilities include development and maintenance of the national standards of measurement, and the provisions of means for making measurements consistent with those standards; determination of physical constants and properties of materials; development of methods for testing materials, mechanisms, and structures, and making such tests as may be necessary, particularly for government agencies; cooperation in the establishment of standard practices for incorporation in codes and specifications; advisory service to government agencies on scientific and technical problems; invention and development of devices to serve special needs of the Government; assistance to industry, business, and consumers in the development and acceptance of commercial standards and simplified trade practice recommendations; administration of programs in cooperation with United States business groups and standards organizations for the development of international standards of practice; and maintenance of a clearinghouse for the collection and dissemination of scientific, technical, and engineering information. The scope of the Bureau's activities is suggested in the following listing of its four Institutes and their organizational units.

Institute for Basic Standards. Electricity. Metrology. Heat. Radiation Physics. Mechanics. Applied Mathematics. Atomic Physics. Physical Chemistry. Laboratory Astrophysics.* Radio Standards Laboratory: Radio Standards Physics; Radio Standards Engineering.** Office of Standard Reference Data.

Institute for Materials Research. Analytical Chemistry. Polymers. Metallurgy. Inorganic Materials. Reactor Radiations. Cryogenics.** Office of Standard Reference Materials.

Central Radio Propagation Laboratory.** Ionosphere Research and Propagation. Troposphere and Space Telecommunications. Radio Systems. Upper Atmosphere and Space Physics.

Institute for Applied Technology. Textiles and Apparel Technology Center. Building Research. Industrial Equipment. Information Technology. Performance Test Development. Instrumentation. Transport Systems. Office of Technical Services. Office of Weights and Measures. Office of Engineering Standards. Office of Industrial Services.

---

* NBS Group, Joint Institute for Laboratory Astrophysics at the University of Colorado.
** Located at Boulder, Colorado.

UNITED STATES DEPARTMENT OF COMMERCE • Luther H. Hodges, *Secretary*
NATIONAL BUREAU OF STANDARDS • A. V. Astin, *Director*

A Study of Lunar Surface Radio Communication

L. E. Vogler

National Bureau of Standards Monograph 85

Issued September 14, 1964

For sale by the Superintendent of Documents, U.S. Government Printing Office
Washington, D.C., 20402 - Price 70 cents

Library of Congress Catalog Card Number: 64-60070

CONTENTS

A STUDY OF LUNAR SURFACE RADIO COMMUNICATION

L. E. Vogler

The problem of point-to-point radio communication on the moon is discussed, and equations and curves are presented to estimate power requirements in lunar communication systems. Assuming a smooth surface, consideration is given to ground wave attenuation over both layered and non-layered grounds, antenna ground losses in situations where ground screens are impractical, noise level estimates in the receiving system, and the effects on propagation of possible lunar ionospheres. An example of the calculation of required power for a particular communication system is given, and further studies are suggested.

1. INTRODUCTION

This monograph presents the results of a study investigating the problem of point-to-point radio communication on the surface of the moon. It is intended as a survey of all the work accomplished in a project sponsored by Jet Propulsion Laboratory and, consequently, much of the material has appeared in previous papers concerned with various phases of the study [Vogler, 1963a, 1963b; Vogler and Noble, 1963, 1964]; the rest of the material, notably the discussions on the effects of layered grounds and possible lunar ionospheres, has not been published before.

No attempt is made here to analyze in detail one particular type of communication system; rather, it is hoped that this study may provide part of the general information necessary to the design of any future lunar surface communication link. For example, the antenna used in a permanently based installation would most likely be much more elaborate than the one needed for communication by a mobile exploring party. Once the purpose of the system is determined, the curves herein may be used to help estimate the frequency, range, and power requirements.

Most of the curves, aside from those figures describing illustrative examples, are plotted in parametric terms for the simple reason that very little information exists at the present time concerning the exact nature of the lunar environment; however, as more and more data become available, the curves, using the better estimates of parametric values, will still be useful in the analysis of communication requirements.

The study is primarily concerned with the propagation aspect of lunar surface communication, although considerable emphasis has been placed on the evaluation of antenna power losses due to the proximity of the ground. For low antenna heights and poorly conducting soils, these losses may be far from negligible, especially where ground screens are impractical. The effects of noise and its relationship to the desired signal is discussed briefly, consideration being given to galactic and receiving system component noise.

The lunar model assumed is that of a smooth sphere of radius $r_o = 1738$ km. The effects of rough terrain on signal propagation are not included in this analysis, although it is recognized that such things as knife-edge diffraction, "obstacle gain", etc., might be important at some locations on the moon's surface; a study including these mechanisms could be undertaken for particular surface areas of interest. The present curves are expected to be most useful for applications in the frequency range from about 1 kc/s to 10 Mc/s. Throughout the present analysis, antenna heights are assumed to be low enough such that height gain effects are negligible.

2. SYSTEM LOSS

The concept of system loss [Norton, 1959; Wait, 1959; CCIR, 1963] will be used to describe the effects of the various system parameters. System loss L_s is defined as the ratio, expressed in decibels, of the radio frequency power input to the terminals of the transmitting antenna p_t and the resultant radio frequency signal power available at the terminals of the receiving antenna p_r:

$$L_s = 10 \log(p_t/p_r) = P_t - P_r \quad . \tag{2.1}$$

Unless otherwise specified, capital letters will be used to designate the decibel equivalent of the corresponding lower case letters; e.g., $P_t = 10 \log_{10} p_t$.

The system loss may be divided further into a free space component that would be the loss expected between isotropic antennas situated in free space, an attenuation A_t relative to a free space inverse distance field which accounts for the effects on propagation of the intervening terrain, and the transmitting and receiving antenna components L_t, L_r, and G_p describing the effects of the particular antennas used. Thus, (2.1) may be written as

$$P_t = L_s + P_r = 10 \log(4\pi d_o/\lambda)^2 + A_t - G_p + L_t + L_r + P_r \quad , \tag{2.2}$$

where d_o is the arc distance separating the two antennas and λ is the free space wavelength expressed in the same units as d_o. The term G_p denotes the path antenna gain which is a function of the transmitting and receiving antenna maximum directivity gains relative to isotropic antennas, G_t and G_r, and any aperture-to-medium coupling loss or polarization coupling loss. For the purposes of this analysis, the latter two losses will be assumed negligible such that $G_p = G_t + G_r$; however, it should be noticed that, in general, the path antenna gain will be less than or equal to the sum of the maximum directivity gains. The symbols L_t and L_r denote antenna losses arising from the antenna's proximity to the ground: $L_{t,r} = 10 \log(r/r_f)$, where r is the actual input resistance and r_f the radiation resistance in free space. Notice that, in order to calculate transmitter power, any transmission line loss and appropriate circuit losses should be added to the right side of (2.2).

The power available at the receiver consists not only of the desired signal but also of radio noise arising both from within and from without the receiving system. If $r(s/n)$ denotes the desired minimum signal-to-noise power ratio that will provide a given grade of reception as measured at the receiver predetection output, and an operating noise factor f[†] is defined as the ratio of (1) the signal to a reference Johnson-noise power ratio that is available from a loss-free receiving antenna to (2) the receiver predetection output signal-to-noise ratio $r(s/n)$, then p_r may be expressed as

$$p_r = f k_B t_o b r(s/n)/\ell_c \quad , \tag{2.3}$$

[†] The relationship between f and the effective "noise temperature" T_{eff} used in some discussions is given by $T_{eff} = t_o f$.

where $k_B t_o b$ is the reference Johnson-noise power. The symbol k_B denotes Boltzmann's constant ($= 1.38054 \times 10^{-23}$ joules/degree), t_o is a reference temperature in degrees Kelvin, b is the effective noise bandwidth in cycles per second, and ℓ_c is the ratio of the antenna input resistance to its radiation resistance.

Using the above definitions and assuming $\ell_c \simeq \ell_r$, (2.2) may now be expressed as

$$P_t = 32.45 + 20 \log d_o(\text{km}) + 20 \log f_{mc} + A_t - (G_t + G_r) + L_t + R + F + B + 10 \log (k_B t_o) , \qquad (2.4)$$

where d_o is measured in kilometers, f_{mc} denotes the radio frequency in megacycles per second, and $R \equiv 10 \log r(s/n)$. The following sections will discuss the various components of (2.4).

3. GROUND WAVE ATTENUATION A_t

Numerical procedures for the calculation of electromagnetic fields diffracted around a smooth homogeneous sphere have been developed by various authors [Norton, 1941; Bremmer, 1949]. The ground wave may be expressed as a series of residues that depend on the radius of the sphere r_o, the arc distance d_o, the antenna heights h_1 and h_2, the free space wavelength λ, the relative dielectric constant ϵ_r and conductivity σ of the ground, and the polarization of the wave. As stated in section 1, the present analysis assumes negligible height gain effects corresponding to antenna heights near zero; for elevated antennas, estimates of height gain may be obtained for beyond the horizon paths from another paper [Vogler, 1964].

In parametric form the ground wave attenuation relative to a free space inverse distance field A_t is conveniently plotted as a function of three parameters: K, b°, and x_o'. Through the recent work of Wait [1962a] both non-layered and layered grounds may be accounted for by generalizations of the definitions of K and b°. Thus, with the subscripts h and v referring to horizontal and vertical polarization respectively,

$$K_h = \left[(2\pi r_o/\lambda)^{\frac{1}{3}} |T_h| \cdot |Q_h| \right]^{-1}, \quad K_v = \left[(2\pi r_o/\lambda)^{\frac{1}{3}} |T_v| \cdot |Q_v| \right]^{-1}, \qquad (3.1)$$

where

$$|T_h| = \left[(\epsilon_r - 1)^2 + s^2 \right]^{\frac{1}{4}}, \quad |T_v| = \left[\sqrt{(\epsilon_r - 1)^2 + s^2} \,/ (\epsilon_r^2 + s^2) \right]^{\frac{1}{2}}; \qquad (3.2)$$

and

$$b_h^\circ = 180^\circ - \tan^{-1}\left(\frac{\epsilon_r - 1}{s}\right) - q_h^\circ, \quad b_v^\circ = 2 \tan^{-1}\left(\frac{\epsilon_r}{s}\right) - \tan^{-1}\left(\frac{\epsilon_r - 1}{s}\right) - q_v^\circ , \qquad (3.3)$$

with

$$s = 2 \times 10^{-7} \, c \lambda \, \sigma \simeq 1.8 \times 10^4 \, \sigma(\text{mhos/m})/f_{mc} .$$

Both ϵ_r and s are dimensionless and refer to the top ground layer unless otherwise specified. The parameters λ and σ are in meters and mhos per meter respectively, and c is the velocity of light.

The symbols $|Q|$ and q° appearing in (3.1) and (3.3) denote the magnitude and phase of a "stratification factor", $Q \equiv |Q| \exp(iq^\circ/2)$, that accounts for the effect of layering in the ground. In general Q is a complex quantity dependent on the heights and electromagnetic ground constants of the various layers, whereas for a homogeneous (non-layered) ground, Q is equal to unity. Wait [1962b] has derived formulas for Q for the general case of n layers and has presented curves [Wait, 1962a] for two and three layer situations; however, unless specific values for the heights and ground constants of the various layers are given, a graphical representation becomes quite complicated for a multi-layered ground. For the present discussion, restriction to vertical polarization over a two-layered model will be assumed.

Letting the subscripts 1 and 2 refer to the upper and lower layers respectively, Q_v may be expressed as

$$Q_v = \frac{\left(|T_{v2}|/|T_{v1}|\right) e^{i\left(b_{v1}^\circ - b_{v2}^\circ\right)/2} + \tanh\left\{(2\pi\ell_1/\lambda)|T_{h1}| \, e^{i\left(270^\circ - b_{h1}^\circ\right)/2}\right\}}{1 + \left(|T_{v2}|/|T_{v1}|\right) e^{i\left(b_{v1}^\circ - b_{v2}^\circ\right)/2} \tanh\left\{(2\pi\ell_1/\lambda)|T_{h1}| \, e^{i\left(270^\circ - b_{h1}^\circ\right)/2}\right\}} \equiv |Q_v| \, e^{iq_v^\circ/2} , \tag{3.4}$$

where ℓ_1 is the height of the upper layer measured in the same units as λ. $|T_h|$ and $|T_v|$ are given by (3.2) using the appropriate values of ϵ_r and σ characterizing layer 1 or layer 2; b_h° and b_v° are obtained from (3.3) after setting $q^\circ = 0$. As ℓ_1 becomes very large (corresponding to homogeneous ground), Q_v approaches unity and $|Q_v| = 1$, $q_v^\circ = 0$.

Graphs of $|T_h|$ and $|T_v|$ as functions of ϵ_r and s are shown in figures 1 and 2 where the expressions for $K_{h,v}$ refer to a homogeneous ground ($|Q| = 1$); similar plots of b_h° and b_v° are given in figures 3 and 4, again for homogeneous ground ($q^\circ = 0$). It can be seen that b° is always positive for either polarization as long as no layering occurs.

The variation of K_v and b_v° for a two-layered ground is shown in figures 5 through 8. The curves were calculated from (3.1), (3.3), and (3.4) using the values of the ground constants and upper layer heights indicated. Only values of K_v for $0.01 \le K_v \le 10$ are plotted since the variation of A_t as a function of b° is negligible outside this range (see figures 9 - 14). The curves of b_v° indicate that, as the conductivity of the lower layer σ_2 increases, b_v° is more likely to become negative. Thus, if it is found that the moon consists of a highly conducting core underlying a thin poorly conducting crust, ground wave communication could encounter "fade-outs" for certain frequencies and ranges. This is indicated in figures 9 through 14 which show the ground wave attenuation A_t for zero antenna heights versus the distance parameter x_o', where

$$x_o' = f_{mc}^{\frac{1}{3}} \, d_o \text{(km)} . \tag{3.5}$$

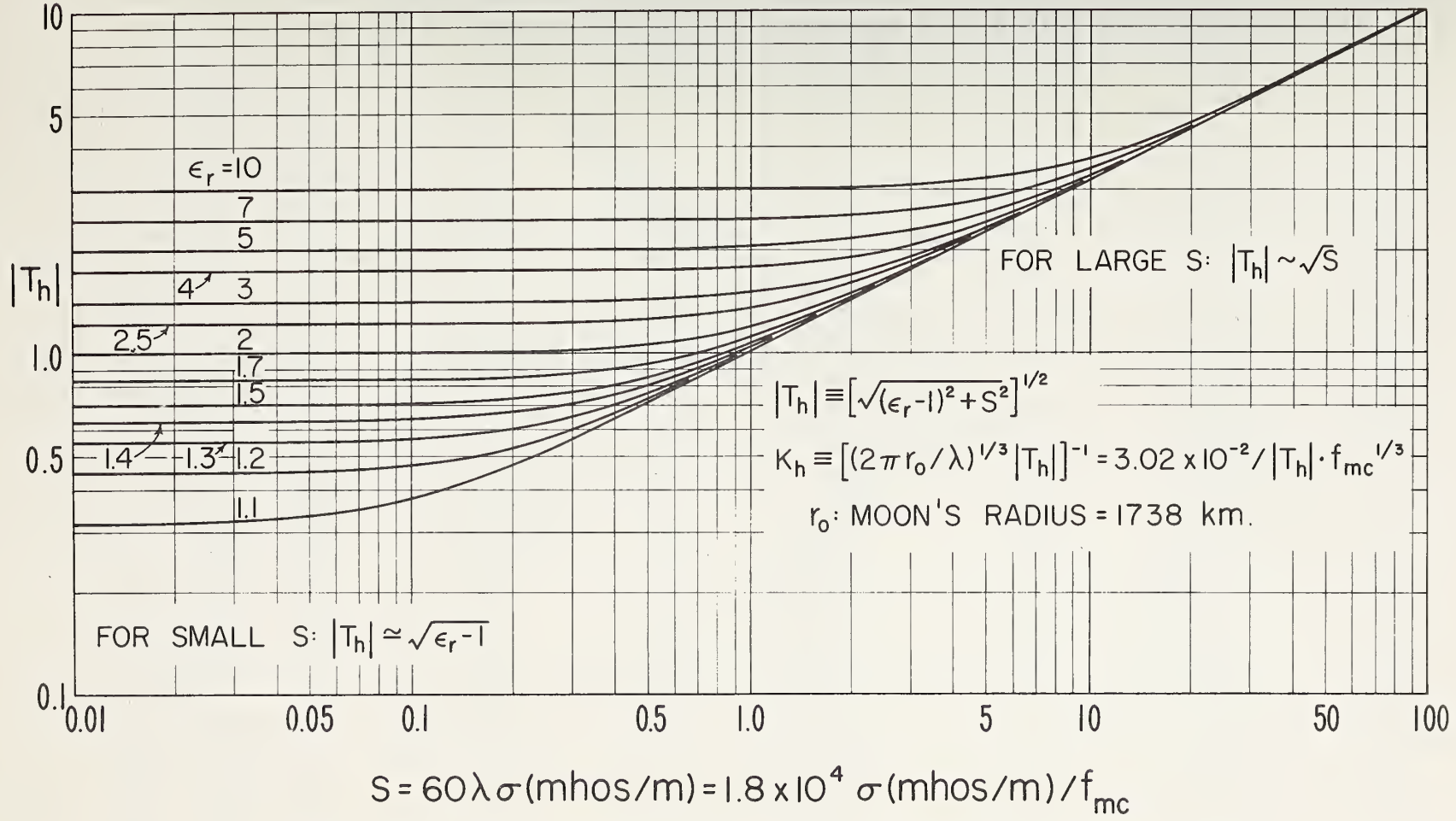

Figure 1. The parameter $|T_h|$ for horizontal polarization. The formula for K_h assumes a homogeneous ground.

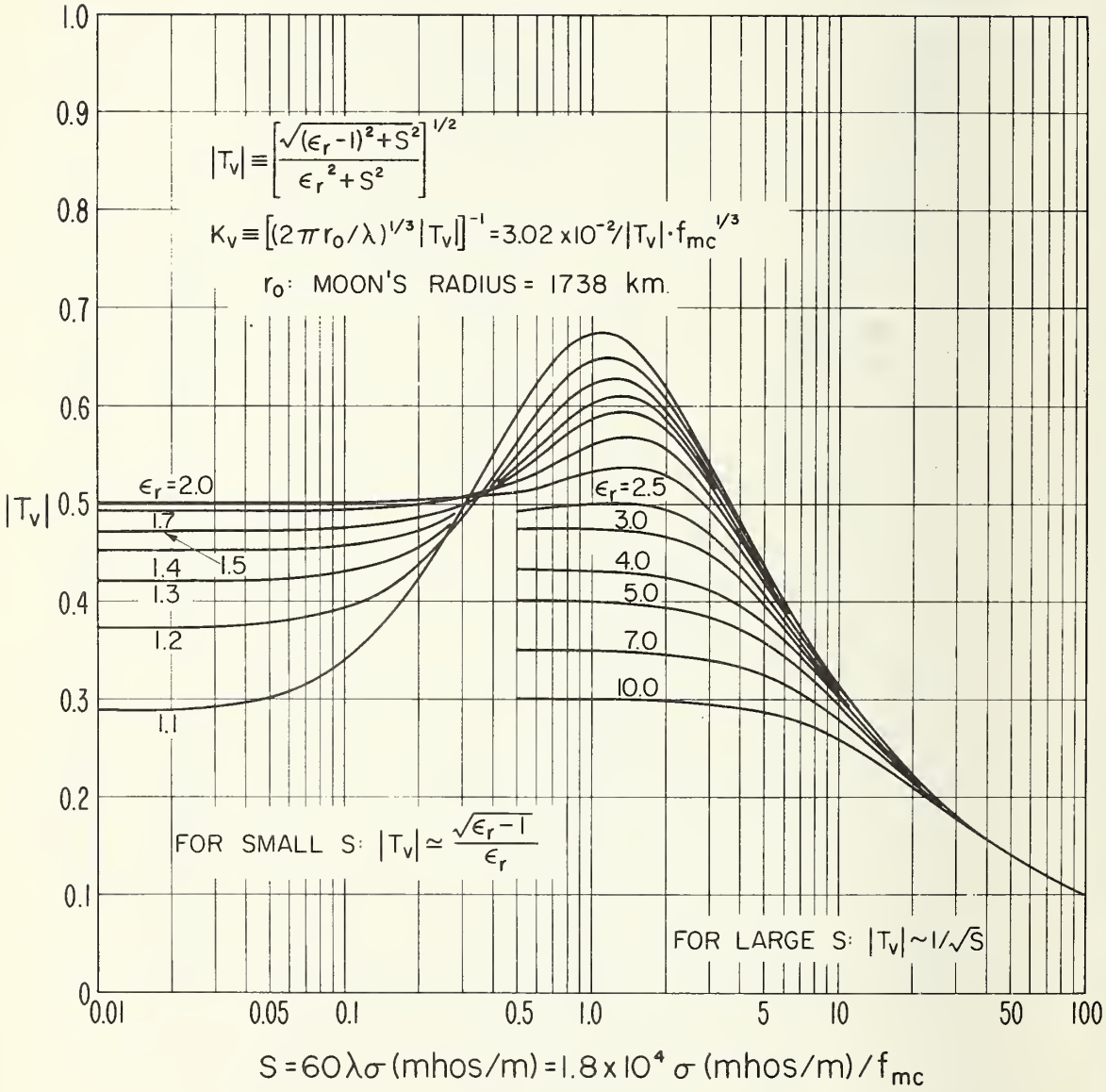

Figure 2. The parameter $|T_v|$ for vertical polarization. The formula for K_v assumes a homogeneous ground.

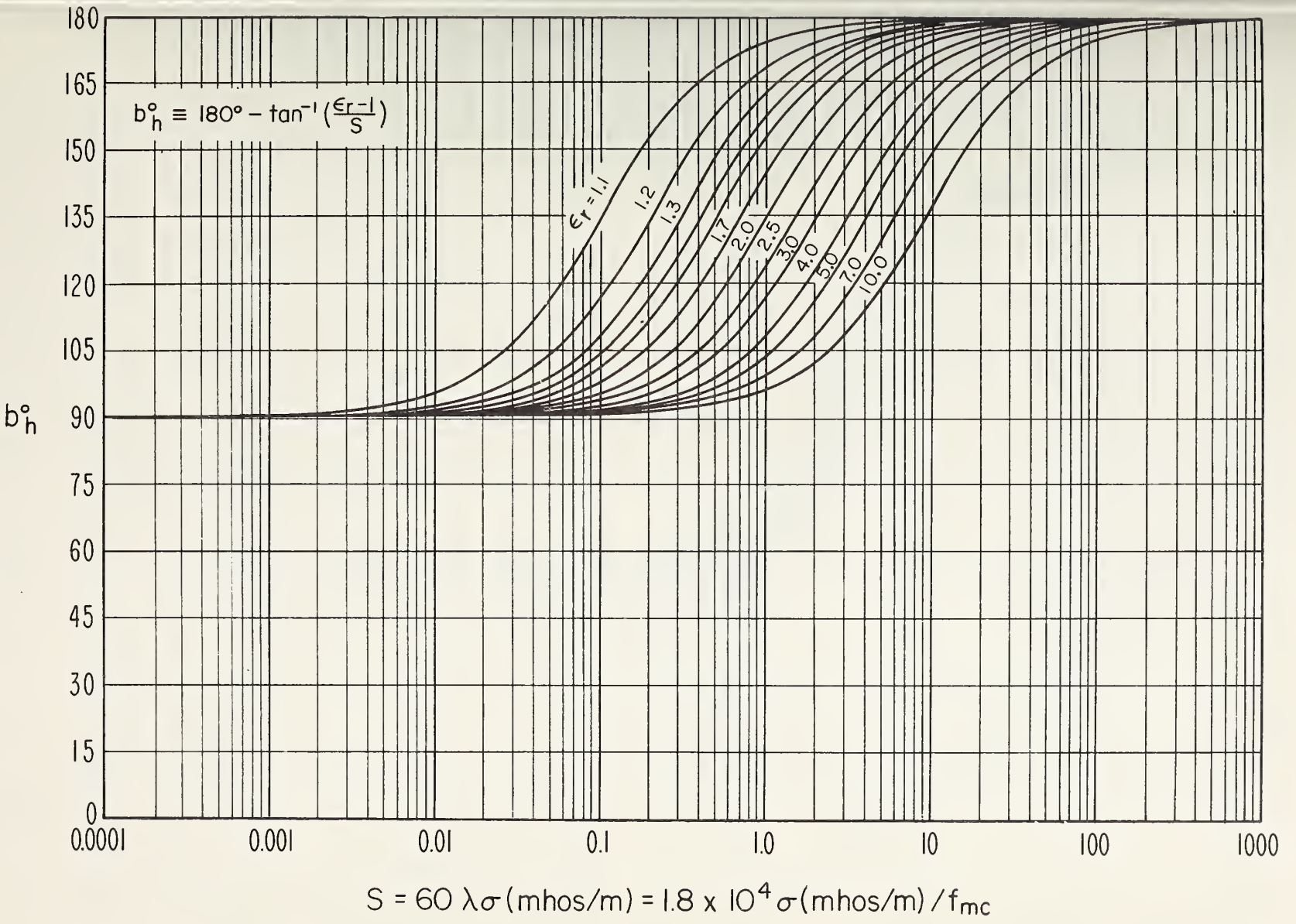

Figure 3. The parameter b_h° for horizontal polarization and homogeneous ground.

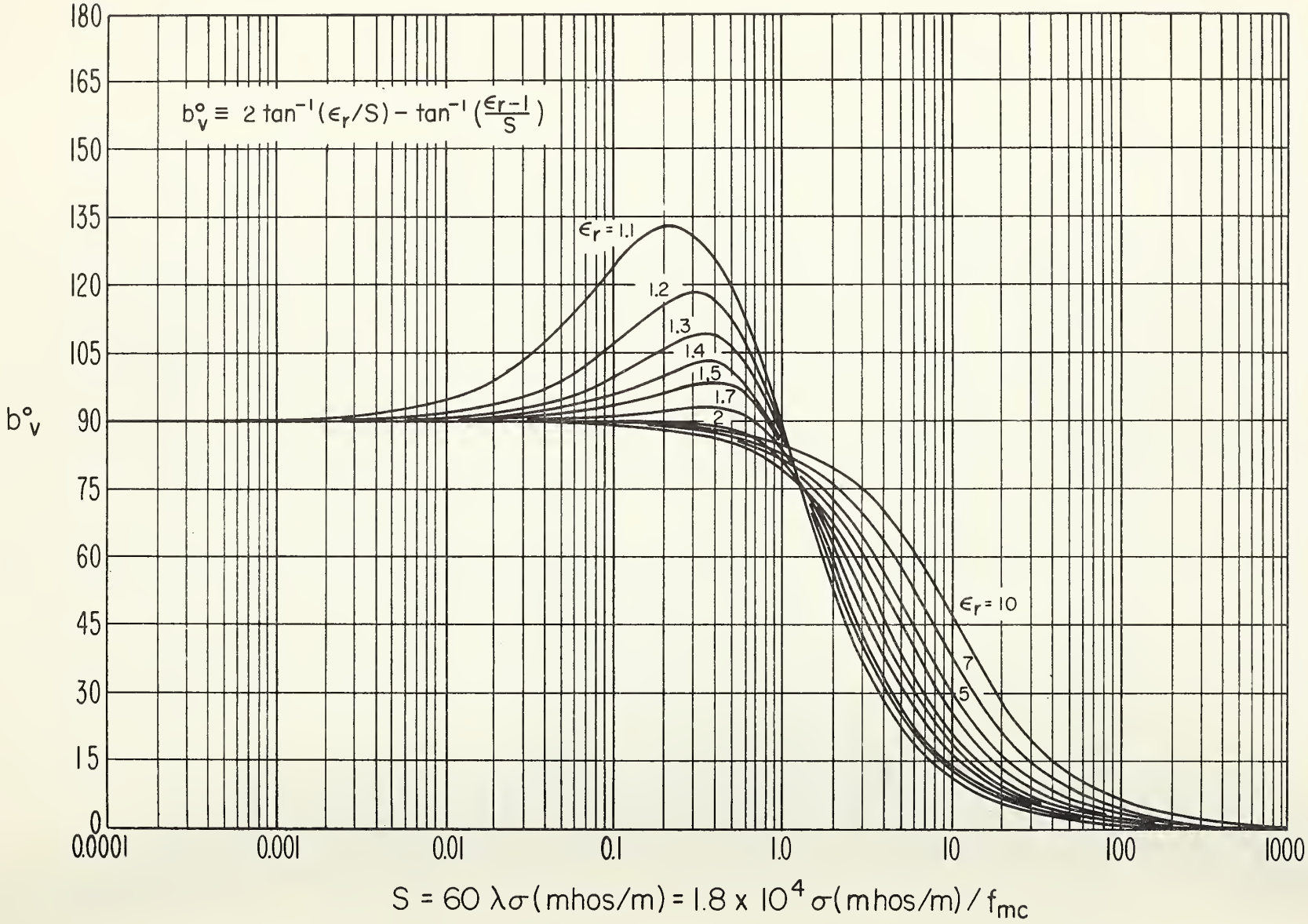

Figure 4. The parameter b°_v for vertical polarization and homogeneous ground.

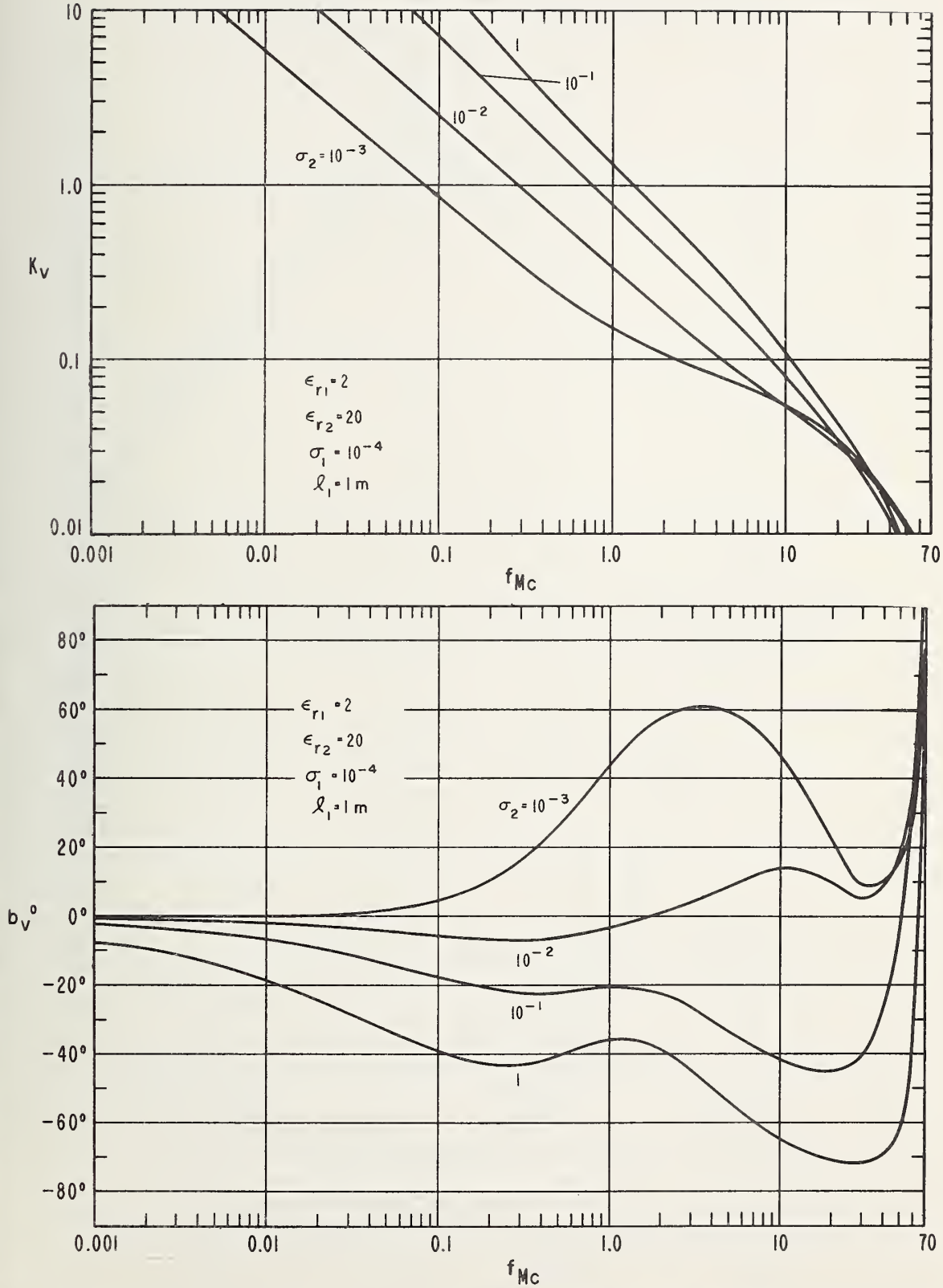

Figure 5. K_v and b_v° for two layers, upper layer height: 1 m.

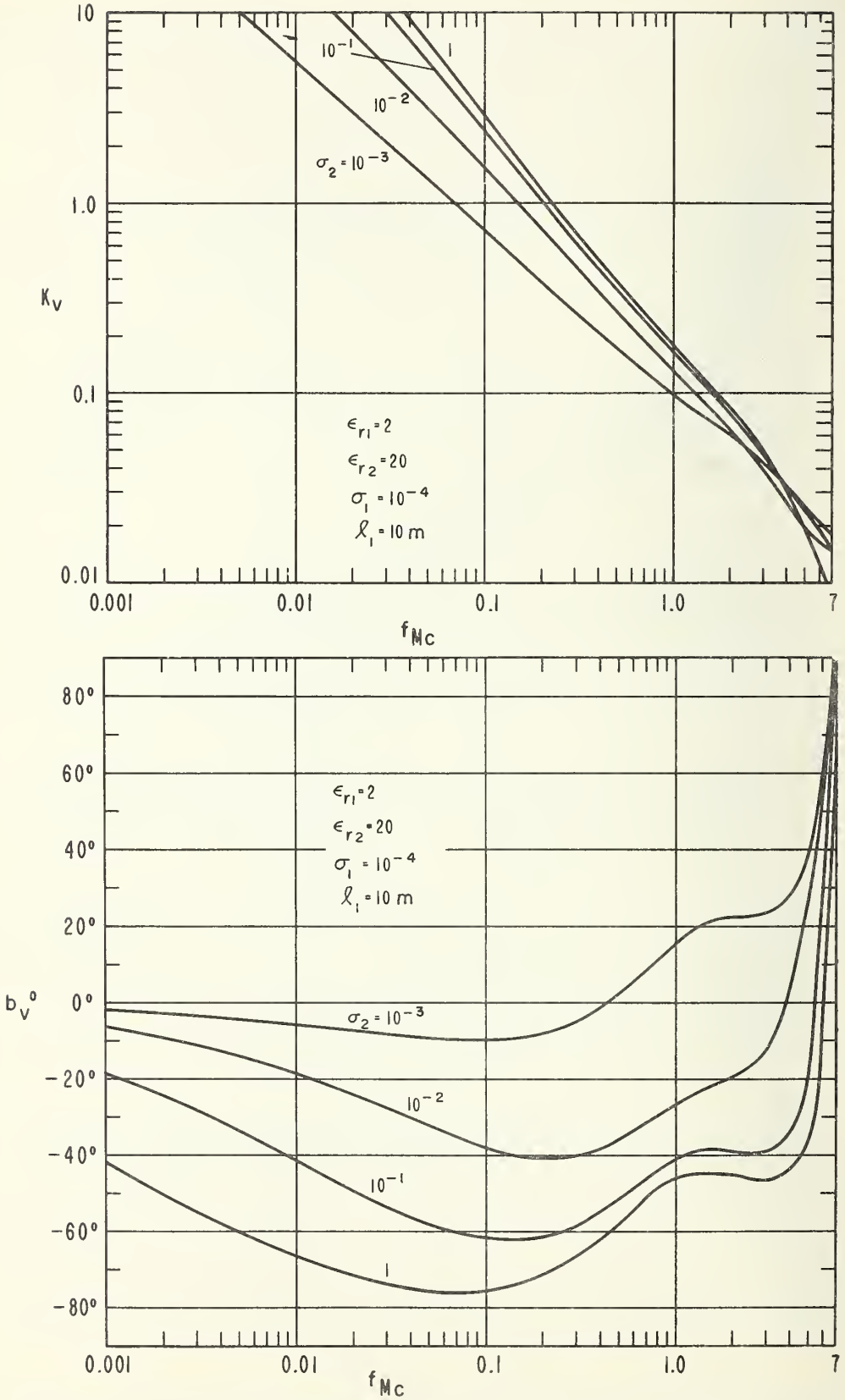

Figure 6. K_v and b_v° for two layers, upper layer height: 10 m.

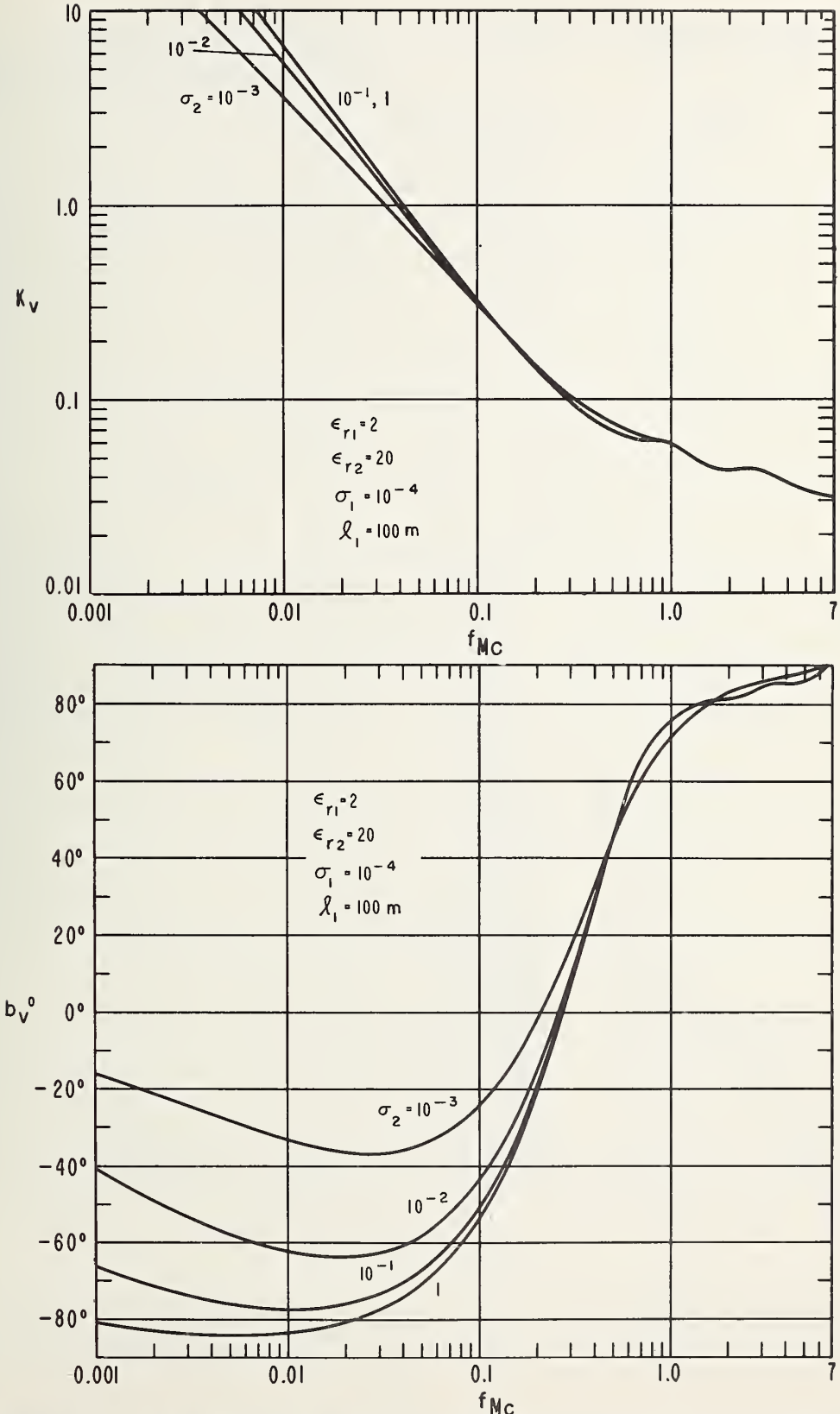

Figure 7. K_v and b_v° for two layers, upper layer height: 100 m.

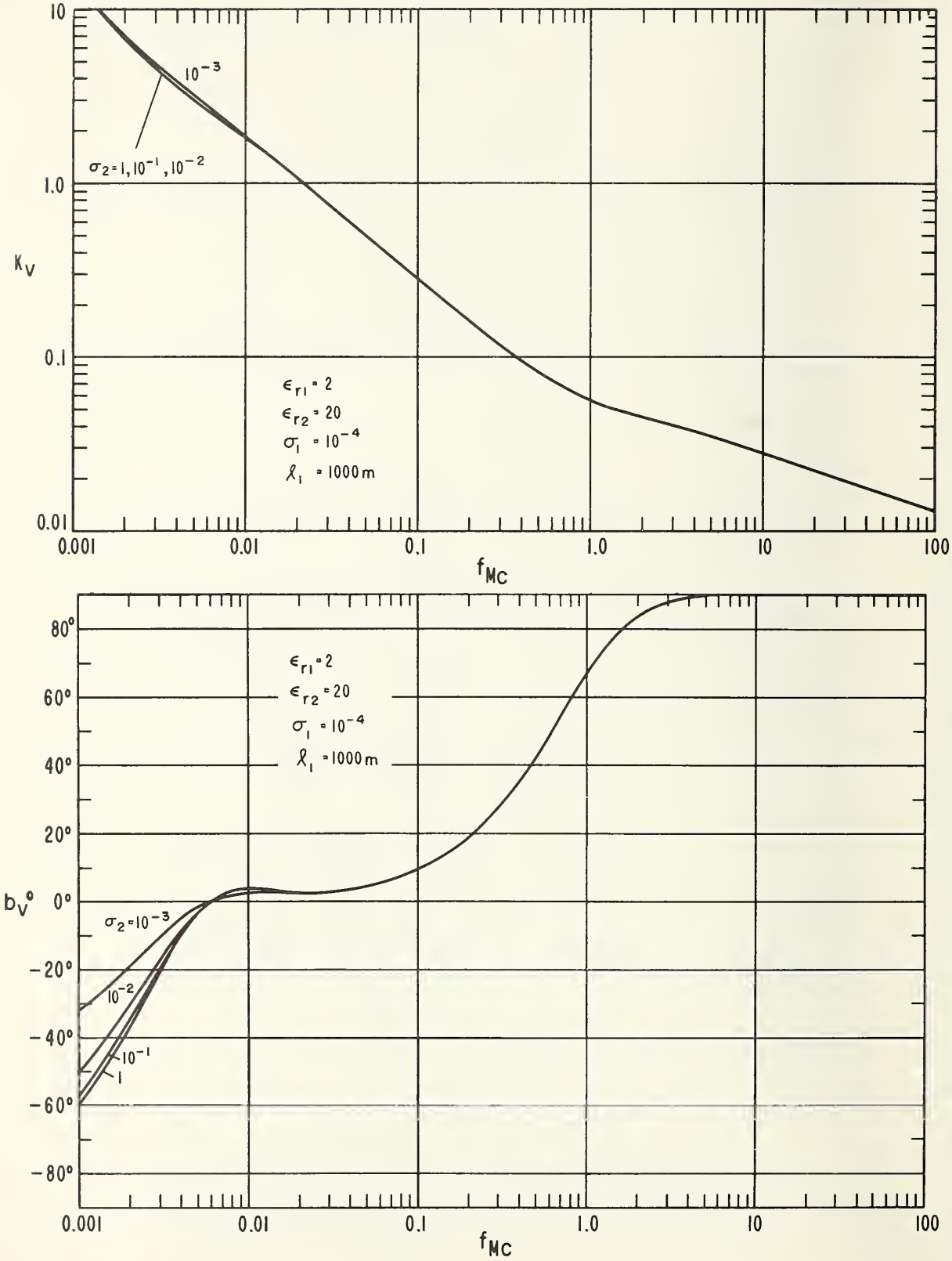

Figure 8. K_v and b_v° for two layers, upper layer height: 1000 m.

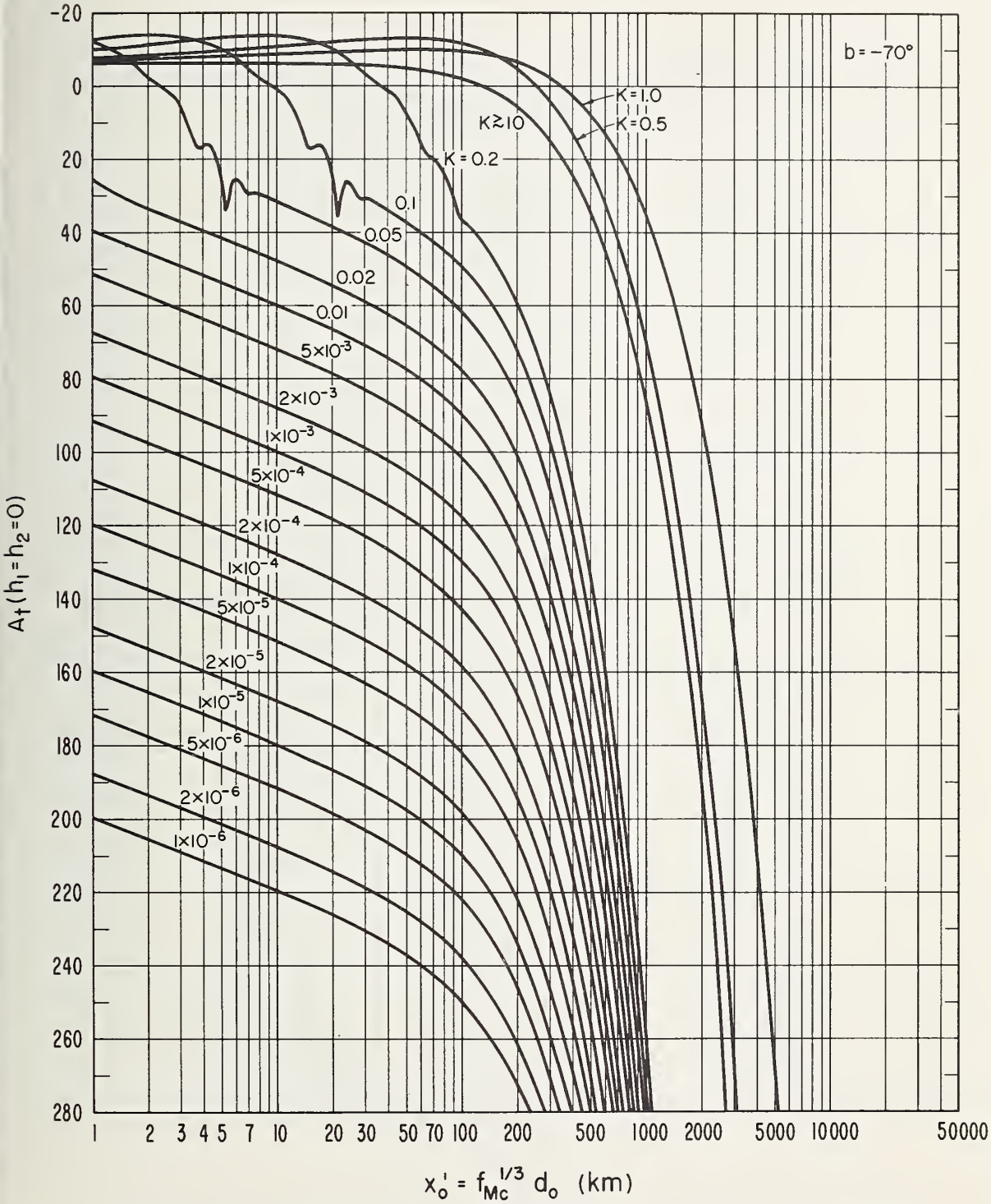

Figure 9. Ground wave attenuation for zero antenna heights, b = -70°.

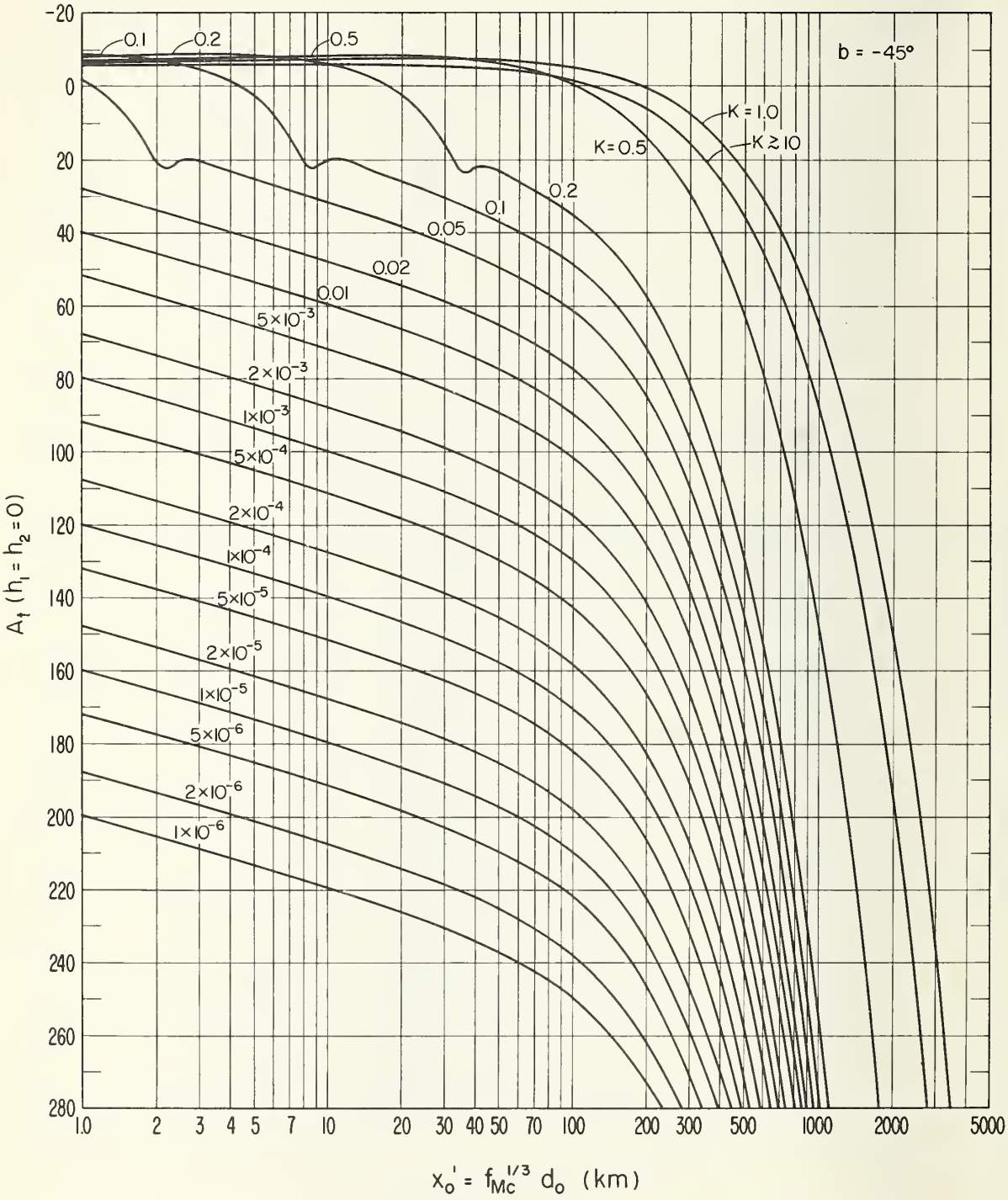

Figure 10. Ground wave attenuation for zero antenna heights, $b = -45^{\circ}$.

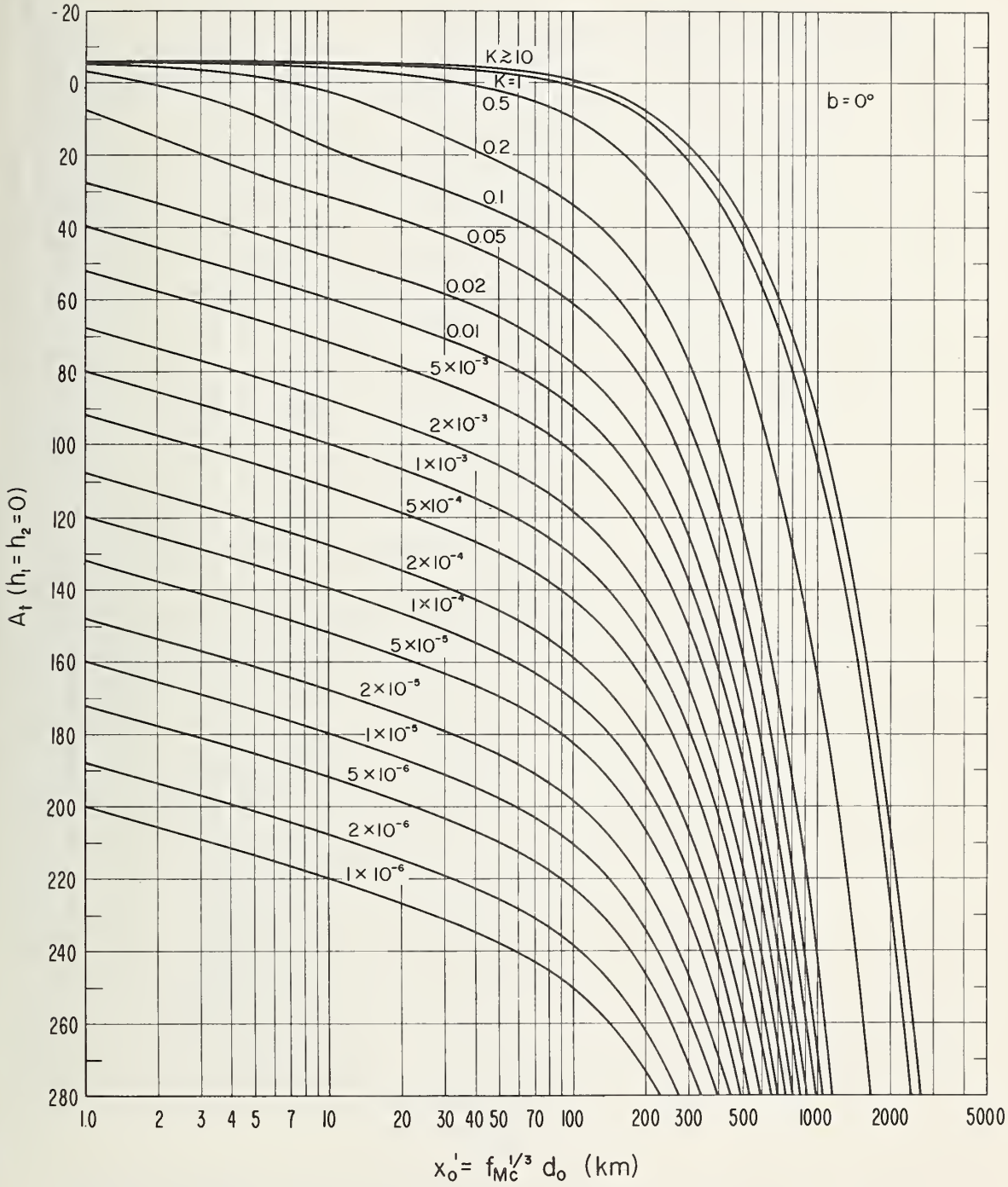

Figure 11. Ground wave attenuation for zero antenna heights, b = 0°.

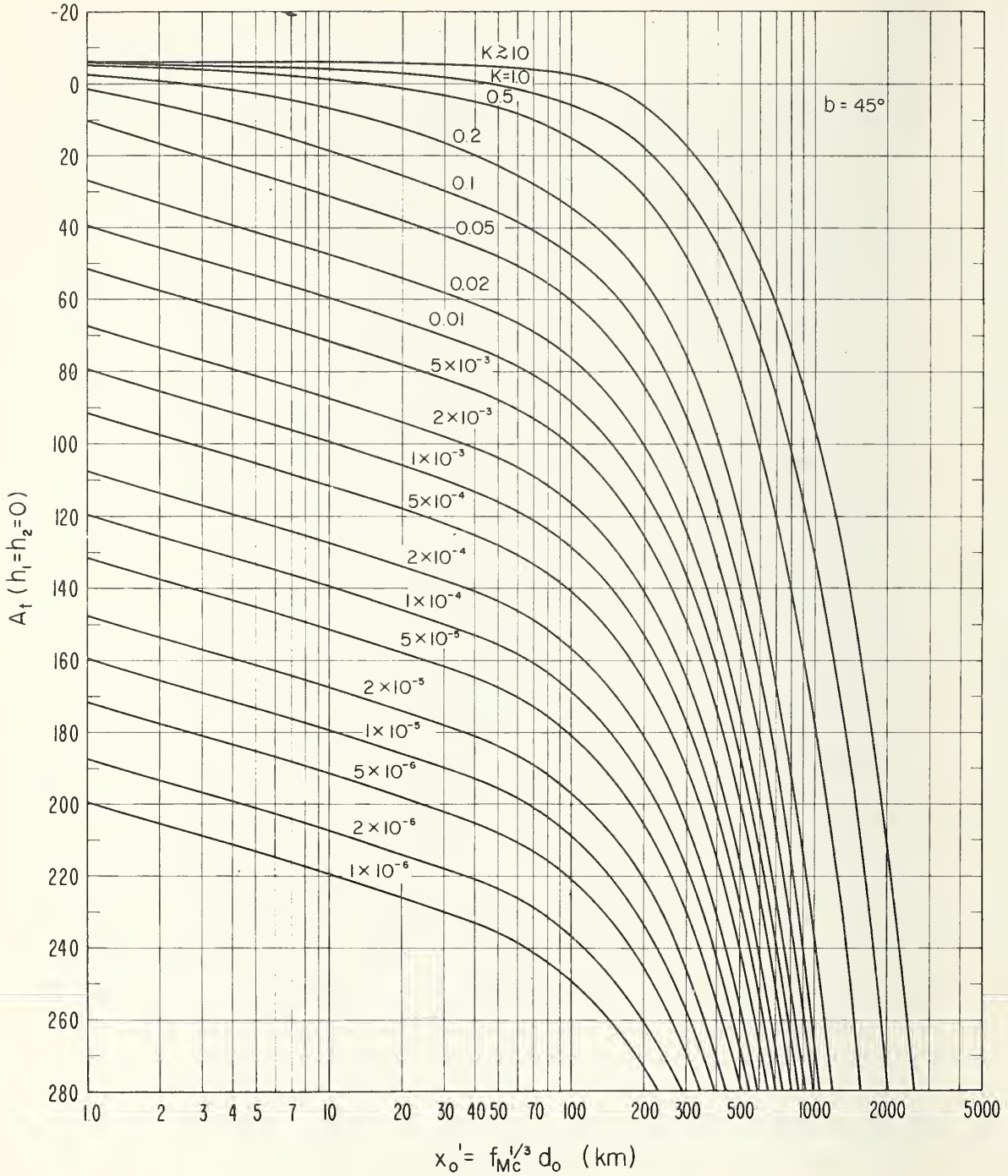

Figure 12. Ground wave attenuation for zero antenna heights, b = 45°.

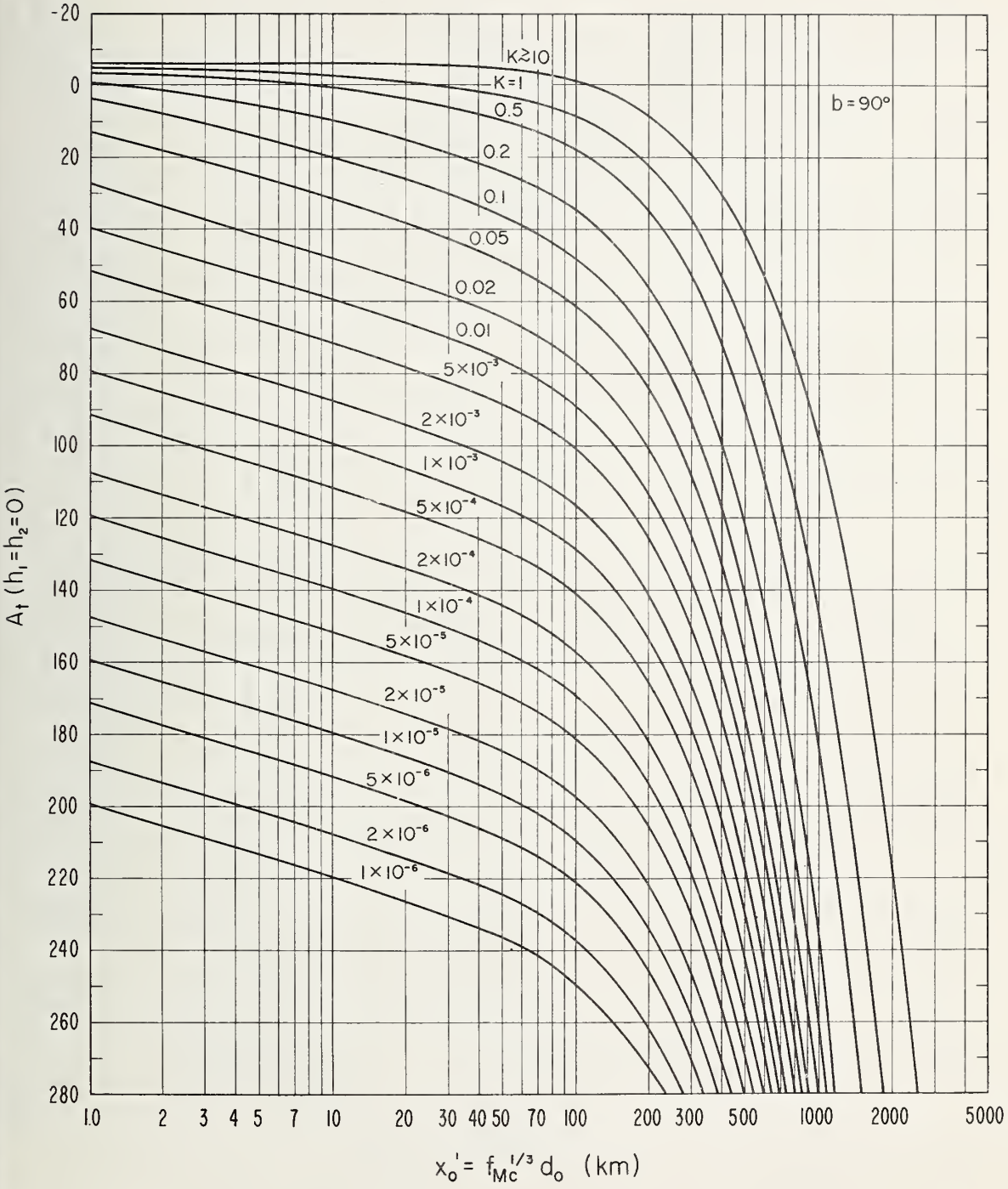

Figure 13. Ground wave attenuation for zero antenna heights, b = 90°.

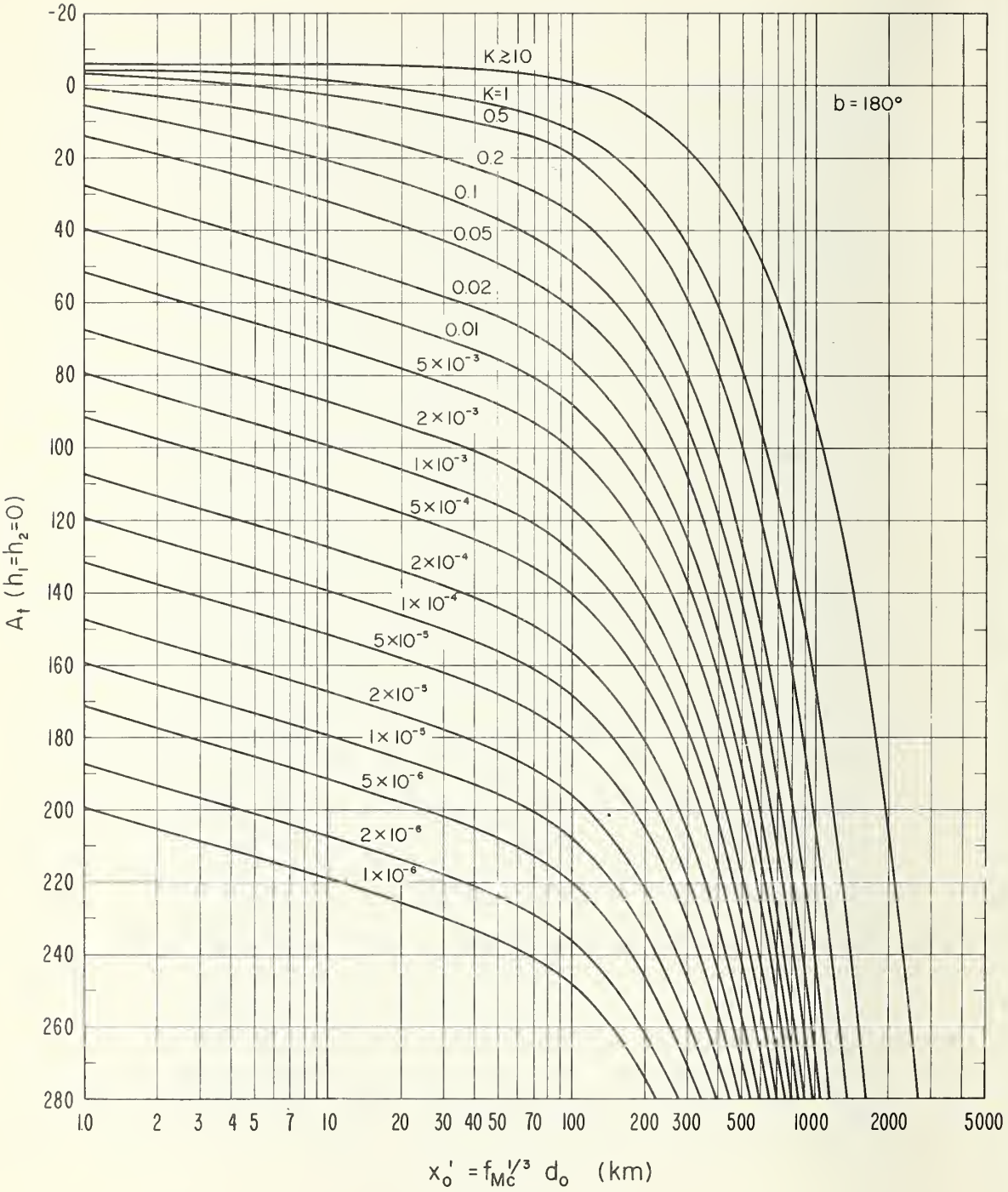

Figure 14. Ground wave attenuation for zero antenna heights, b = 180°.

In figures 9 ($b = -70^\circ$) and 10 ($b = -45^\circ$) the curves show fading effects over short intervals of x_o' for certain values of K. As b becomes positive, these fade-outs disappear and A_t is seen to increase smoothly with distance.

The calculations of the attenuation curves were not done by numerically evaluating the complete residue series, since a prohibitive number of terms are necessary for small values of x_o'. In this region (the left hand portion of figures 9 - 14) use was made of the modified flat earth formula developed by Wait [1962b, see equation (108)] in which the leading term is the plane earth attenuation function and successive terms account for the curvature of the sphere. The formula with two curvature correction terms was employed wherever valid until x_o' became too large, at which point the first term of the residue series could be used from there on out.

Equation (2.4) is strictly applicable only for the case of antennas separated a sufficient distance apart ($d_o >> \lambda$) such that the induction and static fields may be neglected. Because of this restriction, A_t is not shown in the figures for values of $x_o' < 1$. As d_o (or x_o') goes to zero, A_t approaches $20 \log(\frac{1}{2}) = -6.02$, which would correspond to the surface wave field intensity expected between short vertical electric dipoles situated near each other on a perfectly conducting plane.

It is apparent from figures 9 - 14 that the attenuation is less for the larger values of K, these values corresponding to vertically polarized waves at the lower frequencies. For example, for $K \geq 0.1$ and $f_{mc} \leq 1.0$, the attenuation is less than 50 db out to distances of 100 km. On the other hand, with horizontal polarization, K_h is usually much less than unity for all frequencies and the attenuation is greater.

4. ANTENNA EFFECTS

The terms $L_{t,r}$ and $G_p = G_t + G_r$ (the subscripts t,r referring to either transmitting or receiving antenna) in (2.2) describe the effects of the particular transmitting and receiving antennas used in the communication system under consideration. $L_{t,r}$, called the ground proximity loss, is defined as the ratio expressed in decibels of the input resistance of the antenna r to its free space radiation resistance r_f. As the height of the antenna above the surface is increased, the ratio of the resistances approaches unity and L_t or L_r effectively become zero. For heights near the surface, the input resistance is a function of the electromagnetic ground constants ϵ_r and σ, the radio frequency f_{mc}, and the antenna height h above the surface.

$G_{t,r}$ denotes the free space maximum directivity gain of an optimally oriented loss-free antenna above an isotropic antenna, e.g., $G_t = G_r = 10 \log(3/2) = 1.76$ for elementary dipoles and $G_t = G_r = 2.15$ for half-wave dipoles.

Because present estimates indicate the conductivity of lunar surface material to be relatively poor, a numerical evaluation of input impedance was undertaken [Vogler and Noble, 1963, 1964] considering four types of antennas: vertical and horizontal electric and magnetic dipoles. Short dipoles of length $d\ell$ are assumed, the current in which varies as $I_o e^{i\omega t}$ with I_o a constant along the antenna; the magnetic dipoles are then equivalent to small circular loop antennas of area dA, the axis being in the direction of the dipole. The ground beneath the antenna is assumed to be homogeneous and characterized by its relative dielectric constant ϵ_r and conductivity σ.

The input impedance Z, obtained in terms of the field at the antenna, may be divided into a free space component Z_f and a component ΔZ describing the effect of the presence of the ground:

$$Z = Z_f + \Delta Z \ . \tag{4.1}$$

Explicit expressions for the impedance change due to ground normalized by the free space radiation resistance, $\Delta Z/r_f$, where VED, HED, VMD, HMD refer to the initial letters of the four types of dipoles considered, are then given by

$$\text{VED:}\quad \Delta Z/r_f = i(3/2\,\alpha^3)\left[I_1(N^2) + I_2(N^2) \right], \quad r_f = 20\,\beta^2(d\ell)^2 \ , \tag{4.2a}$$

$$\text{HED:}\quad \Delta Z/r_f = i(3/4\,\alpha^3)\left[I_1(1) + I_2(N^2) \right], \quad r_f = 20\,\beta^2(d\ell)^2 \ , \tag{4.2b}$$

$$\text{VMD:}\quad \Delta Z/r_f = i(3/2\,\alpha^3)\left[I_1(1) + I_2(1) \right], \quad r_f = 20\,\beta^4(dA)^2 \ , \tag{4.2c}$$

$$\text{HMD:}\quad \Delta Z/r_f = i(3/4\,\alpha^3)\left[I_1(N^2) + I_2(1) \right], \quad r_f = 20\,\beta^4(dA)^2 \ , \tag{4.2d}$$

where

$$I_1(\delta) = \alpha^2 \int_{i\alpha}^{\infty} \left\{ \frac{\delta x - \sqrt{x^2 - \alpha^2(N^2 - 1)}}{\delta x + \sqrt{x^2 - \alpha^2(N^2 - 1)}} \right\} e^{-x}\, dx \ , \tag{4.3a}$$

$$I_2(\delta) = \int_{i\alpha}^{\infty} x^2 \left\{ \frac{\delta x - \sqrt{x^2 - \alpha^2(N^2 - 1)}}{\delta x + \sqrt{x^2 - \alpha^2(N^2 - 1)}} \right\} e^{-x}\, dx \ , \tag{4.3b}$$

$$\alpha = 2h\beta = 2h(2\pi/\lambda) \ , \quad N^2 = \epsilon_r - is \ , \quad s = 60\lambda\,\sigma(\text{mhos/m}) \ , \tag{4.4}$$

and h denotes the antenna height in meters above the ground.

The variable x in (4.3) assumes purely imaginary values from the lower limit to zero, and from there ranges over real values to the upper limit. The sign of the square root is chosen so that the real part is greater than zero. A derivation of the dipole impedances together with asymptotic expressions of (4.2) is contained in the appendix.

Ground proximity loss in terms of the input impedance as given by (4.1) may be expressed as

$$L_{t,r} = 10 \log(r/r_f) = 10 \log\left[1 + \mathrm{Re}(\Delta Z/r_f) \right] , \tag{4.5}$$

where $\mathrm{Re}(\Delta Z/r_f)$ denotes the real part of $(\Delta Z/r_f)$. Using the relationships of (4.2), $L_{t,r}$ is plotted versus

$$s = 60\lambda\ \sigma(\text{mhos/m})$$

in figures A-1 to A-28 for various values of ϵ_r and α. Notice that for α greater than about 5, i.e., $h/\lambda \gtrsim 0.4$, the ground loss is always negligible; however, as the antenna height in wavelengths approaches zero, $L_{t,r}$ may become quite large for certain combinations of ground conductivity and frequency. It is often possible to reduce the effect of the ground through the use of appropriate ground screens. Discussions of this subject are contained in papers by Wait and Surtees [1954] and by Wait [1956].

To show the variation in the normalized input impedance change for both the resistance $(\mathrm{Re}\ \Delta Z/r_f)$ and the reactance $(\mathrm{Im}\,\Delta Z/r_f)$, equations (4.2) are evaluated and plotted in figures A-29 to A-64 as functions of $|N|$, $\phi/2$, and α where,

$$|N| = \left(\epsilon_r^2 + s^2\right)^{1/4}, \qquad \phi/2 = (1/2)\ \tan^{-1}(s/\epsilon_r)\ , \tag{4.6}$$

with α and s as defined in (4.4). It should be emphasized that figures A-29 to A-64 do not show the <u>total</u> input impedance, but only the variation due to the presence of the ground. Impedance curves such as those in the figures are useful not only in estimating antenna requirements for lunar communication systems, but also may be used in determining the electromagnetic characteristics of material composing the moon.

This section will conclude with a brief discussion of the Beverage wave antenna [Beverage, Rice, and Kellogg, 1923]. If considered for semi-permanent installations on the moon, it has the advantage of relatively simply construction and operates most efficiently over poorly conducting soils. The wave antenna in its simplest form consists of a long horizontal wire situated a short height above the ground and terminated at one end through its characteristic impedance. It is a uni-directional antenna with the maximum gain in the direction of the antenna axis and toward the terminated end.

Wait [1954] has shown that the vertical electric field component of a wave antenna is proportional to a complex factor T_v, termed the "wave tilt" and defined by

$$T_v = \left[(\epsilon_r - 1) - is\right]^{1/2} / (\epsilon_r - is)\ , \tag{4.7}$$

and a function S' which depends on the wavelength λ, antenna length ℓ, an angle ϕ' measuring the direction in which the antenna is pointing, and the propagation constant Γ defined as

$$\Gamma \equiv \alpha' + i\beta m\ , \tag{4.8}$$

where α' and m are real and $\beta = 2\pi/\lambda$.

For low antenna heights h an approximate expression for the values of α' and m has been given by Carson [1926]:

$$\alpha'/\beta \simeq m - 1 \simeq \left[2^{3/2} (\beta h) \sqrt{\epsilon_r^2 + s^2} \ \ln(4h/d_a) \right]^{-1} , \tag{4.9}$$

where d_a is the diameter of the antenna wire. For an uninsulated infinitesimally thin antenna actually lying on the ground, Γ may be expressed as [Coleman, 1950]

$$\Gamma \equiv \alpha' + i\beta m = \beta \sqrt{m^2 - (\tfrac{1}{2})(\epsilon_r + 1)} + i(\beta/2) \left[\sqrt{(\epsilon_r + 1)^2 + s^2} + (\epsilon_r + 1) \right]^{\frac{1}{2}} . \tag{4.10}$$

The function S', obtained by integrating the contributions of all the elements along the antenna, is given by

$$S' = \frac{1 - \exp[-(\Gamma - i\beta \cos\phi')\ell]}{(\Gamma - i\beta \cos\phi')\ell} . \tag{4.11}$$

It can be seen from (4.10) that the propagation constant of a wave antenna lying on the ground approaches its free space value $i\beta$ if the relative dielectric constant is very near unity and the conductivity is extremely small; in this case S' approaches unity.

The wave antenna power gain [Martin and Wickizer, 1949] referred to an isotropic antenna, (p_{wa}/p_{iso}), may now be expressed as

$$(p_{wa}/p_{iso}) = (\beta \ell \cos\phi')^2 \ |S'|^2 \cdot |T_v|^2 (120 R_o/|Z_o|^2) , \tag{4.12}$$

where $Z_o = R_o + i X_o$ is the characteristic impedance of the wave antenna. The factor $|T_v|$, which was discussed in section 3 and defined by (3.2), is shown in figure 2, and $|S'|$ is graphed in figure 15 as a function of the two parameters $(\alpha'\ell)$ and $(\beta\ell)(m - \cos\phi')$. An example of the wave antenna pattern,

$$|S| = (\beta \ell \cos\phi') \cdot |S'| ,$$

as a function of the direction angle ϕ' is shown in figure 16 for several values of $\beta\ell = 2\pi(\ell/\lambda)$ and for $m = 1$, $\alpha' = 0$. It is seen that the antenna is highly directional in the forward direction $(\phi' = 0)$; other values of m and α' modify the pattern somewhat, but the general shape is the same.

A modification of the wave antenna which is also discussed in the paper by Wait [1954] is one in which the horizontal wire of length $\ell = 2b$ is center-fed and the ends of the antenna are not terminated with a load impedance. Assuming a current distribution along the wire of

$$I(y) = I_o [\sinh(\Gamma b)]^{-1} \ \sinh\left\{\Gamma(b - |y|)\right\} , \tag{4.13}$$

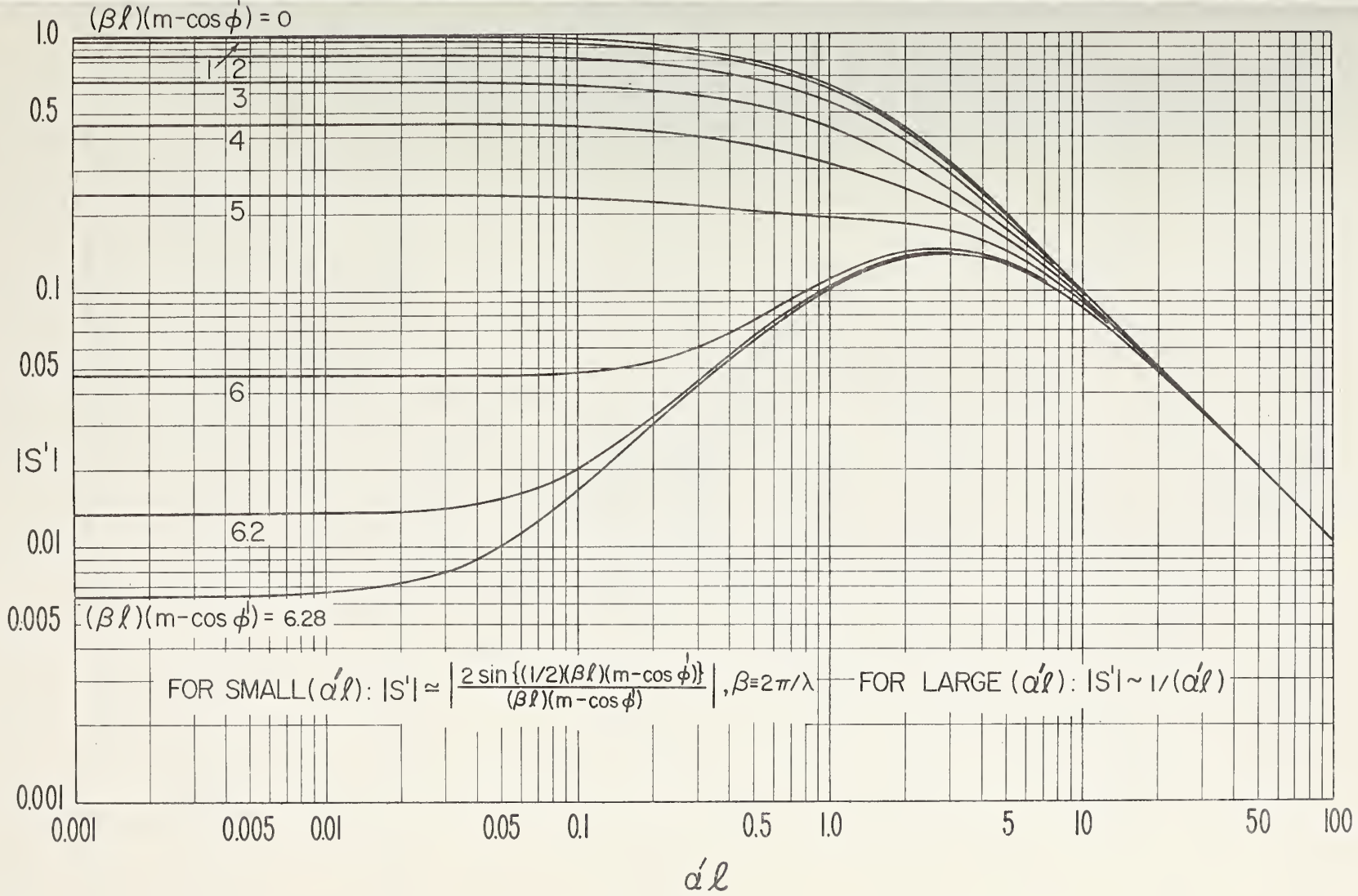

Figure 15. Pattern factor $|S'|$ for wave antenna of length ℓ and propagation constant $\Gamma = \alpha' + i\beta m$.

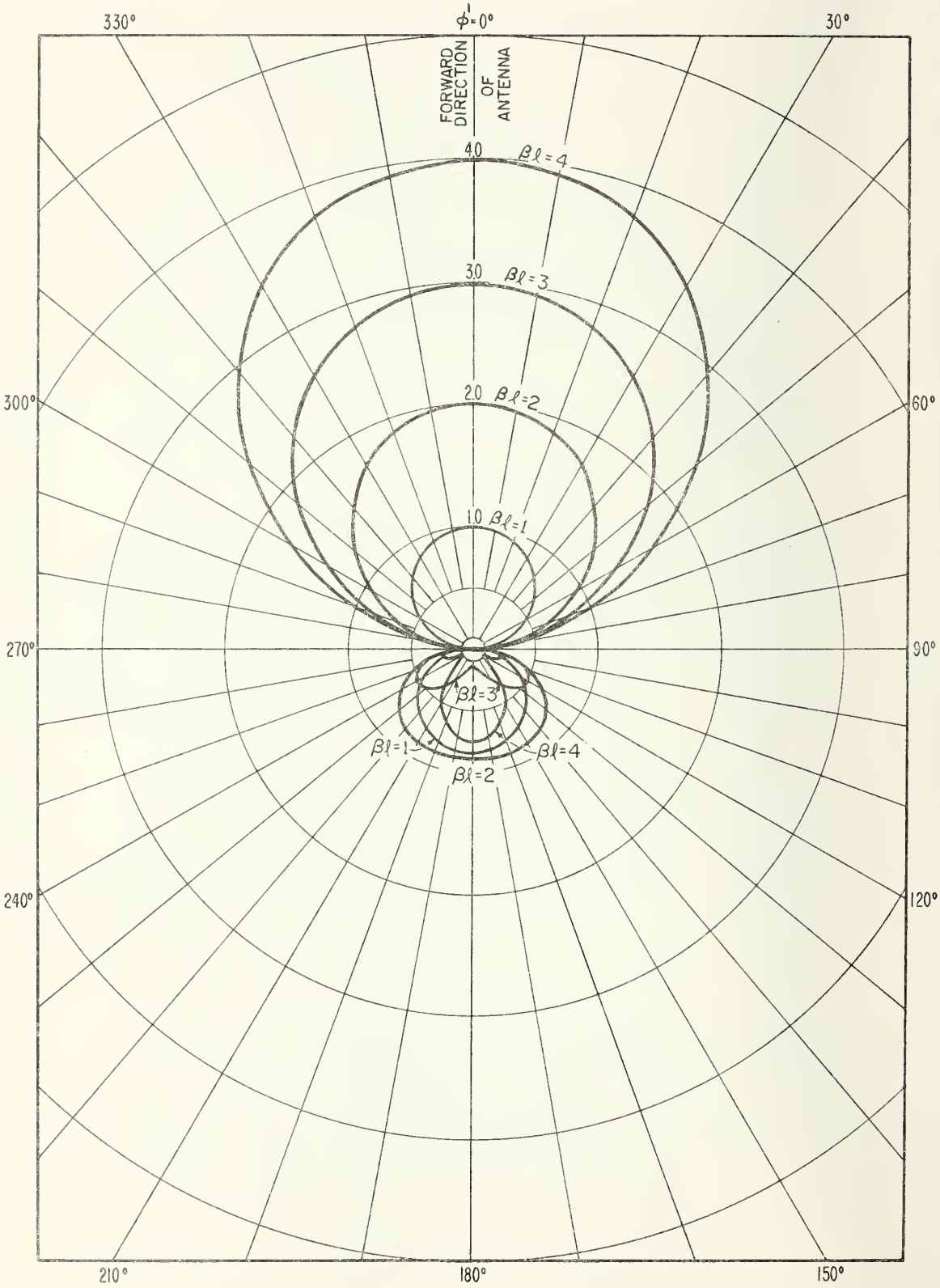

Figure 16. Wave antenna pattern $|S| = \beta\ell \cos\phi'$. $|S'|$ for $\alpha' = 0$, $m = 1$.

where I_o and y are respectively the current at and the distance from the feed point, an integration of the elements over the length of the antenna yields for the antenna pattern $|S|$:

$$|S| = |\beta b \cos\phi'| \cdot |S_1'|$$

$$= |x_3| \left[\frac{2\{\cosh x_1 - \cos(x_2 - x_3)\}}{x_1^2 + (x_2 - x_3)^2} \times \frac{2\{\cosh x_1 - \cos(x_2 + x_3)\}}{x_1^2 + (x_2 + x_3)^2} \times \frac{x_1^2 + x_2^2}{\cosh^2 x_1 - \cos^2 x_2} \right]^{1/2} , \quad (4.14)$$

where $x_1 = \alpha' b$, $x_2 = \beta b m$, and $x_3 = \beta b \cos\phi'$.

Graphs of (4.14) are shown in figure 17 for the case of $\alpha' = 0$, which corresponds to very poorly conducting ground. The values of $|S|$ shown on the figure, however, should be used only with antenna lengths ℓ such that the quantity $(\alpha' \ell)$ is very near zero; if this is not the case, $|S|$ should be calculated from (4.14). The center-fed wave antenna power gain corresponding to (4.12) is given by

$$\left(p_{wa}/p_{iso}\right) = |S|^2 \cdot |T_v|^2 \left(120 R_o / |Z_o|^2\right) , \quad (4.15)$$

where $|T_v|$, R_o, and Z_o have been defined previously.

The theoretical determination of L_t or L_r for a wave antenna in terms of its input resistance is quite difficult. However, considering these quantities essentially as power ratios measuring the effectiveness of the antenna, an estimate of their magnitude may be obtained from (4.12) by assuming that

$$L_{t,r} - G_{t,r} \simeq -10 \log\left(p_{wa}/p_{iso}\right) . \quad (4.16)$$

5. NOISE EFFECTS

The operating noise factor f [Norton, 1962] appearing in (2.4) provides a measure of the effects of noise on the receiving system (in previous papers [Vogler, 1963a, 1963b] f is called the effective noise figure). It is defined by

$$f \equiv [p_a/(k_B t_o b)]/[r(s/n)] , \quad (5.1)$$

where p_a is the signal power available from an equivalent loss-free receiving antenna, $(k_B t_o b)$ is a reference Johnson-noise power [see (2.3)], and $r(s/n)$ is the receiver predetection output signal-to-noise ratio.

Since p_a is the power available from a loss-free antenna, its relationship to the power available from the actual antenna, p_r, may be expressed as

$$p_a = \ell_c p_r , \quad (5.2)$$

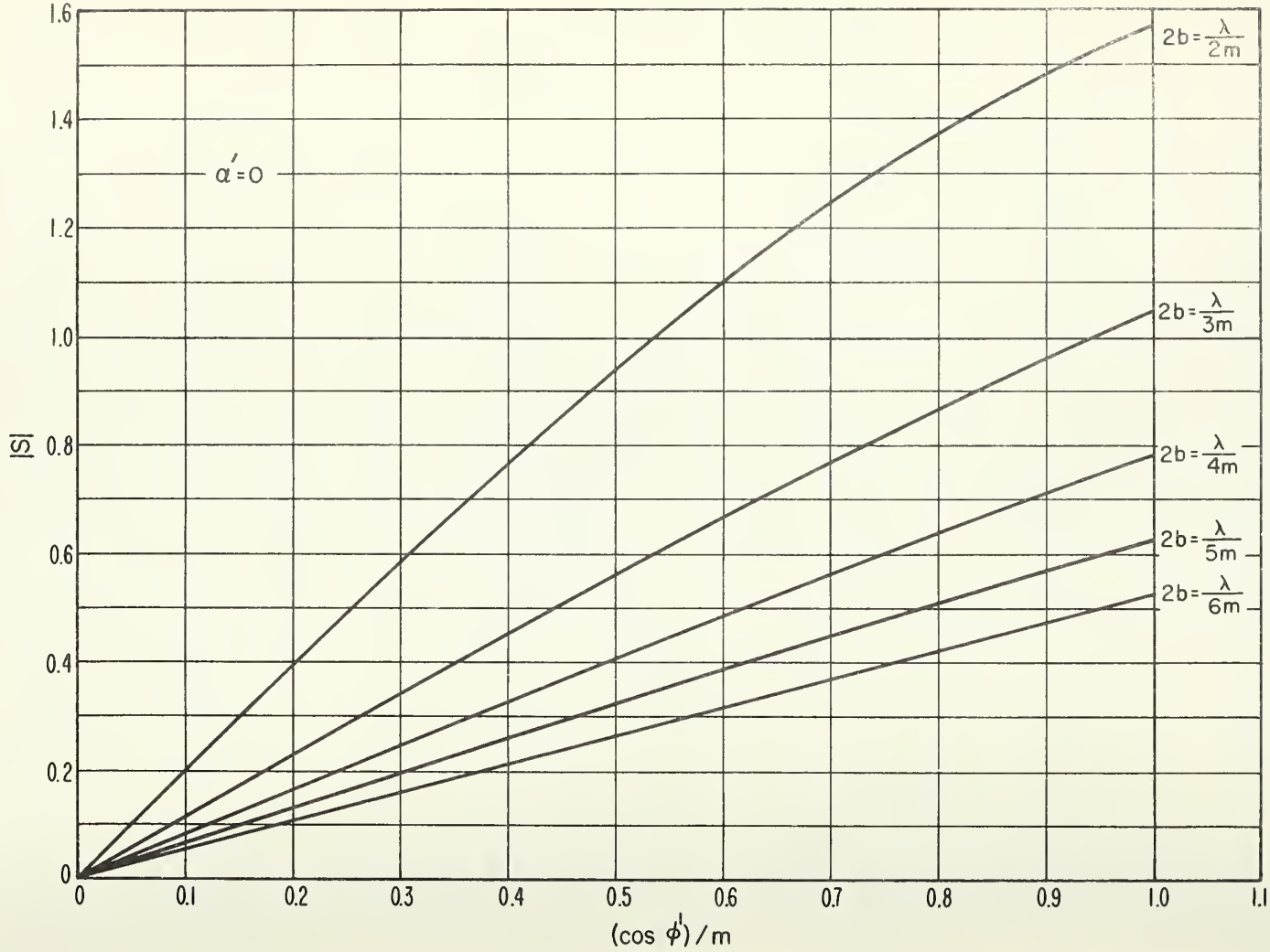

Figure 17. $|S|$ for center-fed antenna of length $\ell = 2b$ with $\alpha' = 0$.

where ℓ_c is the antenna circuit loss factor. Because the present study is primarily concerned with low antennas over poorly conducting ground, the assumption is made throughout that $\ell_c \simeq \ell_r$, where ℓ_r is the ground proximity loss discussed in section 4.

In terms of the noise factors of the receiving system's component parts, f can be expressed in the following form:

$$f = f_e - 1 + f_c + \ell_c (f_{t\ell} - 1) + \ell_c \ell_{t\ell} (f_r - 1) , \tag{5.3}$$

where f_e, f_c, $f_{t\ell}$, and f_r denote respectively the noise factors of the external noise, antenna circuit, transmission line, and receiver. In terms of the loss factors ℓ_c and $\ell_{t\ell}$ of the antenna circuit and transmission line (i.e., the ratio of the available input to output powers of the component), f_c and $f_{t\ell}$ are given by

$$f_c = 1 + (\ell_c - 1)(t_c/t_o), \quad f_{t\ell} = 1 + (\ell_{t\ell} - 1)(t_{t\ell}/t_o) , \tag{5.4}$$

where t_c and $t_{t\ell}$ designate the absolute temperatures of the corresponding components and t_o is a reference temperature.

Generally speaking, the factors f_e and f_c will predominate in calculating values of f, especially at the lower frequencies [Crichlow, Smith, Morton, and Corliss, 1955]; at high frequencies f depends more on $f_{t\ell}$ and f_r, which are best obtained by direct measurement. By arbitrarily assuming the transmission line loss to be negligible ($\ell_{t\ell} = 1$) and the antenna circuit temperature very near the reference temperature, (5.1) may be written as

$$f = f_e + \ell_c f_r - 1 , \quad \ell_{t\ell} = 1 , \quad t_c = t_o . \tag{5.5}$$

With the approximation $\ell_c \simeq \ell_r$, this then becomes

$$f \simeq f_e + \ell_r f_r - 1 , \tag{5.6}$$

where ℓ_r has been defined in section 4.

The principal sources of external noise received by an antenna located on the moon are (1) galactic or cosmic, (2) earth-based, and (3) solar. The amount of noise affecting the signal depends on the location, orientation, and directional gain of the particular antenna under consideration. Some preliminary studies [Page, 1962] of earth-based and solar noise components indicate that, in the case of a quiescent sun, solar noise is negligible compared with galactic noise unless the antenna beam is oriented directly toward the sun. On the other hand terrestrial atmospheric noise might become comparable to the galactic noise in the lower frequency range; however, this assumes a negligible ionospheric shielding effect.

Galactic noise levels have been fairly well established at the higher frequencies through earth-based measurements. Figure 18 shows an estimate of the external noise factor $F_e = 10 \log f_e$ obtained from galactic noise data compiled by Menzel [1961] and by Hartz [1963]; the reference

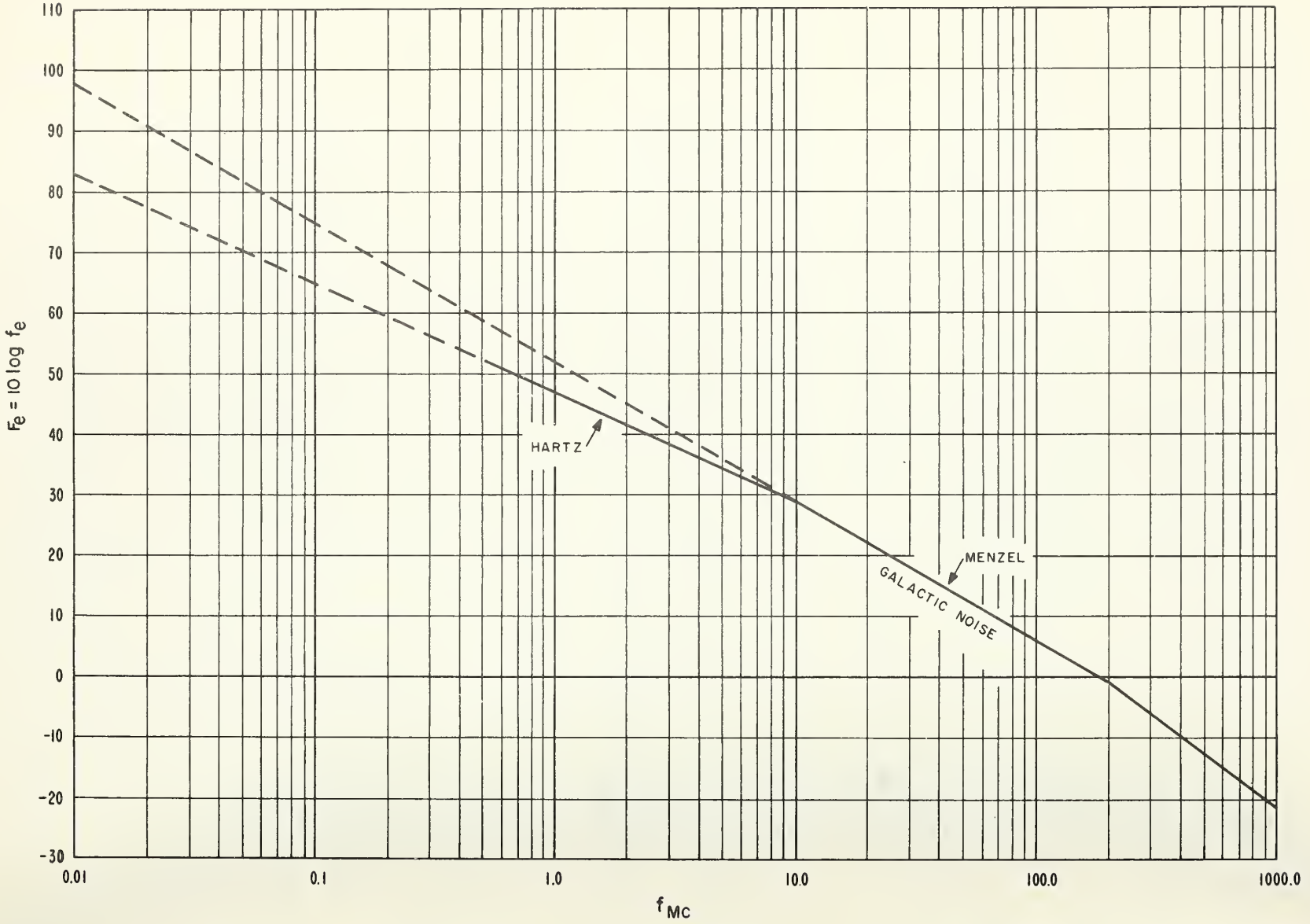

Figure 18. External noise factor, F_e, considering galactic noise only.

temperature assumed here is $t_o = 288.37^\circ K$. Empirical expressions used to plot the galactic noise curve are

$$f_e = 6.467 \times 10^6 f_{mc}^{-3}, \quad f_{mc} \geq 200,$$
$$f_e = 1.585 \times 10^5 f_{mc}^{-2.3}, \quad 10 \leq f_{mc} \leq 200, \tag{5.7a}$$

from the Menzel data, and

$$f_e = 5.012 \times 10^4 f_{mc}^{-1.8}, \quad 0.5 \leq f_{mc} \leq 10, \tag{5.7b}$$

from the Hartz data obtained from Topside Sounder measurements. The upper and lower dashed lines on the figure are extrapolations of the $f_{mc}^{-2.3}$ and $f_{mc}^{-1.8}$ frequency variations.

It is physically apparent that at some lower frequency the galactic noise curve will at least level off. Until information from low frequency measurements are available, the extrapolations of figure 18 may be used to provide (hopefully pessimistic) estimates of galactic noise.

6. POSSIBLE IONOSPHERIC EFFECTS

At the present time there is no indication that the moon possesses a neutral atmosphere of any significant magnitude. Because of this, it is unlikely that lunar surface propagation will be affected by ionospheric considerations to the same extent as terrestrial propagation. However, studies have been made showing the possible existence of a weak lunar ionosphere caused by solar wind. This section will discuss briefly the effect on propagation of two forms of possible ionospheres.

If a negligible magnetic field is assumed and the motion of heavy ions is neglected, the ionosphere may be characterized by its index of refraction N_i as follows:

$$N_i^2 = \left\{ 1 - \frac{f_{cr}^2}{f_{mc}^2 + f_\nu^2} \right\} - i \left\{ \frac{f_\nu f_{cr}^2}{f_{mc}\left(f_{mc}^2 + f_\nu^2\right)} \right\}, \tag{6.1}$$

where f_{mc} denotes the signal frequency, f_ν the collision frequency, and f_{cr} the critical or plasma frequency, all measured in Mc/s. In terms of the electron density/cm^3, n, the critical frequency is given by

$$f_{cr}^2 \simeq 8.1 \times 10^{-5} n, \tag{6.2}$$

where, in general, n is a function of the height h above the ground: $n = n(h)$.

One form of ionosphere that may possibly occur extends from the moon's surface to some distance above, the electron density decreasing with height. Elsmore [1957], using studies of lunar occultation of the Crab Nebula, has hypothesized surface electron densities on the order of 10^3 to 10^4 electrons/cm^3. For signal frequencies near or less than the collision frequency, this ionospheric model presents a propagation problem which, as far as the author is aware, has never

been investigated and is beyond the scope of the present paper. Considerable theoretical study would be necessary to determine propagation characteristics at these low frequencies.

For radio frequencies such that $f_\nu/f_{mc} << 1$, an estimate of the effect of a surface ionosphere on propagation at frequencies greater than the plasma frequency may be obtained through the concept of effective radius [Burrows and Atwood, 1949]. The effective radius, r_e, introduces a correction to the actual radius, r_o, that allows for the refraction of the radio wave as it travels through the medium (in this case the model ionosphere) above the ground. Expressed in terms of an effective radius factor k [Wait, 1961]:

$$k = \frac{r_e}{r_o} = \left[1 + \frac{r_o N_i'(h=0)}{N_i(h=0)} \right]^{-1} , \tag{6.3}$$

where $N_i'(h=0)$ denotes the gradient of the refractive index with respect to height evaluated at the surface.

With the restriction that $f_\nu/f_{mc} << 1$, (6.1) may be rewritten as

$$N_i^2 \simeq 1 - f_{cr}^2/f_{mc}^2 = 1 - 8.1 \times 10^{-5} n(h)/f_{mc}^2 , \tag{6.4}$$

and k then becomes

$$k \simeq \left[1 + \frac{4.05 \times 10^{-5} r_o \{-n'(0)\}}{N_i^2(0) \cdot f_{mc}^2} \right]^{-1} \simeq \left[1 + \frac{0.07 \{-n'(0)\}}{f_{mc}^2 - 8.1 \times 10^{-5} n(0)} \right]^{-1} , \tag{6.5}$$

where $n(0)$ is the electron density/cm^3 at the surface and $n'(0)$ is the electron density gradient with respect to height in km evaluated at the surface. It can be seen that (6.5) may be used only for radio frequencies such that

$$f_{mc} > f_{cr} = 9 \times 10^{-3} \sqrt{n(0)} ;$$

thus, for an electron density at the surface of, say, $n(0) = 10^4$, the effective radius concept should be restricted to frequencies of 1 Mc/s or greater.

The curves of figures 9 - 14 will now provide estimates of the attenuation A_t if they are read as functions of a modified x_o', $x_o'(k)$, and a modified $K_{h,v}$, $K_{h,v}(k)$, where

$$x_o'(k) = k^{-\frac{2}{3}} f_{mc}^{\frac{1}{3}} d_o(km) , \quad K(k) = 3.02 \times 10^{-2} k^{-\frac{1}{3}} / |T| \cdot |Q| \cdot f_{mc}^{\frac{1}{3}} , \tag{6.6}$$

and k is given by (6.5). Notice that $x_o'(1)$ and $K(1)$ are simply those parameters discussed in section 3 and defined by (3.5) and (3.1); the effective radius factor k does not modify $b_{h,v}^\circ$.

To show the variation of k with frequency, (6.5) is plotted in figure 19 for several values of the surface electron density gradient n'(0). The values chosen do not represent any experimental evidence but are used merely to show the variation of k with the gradient. Figure 19 shows that, as the gradient becomes more negative, k decreases and, in general, a higher attenuation of the signal is to be expected. Should a positive gradient exist, less attenuation of the signal would occur.

Another possible lunar ionosphere that has recently been investigated [Weil and Barasch, 1963] is similar in form to the terrestrial ionosphere. Weil and Barasch, through theoretical considerations of solar wind influence near the moon together with solar stream data, postulate an ionized elevated layer with an electron density of about $350/cm^3$ at 0.6 lunar radii above the surface. The layer occurs only in the general direction of the sun, and their numerical values are based on quiet sun data.

The theory of this form of ionospheric propagation is well established and, given the necessary data, will provide good estimates of propagation capabilities. The remainder of the section will discuss briefly the simple geometrical-optics approximation to ionospheric propagation. A detailed account of the subject is contained in a paper by Wait [1962 c].

In the geometrical-optics approximation, the field at a point is considered to be the sum of multiply-reflected radio rays arriving from the transmitting source, the reflections occurring between the ground surface and the ionosphere. At distances less than its caustic, the single hop component of the field, i.e., the ray undergoing only one reflection from the ionosphere, will be the most significant. However, the total field is given by the sum of all the rays added together in proper phase; at short distances from the transmitting antenna, the ground wave component must also be included.

In order to gain some idea of the effect on lunar propagation of an elevated ionosphere, the attenuation of the single-hop sky wave is evaluated, assuming the Weil and Barasch model ionosphere with a sharp lower boundary. The assumption of a sharp boundary rather than a more realistic one will give a lower estimate of the attenuation than is actually obtainable, but will still provide a reasonable estimate for the purposes of the present study. Letting $\theta(=d_o/r_o)$, $\rho(=h/r_o)$, ϕ_g, and ϕ_i denote the geometrical quantities indicated in figure 20, the sky wave attenuation A_s may be expressed as

$$A_s \sim -20 \log \left[\left(\frac{C \sin^2 \phi_g}{2\theta_1/\theta} \right) |1 + R_g|^2 \cdot |R_i| \right] , \tag{6.7}$$

where R_g and R_i are Fresnel reflection coefficients of the ground and ionosphere respectively:

$$R_g = \frac{N_g^2 \cos \phi_g - \sqrt{N_g^2 - \sin^2 \phi_g}}{N_g^2 \cos \phi_g + \sqrt{N_g^2 - \sin^2 \phi_g}}, \quad N_g^2 = \epsilon_g - i s_g , \tag{6.8}$$

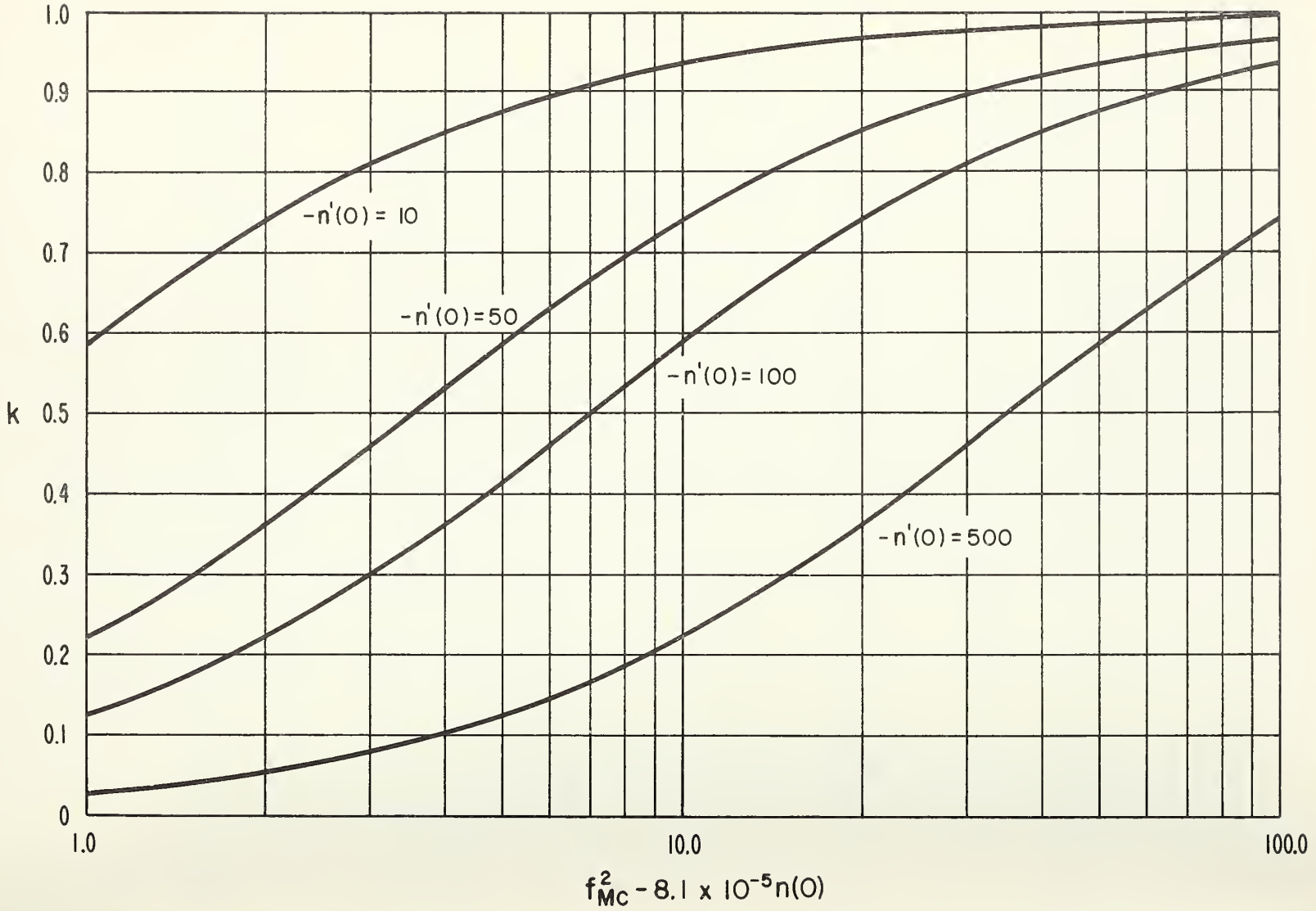

Figure 19. Effective radius factor k as a function of the surface electron density gradient, $n'(0)$.

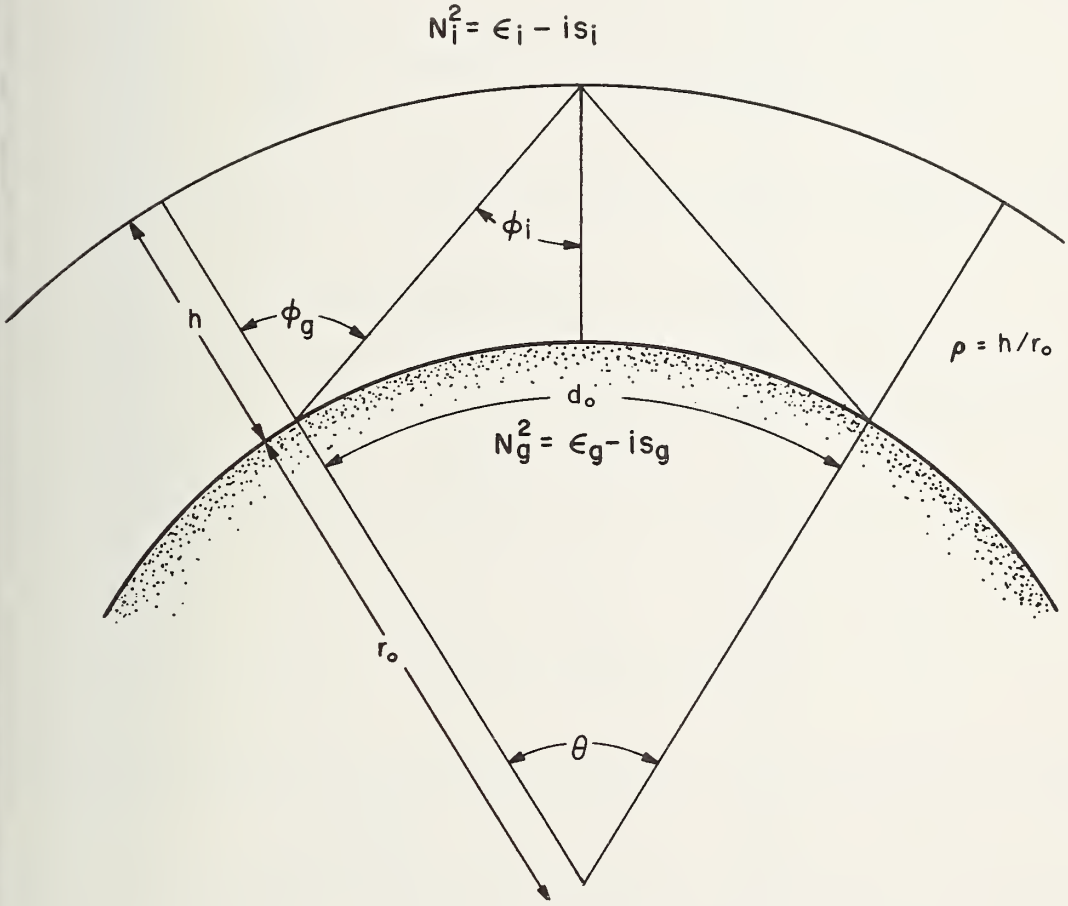

Figure 20. Geometry for single-hop sky wave propagation.

$$R_i = \frac{N_i^2 \cos\phi_i - \sqrt{N_i^2 - \sin^2\phi_i}}{N_i^2 \cos\phi_i + \sqrt{N_i^2 - \sin^2\phi_i}} , \qquad N_i^2 = \epsilon_i - i\, s_i , \tag{6.9}$$

and the angles ϕ_g and ϕ_i may be calculated from

$$\phi_g = \tan^{-1}\left[\frac{(1+\rho)\sin(\theta/2)}{(1+\rho)\cos(\theta/2) - 1} \right], \qquad \phi_i = \sin^{-1}\left[\frac{\sin\phi_g}{1+\rho} \right] . \tag{6.1}$$

The quantity C in (6.7) is a convergence coefficient defined by

$$C = \left[\frac{1+\rho}{\cos(\theta/2)} \right] \left[1 + \frac{\sin^2(\theta/2)}{(1+\rho)\cos(\theta/2) - 1} \right]^{1/2} , \tag{6.1}$$

and θ_1 is related to the total distance traversed by the ray:

$$\theta_1 = \sqrt{\rho^2 + 4(1+\rho)\sin^2(\theta/4)} . \tag{6.1}$$

Notice that (6.11) [and therefore (6.7)] is valid only as long as

$$\theta < \theta_c = 2\cos^{-1}[1/(1+\rho)] .$$

θ_c corresponds to the distance at which a caustic is encountered, and other formulas must be used to calculate the attenuation in this region. The distances considered here will be only those such that $\theta << \theta_c$.

At VLF and for the distances of interest, the reflection coefficient of the ground R_g is near unity even for the very poorly conducting ground expected on the moon. On the other hand, the ionospheric reflection coefficient R_i can have a pronounced effect on propagation estimates. Figure 21 shows a plot of $|R_i|$ as a function of the ionosphere height $\rho = h/r_o$ and

$$s_i = f_\nu f_{cr}^2 / f_{mc}\left(f_{mc}^2 + f_\nu^2\right)$$

obtained from (6.1). Notice that $|R_i|$ depends quite critically on the parameter ϵ_i and, hence, on estimates of n and f_ν. If an elevated lunar ionosphere does exist, data concerning these quantities are necessary for VLF propagation predictions. The purely geometric factor

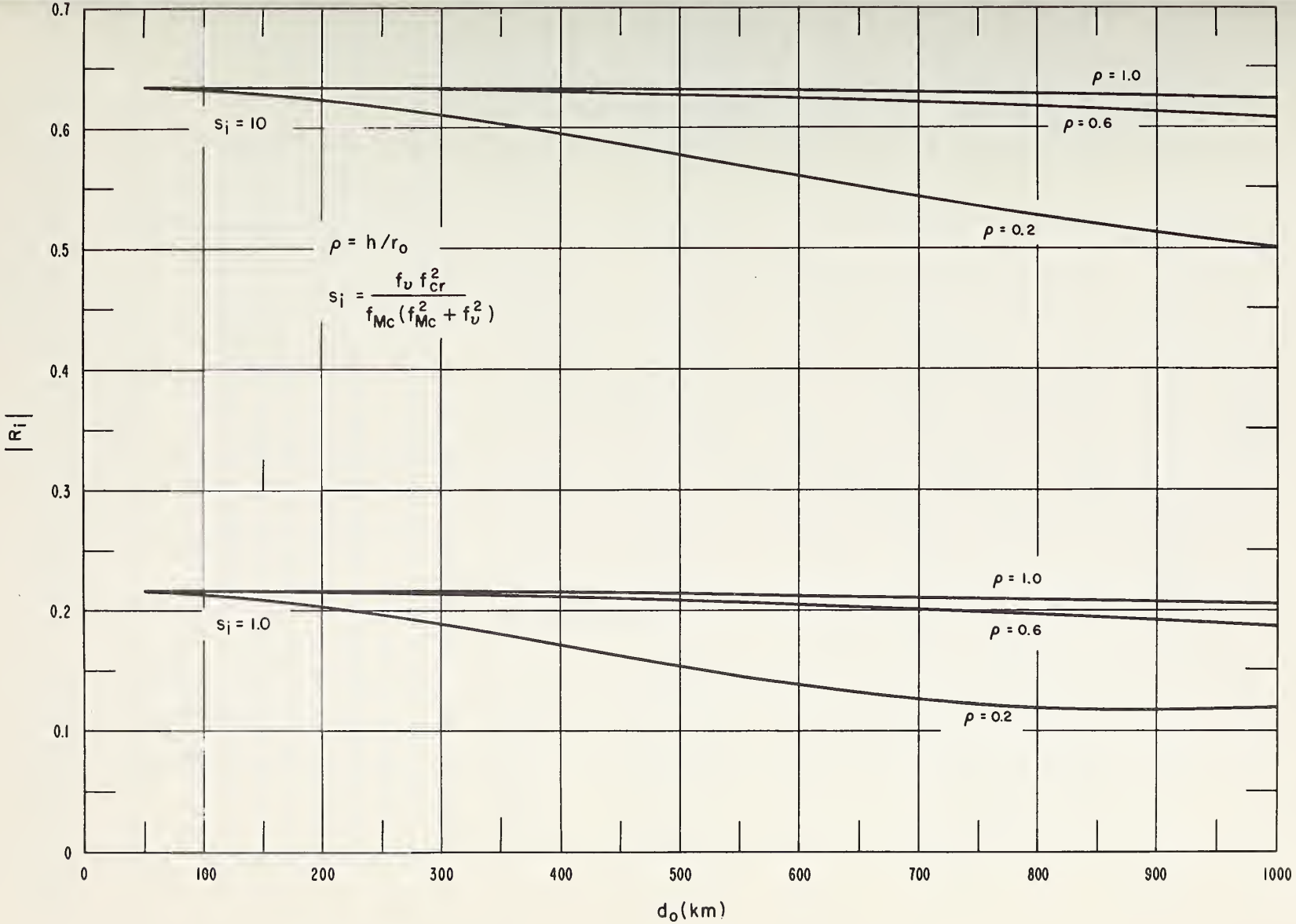

Figure 21. Magnitude of the ionospheric reflection coefficient, $|R_i|$.

$$\left(C \sin^2 \phi_g\right) \Big/ \left(2\, \theta_1 / \theta\right)$$

appearing in (6.7) depends only on the distance d_o between the transmitting and receiving points and on the height of the ionosphere; curves of this factor are presented in figure 22 for various values of ρ.

The attenuation A_s of a single-hop sky wave relative to a free space inverse distance field is shown in figure 23 as calculated from (6.7). For these curves the ground is described by $N_g^2 = 2 - i\ 180$, and the ionosphere at a height $\rho = 0.6$ is described by $N_i^2 = 1 - i\, s_i$, where s_i assumes the values 1 and 10. At a radio frequency of $f_{mc} = 0.01$, for example, the curves would be valid for a ground conductivity $\sigma_g = 10^{-4}$ mhos/m and an ionosphere described by two values of the ratio $(n/f_\nu) \simeq 125$ and $(n/f_\nu) \simeq 1250$; the latter values assume $f_\nu >> f_{mc}$. The dashed curves in the figure show the vertically polarized ground wave attenuation A_t for $f_{mc} = 0.01$ and 0.1; this component of the field is dominant at the shorter distances. It can be seen that over the range of distance shown, the difference in attenuation between the two sky wave curves is about 10 db, this difference arising from the ionospheric reflection coefficient R_i. A change in ground constants at VLF produces very little difference in attenuation for a given s_i.

According to Weil and Barasch [1963] the ionosphere would exist (with any appreciable magnitude) only within about 60° from the sun-moon line; thus, it would not be a dependable mechanism for long-term propagation. It should be remembered, however, that it could occasion interference effects in VLF ground wave communication circuits at those distances where the ground wave and sky wave components are comparable in magnitude.

7. CALCULATION OF REQUIRED POWER

Attempts have been made recently to deduce the electromagnetic properties of the moon's surface material through the use of radar data [Senior and Siegel, 1960]. Although differences exist concerning the exact interpretation of the data [Brown, 1960; Daniels, 1961], there is general agreement that the relative permittivity is not far above unity and that the conductivity is quite low. In any case, most of the graphs discussed in the preceding sections are applicable to a wide range of values of ϵ_r and σ.

Senior and Siegel estimate the relative dielectric constant and conductivity of lunar surface material to be $\epsilon_r = 1.1$ and $\sigma = 3.4 \times 10^{-4}$ mhos/m. Materials constituting the earth's crust have been found with conductivities of this order, but not with such a low permittivity. For the purpose of arriving at some estimate of lunar propagation conditions, it will be assumed that ϵ_r ranges from 1.1 to 2.0 and σ lies between 10^{-3} and 10^{-4} mhos/m.

By choosing a reference temperature $t_o = 288.37^\circ$ K (as in section 5), the required power given by (2.4) may be rewritten as

$$P_t = L_p - (G_t + G_r) + L_t + R + F + B - 204 \qquad (7.1)$$

where the propagation loss L_p for ground wave attenuation between isotropic antennas is given by

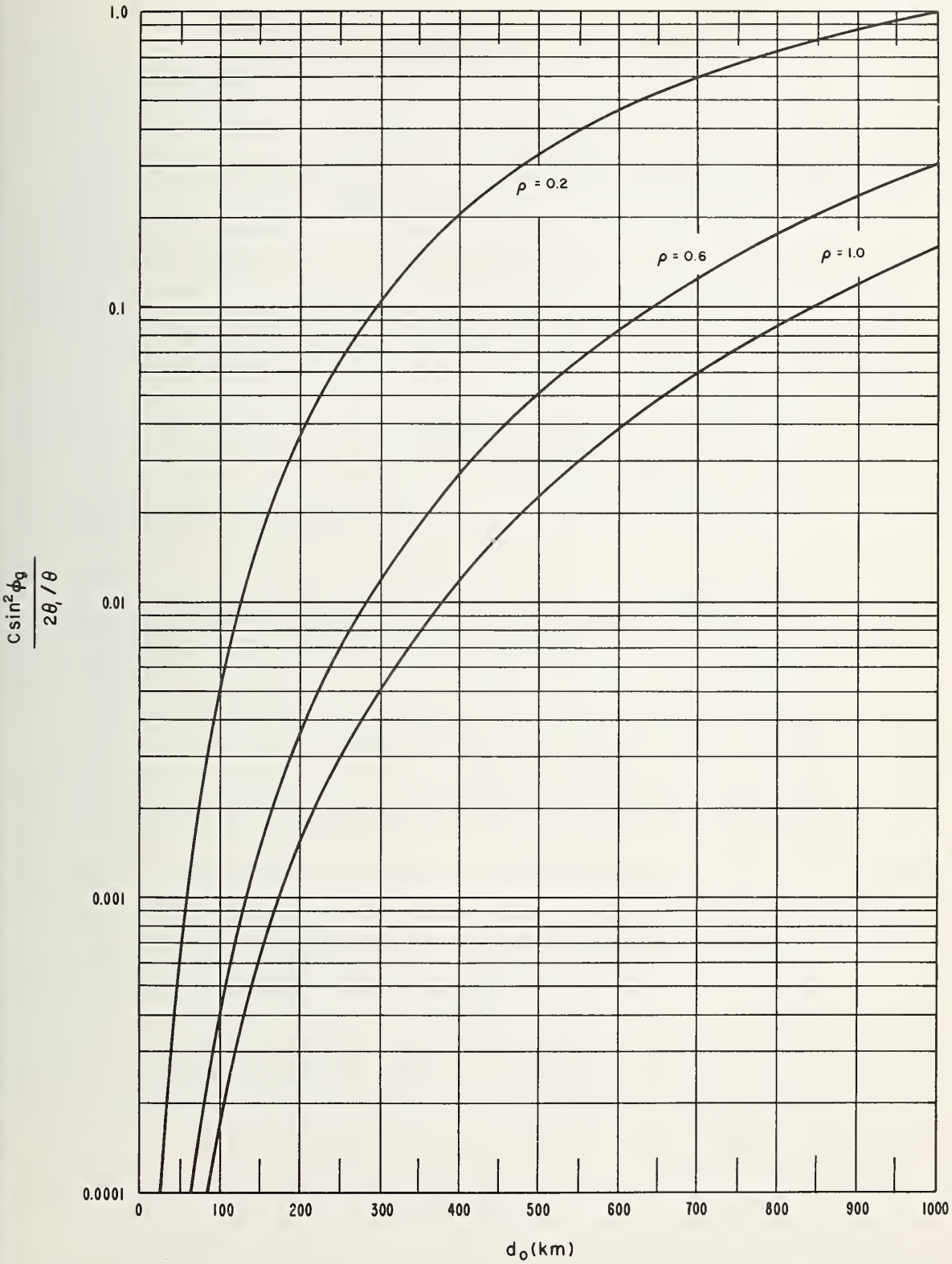

Figure 22. The geometric factor, $(C \sin^2 \phi_g)/(2\theta_1/\theta)$, for use in (6.7).

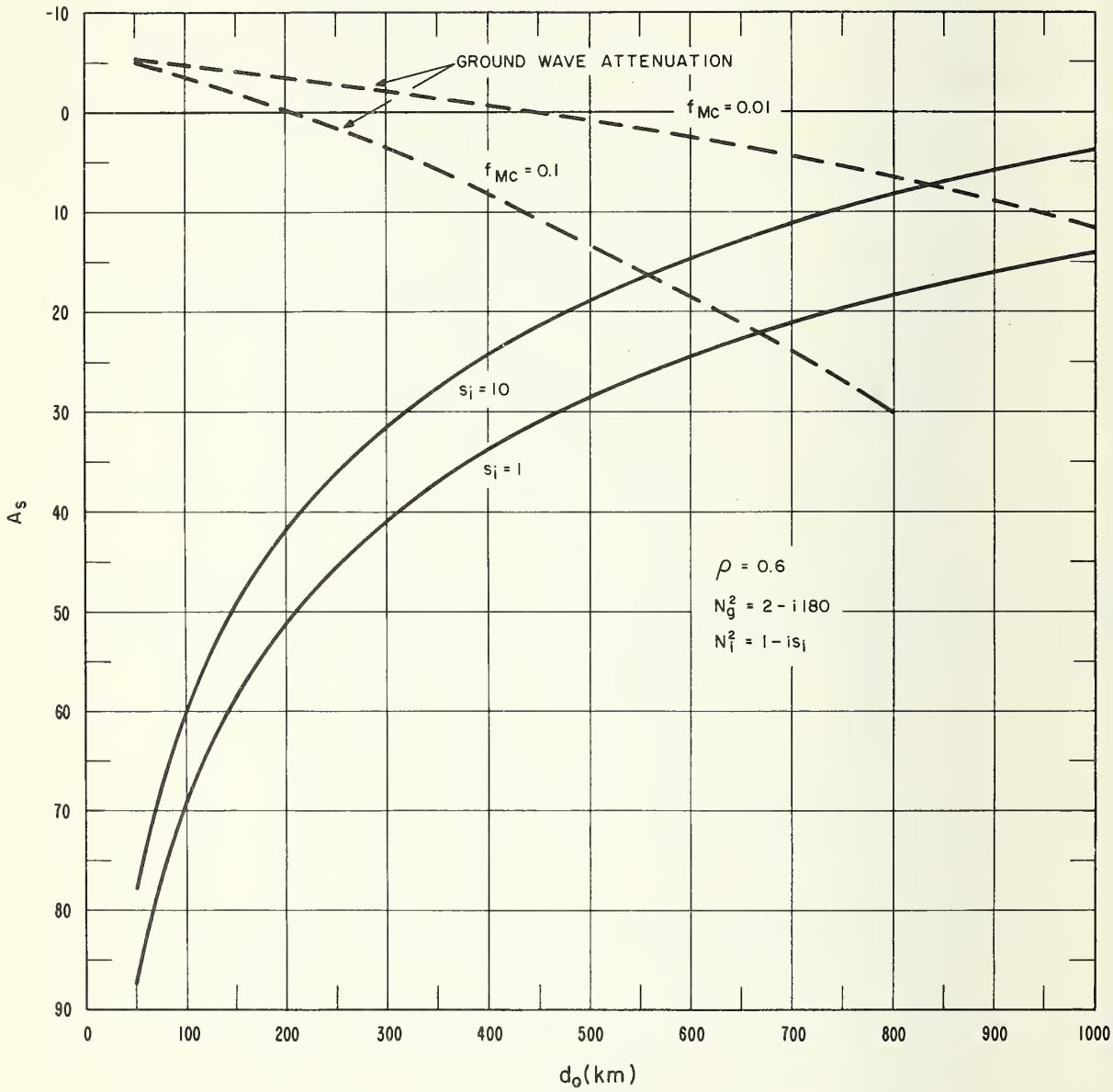

Figure 23. Single-hop sky wave attenuation A_s.

$$L_p = 32.45 + 20 \log d_o(\text{km}) + 20 \log f_{mc} + A_t \ . \qquad (7.2)$$

For sky wave propagation, L_p would be calculated by (7.2) after replacing A_t by the A_s discussed in section 6.

Figure 24 shows curves of L_p for a vertically polarized ground wave over homogeneous ground as a function of frequency and distance. Values of A_t were obtained from figures 11 through 14 by linear interpolation in both the K_v and b_v° directions, K_v being given by figure 2 and (3.1) with $|Q_v| = 1$, and b_v° being read from figure 4. Notice that L_p varies inversely with conductivity at the lower frequencies, while at high frequencies the effect of σ variation becomes negligible.

To show the use of (7.1) in estimating required power for a particular communication system, the following example will be considered. Assume a communication system consisting of a wave antenna lying on the moon's surface and transmitting towards a short vertical electric dipole placed some distance away and in an optimum direction from the transmitter ($\phi' \simeq 0^\circ$). An estimate of $L_t - G_t$ may be obtained from (4.16) and (4.12) by assuming the free space value for the wave antenna characteristic impedance:

$$|Z_o| \simeq R_o \simeq 120\pi \ .$$

For the case of an antenna of length $\ell = \lambda/4$, $L_t - G_t$ is plotted versus frequency in figure 25. Again, the antenna loss varies noticeably with conductivity at the lower frequencies, but not at the higher ones.

A comparison of figure 18 and figures A-1 and A-2 shows that for a dipole at a height of, say, $h = \lambda/16$ the external noise tends to "blanket out" the effect of the antenna circuit loss. This is shown in figure 26, which is a plot of the operating noise factor as given by (5.6) with an assumed receiver noise factor of $f_r = 4$. Now by using figures 24, 25, and 26, and the dipole gain of $G_r = 1.76$, the required power delivered to the transmitting antenna terminals for a given type of service may be estimated from (7.1). Figure 27 shows values of $P_t - (R+B)$ as a function of frequency for antenna separation distances of 10, 100, and 500 km.

To estimate the required power delivered to the terminals of the transmitting antenna, the type of communication service desired must be designated, thus specifying R and B. For example, with standard broadcast service and a bandwidth of 10 kc/s, R may have the value 39 db [CCIR, 1951] and B = 40 db so that 79 db should be added to the curves of figure 27 to obtain the required power in decibels above 1 watt. Thus the power required for this type of service in the example system at a range of 10 km and for a frequency of 300 kc/s would be about 10 db or 10 w. For a low-grade voice communication service and 6 kc/s bandwidth, R = 9 db [CCIR, 1951], B = 38 db, and 47 db would be added to the curves. The required power in this case at a distance of 100 km and for a frequency of 100 kc/s would be about 16 w.

If fixed wave antenna lengths and dipole heights are considered, rather than the variable lengths and heights assumed for figure 27, ground proximity loss curves may be recalculated from the equations and graphs of section 4 and required power estimates obtained from (7.1). Figure 28

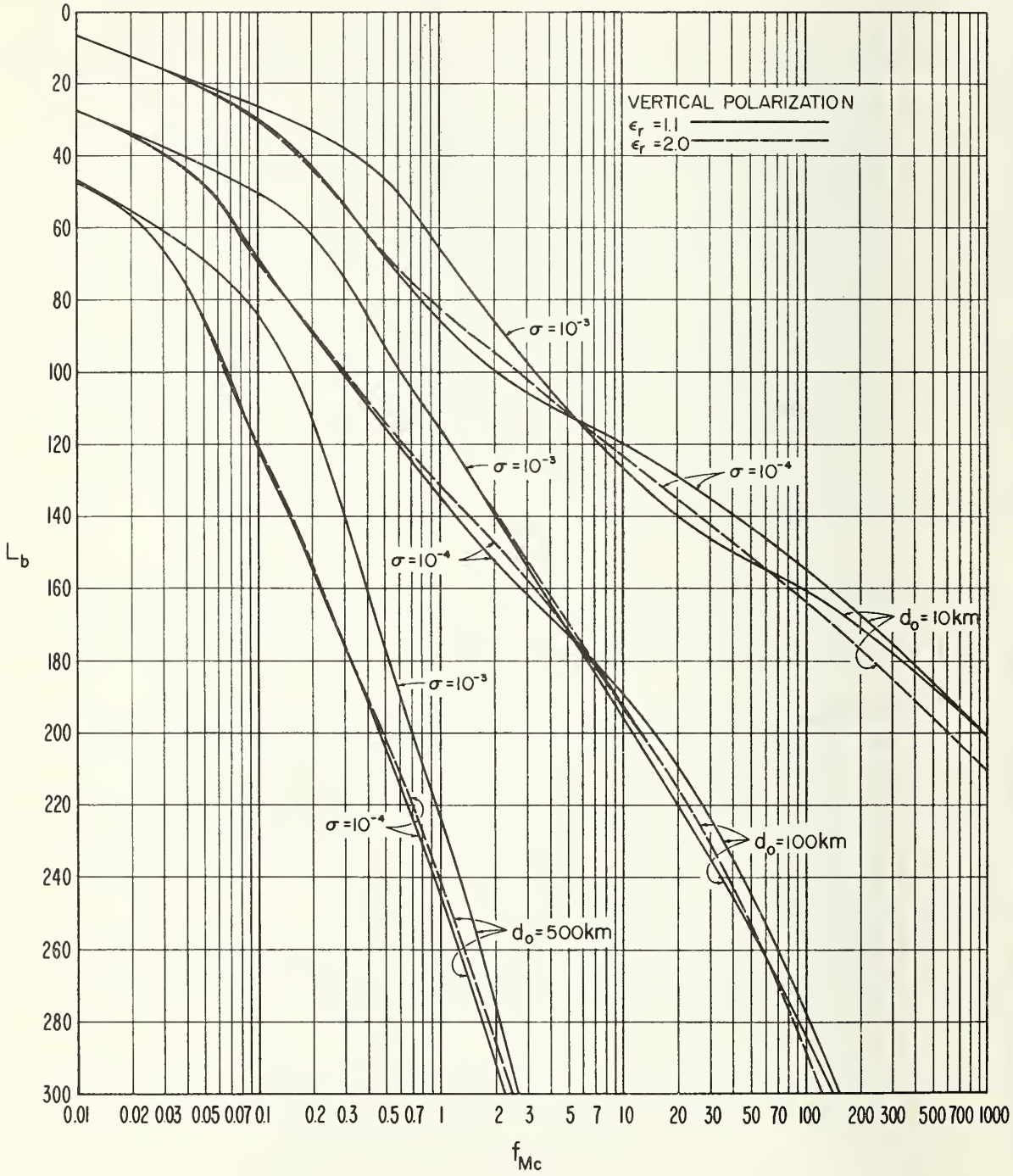

Figure 24. L_b for vertically polarized ground waves over homogeneous ground.

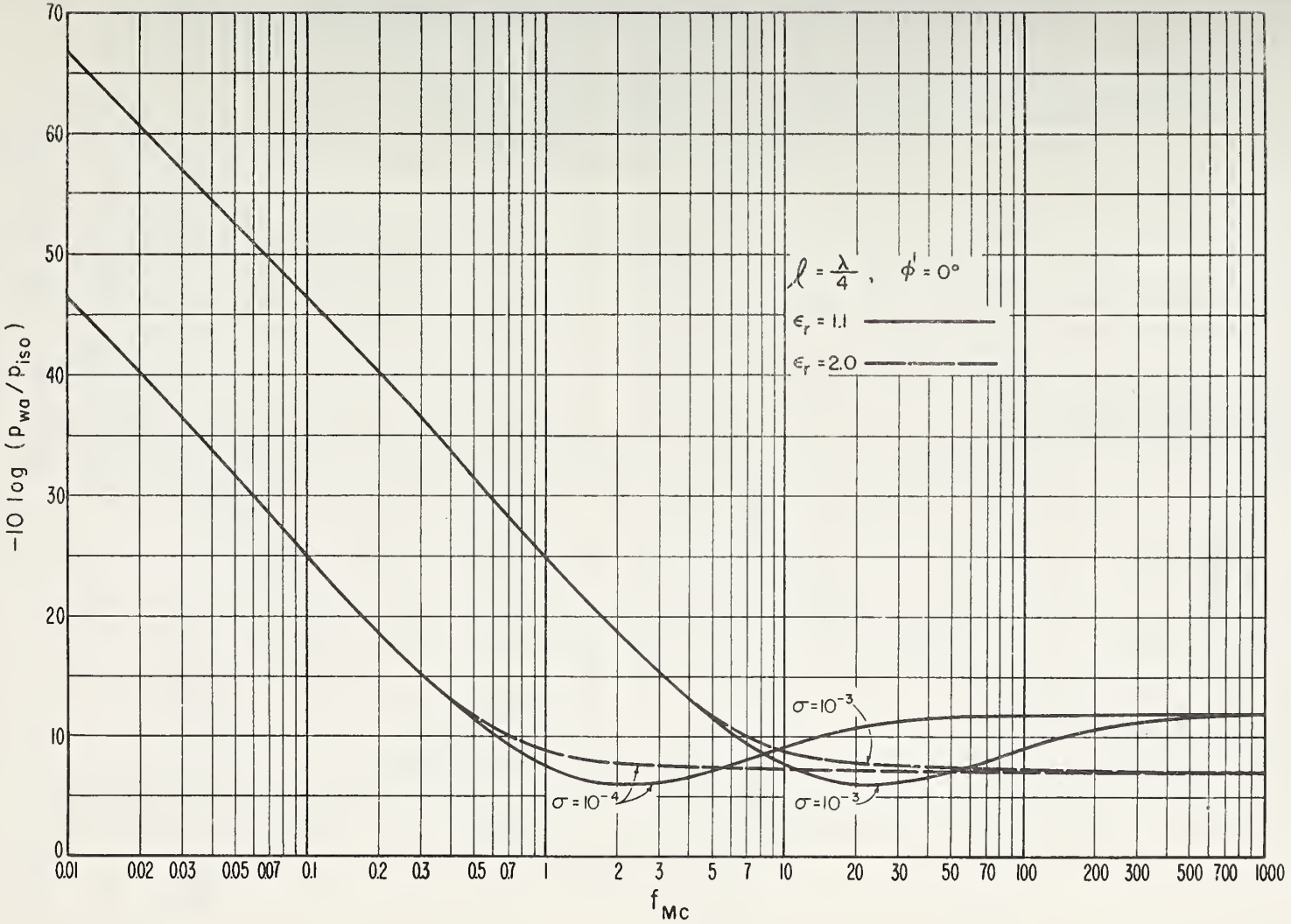

Figure 25. Estimates of $L_t - G_t$ for a wave antenna of length $\ell = \lambda/4$ lying on the ground.

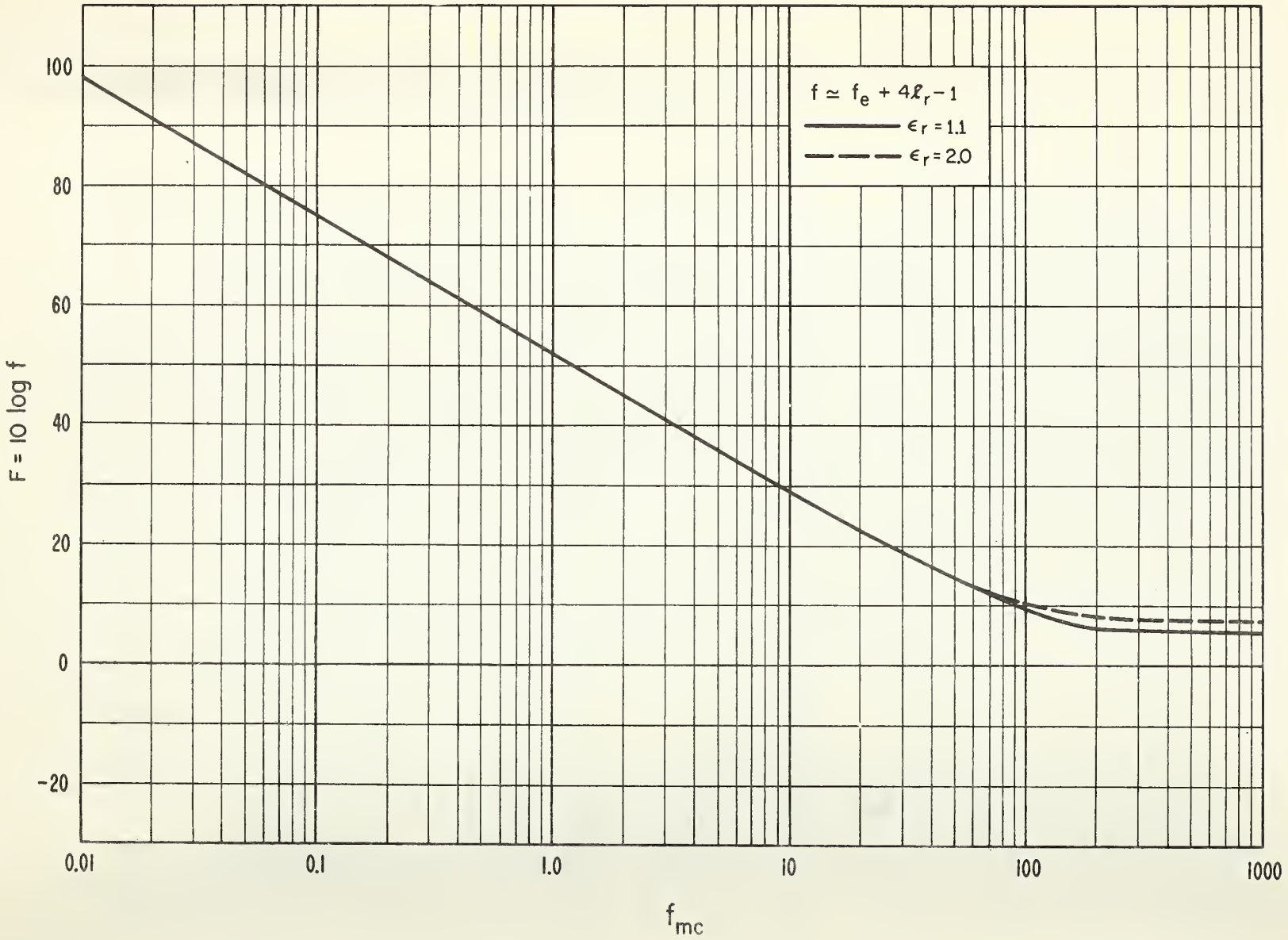

Figure 26. Operating noise factor F using (5.6) and assuming VED at a height h = λ/16.

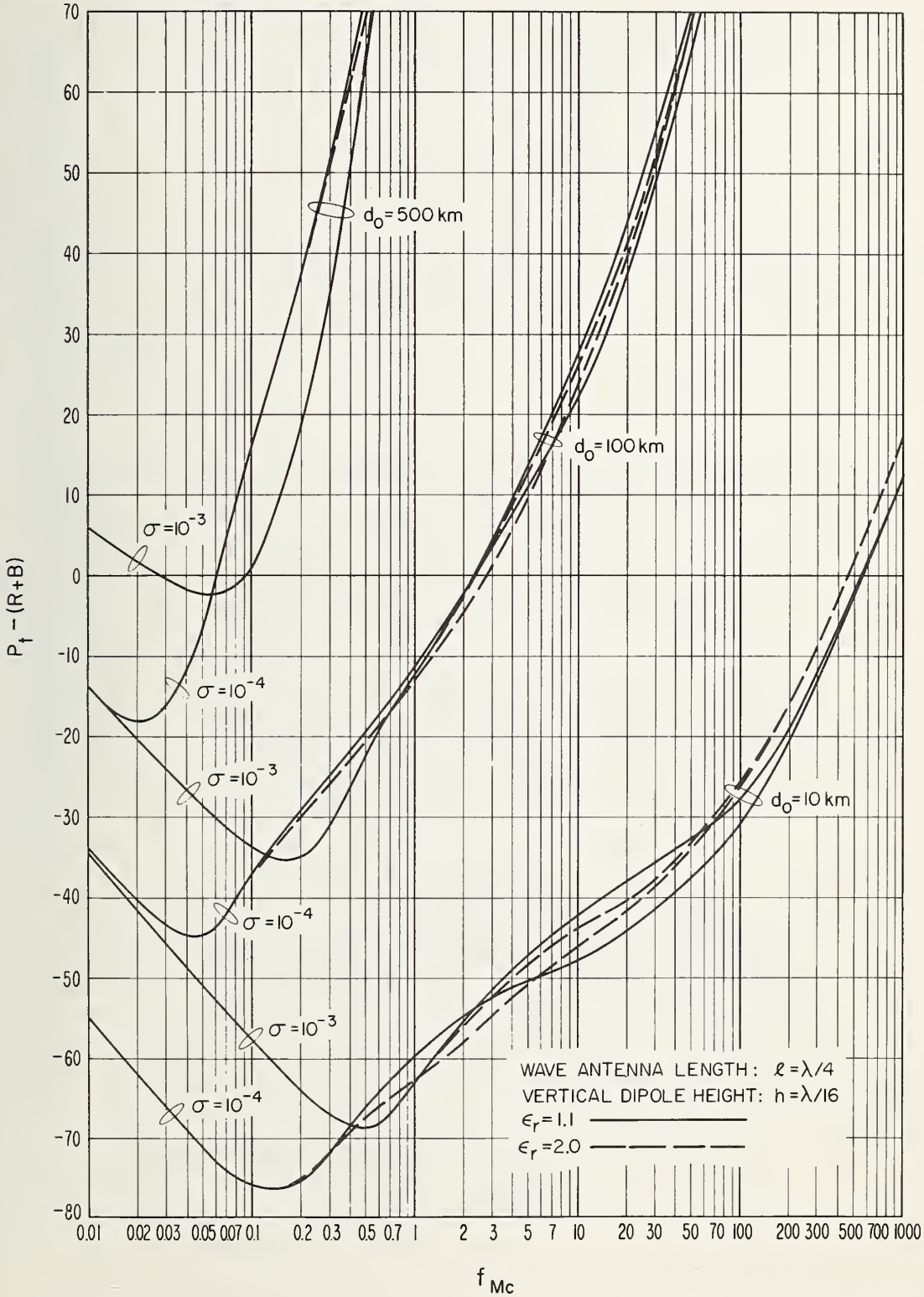

Figure 27. $P_t - (R+B)$ for wave antenna and vertical dipole over homogeneous ground.

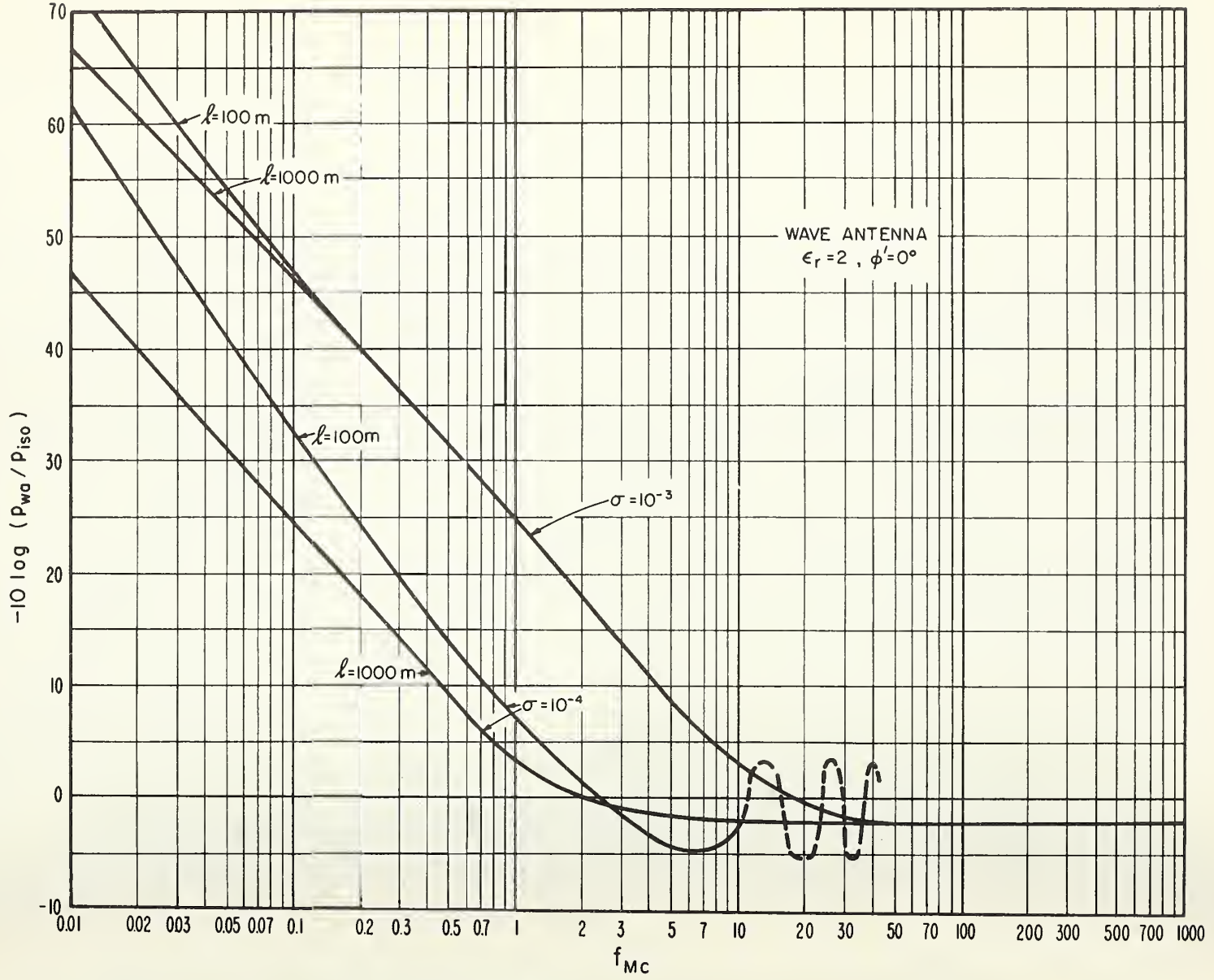

Figure 28. Estimates of L_t - G_t for a wave antenna of fixed lengths ℓ= 100 m and 1000 m.

shows a plot of the quantity $L_t - G_t$ for fixed wave antenna lengths of $\ell = 100$ m and 1000 m and ground conductivities of $\sigma = 10^{-3}$ and 10^{-4} mhos/m with $\epsilon_r = 2$. It can be seen that, at the lower frequencies, the loss associated with the 1000 m antenna is about the same as that shown in figure 25; however, a higher loss occurs at the lower frequencies if the 100 m length wave antenna is used.

The ground proximity loss for a short vertical electric dipole at fixed heights $h = 10$ m and 100 m is shown in figure 29 for the same ground constants assumed in figure 28. As before, the extrapolated values of the external noise factor of figure 18 will tend to override the dipole loss at the lower frequencies, but it should be emphasized that this loss will contribute significantly to the calculation of f at low frequencies if future measurements show f_e to be considerably lower than the extrapolated values assumed here.

Using figures 24, 26, and 28, the quantity $P_t - (R+B)$ is shown in figure 30 for the case of a wave antenna of length $\ell = 100$ m transmitting in the optimum direction towards a short vertical electric dipole at a height $h = 10$ m. For the example of standard broadcast service used previously, the required power P_t at a range of 10 km and for a frequency of 300 kc/s would be about 12 db or 16 w. For the low-grade voice communication service the required power at a distance of 100 km and for a frequency of 100 kc/s would be about 30 w. At high frequencies the estimates of P_t shown in figure 30 will be somewhat pessimistic, since a small height gain effect will occur due to the height of the dipole. Graphs for calculating this effect may be obtained from another paper [Vogler, 1964].

The combination of a wave antenna and dipole and the particular lengths and heights used in the preceding example were arbitrarily chosen. As pointed out in section 1, the purpose of the communication system together with the necessary restrictions placed on its physical components must first be established before specific power requirements may be estimated. Combinations of antennas other than the one assumed in the present example should be investigated before a decision is made as to what will constitute an efficient lunar communication system.

In the particular idealized system described by figures 27 and 30, a number of points should be noted: (1) the required power does not vary appreciably over the range of ϵ_r assumed, but does depend significantly on the conductivity at low frequencies; (2) propagation out to somewhat beyond 100 km is practical for most types of systems and service, at least at MF or below; (3) the curves indicate an optimum frequency exists, depending on the conductivity of the lunar surface and the range of propagation; for the model assumed and for the conductivities and distances shown, the optimum frequency lies in the LF band. It should be kept in mind that the operating noise factor of the receiving system was considered to be a function only of the galactic noise (which, of course, is extrapolated at the lower frequencies) and a rather low receiver noise factor. If the receiving antenna loss ℓ_c were large enough, it is apparent from (5.3) that F would have higher values than those assumed. Also, during the lunar day, the antenna temperature t_c would increase, thus making the operating noise factor even higher.

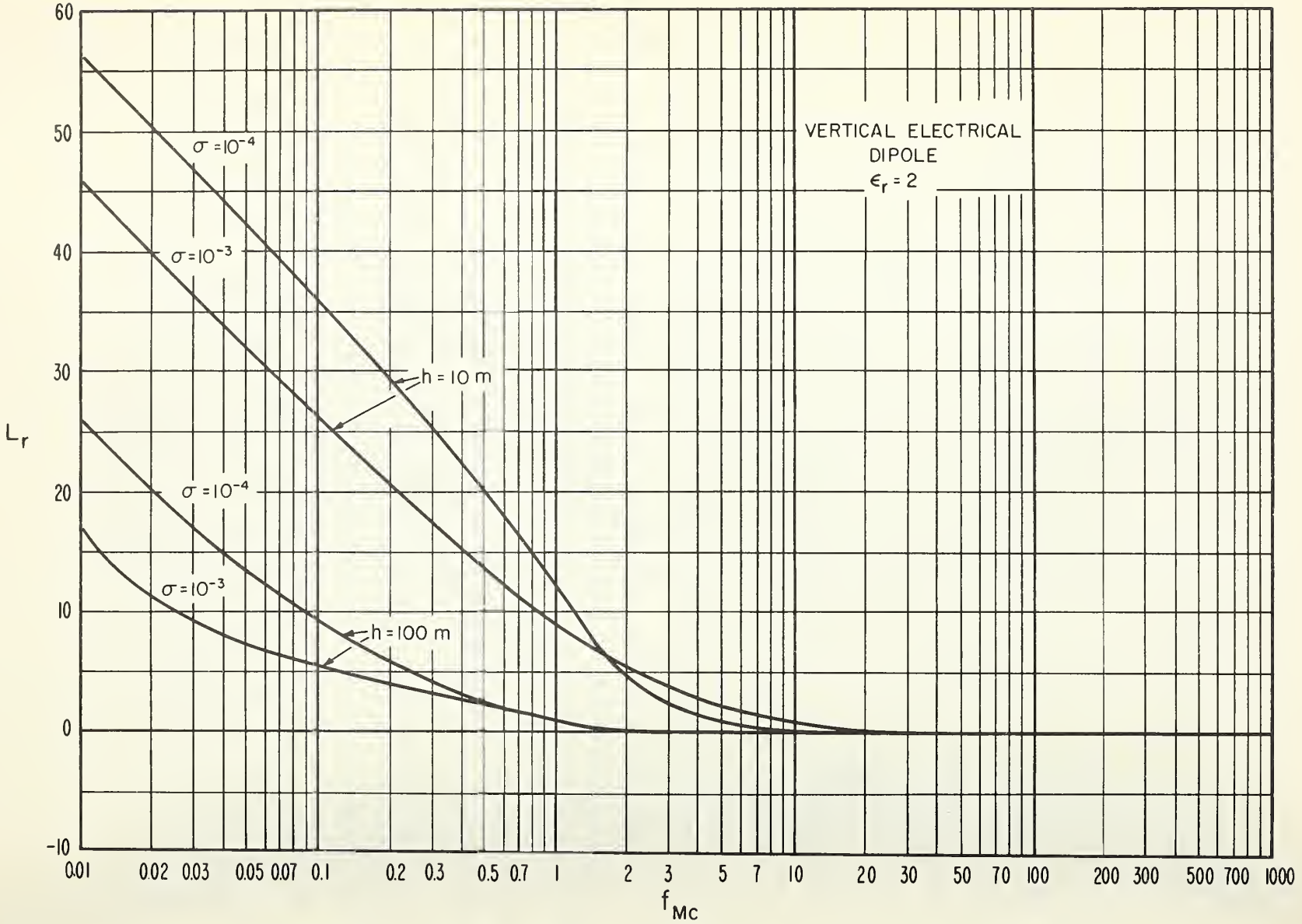

Figure 29. Ground proximity loss L_r for a short vertical electric dipole at fixed heights h = 10 m and 100 m .

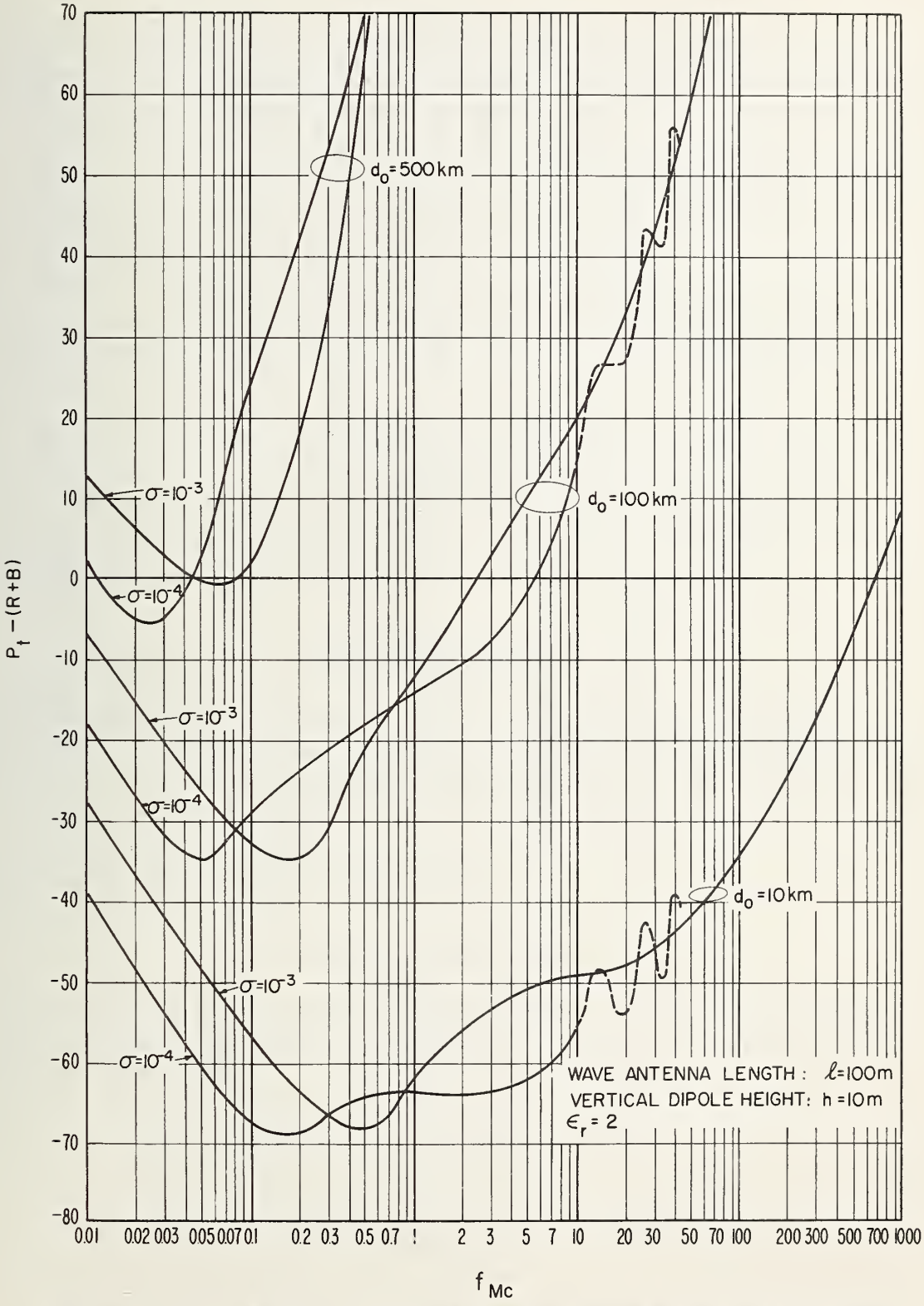

Figure 30. $P_t-(R+B)$ for fixed length wave antenna and fixed height VED over homogeneous ground.

8. CONCLUSIONS

A study has been presented concerning various aspects of lunar surface communication; it is hoped that these results may serve as a basis for future investigations of the subject. An attempt has been made to present the main curves in a generalized form such that, as changes and refinements in our knowledge of the moon arise, the curves may still be useful in predicting lunar communication requirements.

It is apparent that further studies, both theoretical and experimental, would be useful in the following areas:

1. A more precise evaluation of lunar ground conductivity, together with more information concerning layering (if any) of the materials composing the moon.
2. Further investigation into the structure and magnitude of possible lunar ionospheres, especially the determination as to whether an ionized layer exists at the surface, and if so, its effects on propagation at the lower frequencies.
3. Further studies of noise effects including terrestrial noise sources, noise during high solar activity, and low frequency galactic noise.
4. Investigations of various antenna combinations, taking into account antenna ground losses for those situations in which a ground screen will be impractical.
5. A study of knife-edge diffraction and obstacle gain effects caused by irregularities in the moon's surface structure.

9. ACKNOWLEDGMENTS

The author gratefully acknowledges the assistance of J. L. Noble who programmed most of the mathematical formulas used in the calculations of the many graphs appearing in this paper. His thanks also go to K. A. Norton and J. R. Wait of the NBS Boulder Laboratories, and to Paul S. Goodwin of Jet Propulsion Laboratory for their suggestions and guidance.

10. APPENDIX: INPUT IMPEDANCE OF DIPOLE ANTENNAS

It is assumed that an elementary dipole of length $d\ell$ is located at the origin of a cylindrical coordinate system (ρ, θ, z) at a height h above an isotropic and homogeneous conducting half-space characterized by a dielectric constant ϵ_1 and conductivity σ_1. The interface between the two media is the plane $z = -h$, and for $z > -h$ the dielectric constant is assumed to be equal to the free space value ϵ_o. The magnetic permeability of the whole space is taken as the free space value μ_o (MKS units are used here). In the case of a vertical dipole, the antenna is oriented in the z direction, whereas for a horizontal dipole the orientation is in the $\theta = 0$ direction. The elementary magnetic dipole may be considered equivalent to a small circular loop with its axis in the direction of the dipole and with an area $dA = d\ell/\beta_o$, where β_o is the free space wave number $(= 2\pi/\lambda)$. For practical short dipoles having a linear distribution of current, $d\ell$ should be replaced by an effective length $\ell_e = d\ell/2$.

The electromagnetic field of an elementary dipole above a conducting plane may be obtained from the electric and magnetic Hertzian potentials, $\vec{\Pi}_e$ and $\vec{\Pi}_m$, the components of which, if the vectors are referred to a cartesian coordinate system (x, y, z), satisfy the scalar wave equation $(\nabla^2 + \beta^2)\,\Pi = 0$. Using the cylindrical coordinate form of the wave equation, particular solutions are found by the method of separation of variables resulting in expressions for the Π components involving combinations of the eigenfunction

$$\cos n\theta\, J_n(\lambda\rho)\, C(\lambda, \beta) \exp\left\{ \pm \sqrt{\lambda^2 - \beta^2}\, z \right\}, \tag{A-1}$$

where λ denotes the eigenvalue (following Sommerfeld's notation), J_n is a Bessel function of the first kind and order n, and the C's are functions determined from the boundary conditions. These conditions in the present instance require that the tangential components of the electric vector $\vec{E}$ and the magnetic vector $\vec{B}$ be continuous at the interface between the two media (air and ground).

In the case of vertical dipoles, $\vec{E}$ and $\vec{B}$ may be expressed in terms of Hertzian potentials having a z-component only. Thus in the upper medium

$$\vec{\Pi}_{vert} = \Pi_z \vec{z} = \left(\Pi_z^d + \Pi_z^r \right) \vec{z}, \tag{A-2}$$

where the superscripts d and r refer to the direct or primary stimulation and the reflected or secondary stimulation, respectively. After solving for the coefficients C through the boundary conditions, one finds that for

$$\text{VED:} \quad \Pi_{ez}^d = \frac{iK_e}{\beta_o} \int_o^\infty J_o(\lambda\rho)\, e^{-z u_o (\lambda/u_o)}\, d\lambda,$$

$$\Pi_{ez}^r = \frac{iK_e}{\beta_o} \int_o^\infty J_o(\lambda\rho) \left\{ \frac{N^2 u_o - u_1}{N^2 u_o + u_1} \right\} e^{-(z+2h)u_o (\lambda/u_o)}\, d\lambda, \tag{A-3}$$

$$\text{VMD:}\quad \Pi^{d}_{mz} = \frac{iK_m}{\beta_o}\int_o^\infty J_o(\lambda\rho)\, e^{-z u_o}(\lambda/u_o)\,d\lambda,$$

$$\Pi^{r}_{mz} = \frac{iK_m}{\beta_o}\int_o^\infty J_o(\lambda\rho)\left\{\frac{u_o - u_1}{u_o + u_1}\right\} e^{-(z+2h)u_o}(\lambda/u_o)\,d\lambda, \tag{A-4}$$

where

$$u_o = \sqrt{\lambda^2 - \beta_o^2},\quad u_1 = \sqrt{\lambda^2 - \beta_1^2},\quad N^2 = (\epsilon_1/\epsilon_o) - i(\sigma_1/\omega\epsilon_o). \tag{A-5}$$

β_o and β_1 are propagation constants of the upper and lower media, respectively, and the K's are amplitude factors given by

$$K_e = \frac{\beta_o I_o(d\ell)}{4\pi\omega\epsilon_o},\quad K_m = \frac{\beta_o \mu_o I_o(dA)}{4\pi}. \tag{A-6}$$

For horizontal dipoles, the Hertzian potentials require both an x- and a z-component. Thus, corresponding to (A-2),

$$\vec{\Pi}_{hor} = \Pi_x \vec{x} + \Pi_z \vec{z} = (\Pi^{d}_{x} + \Pi^{r}_{x})\vec{x} + \Pi_z \vec{z}. \tag{A-7}$$

After solving for the C's through the boundary conditions, one obtains:

$$\left.\begin{aligned}
\text{HED:}\quad \Pi^{d}_{ex} &= \frac{iK_e}{\beta_o}\int_o^\infty J_o(\lambda\rho)\, e^{-z u_o}(\lambda/u_o)\,d\lambda,\\
\Pi^{r}_{ex} &= \frac{iK_e}{\beta_o}\int_o^\infty J_o(\lambda\rho)\left\{\frac{u_o - u_1}{u_o + u_1}\right\} e^{-(z+2h)u_o}(\lambda/u_o)\,d\lambda,\\
\Pi_{ez} &= -\frac{iK_e\cos\theta}{\beta_o}\int_o^\infty J_1(\lambda\rho)\left\{\frac{2(u_o - u_1)}{N^2 u_o + u_1}\right\} e^{-(z+2h)u_o}(\lambda^2/\beta_o^2)\,d\lambda,
\end{aligned}\right\} \tag{A-8}$$

$$\left.\begin{aligned}
\text{HMD:}\quad \Pi^{d}_{mx} &= \frac{iK_m}{\beta_o}\int_o^\infty J_o(\lambda\rho)\, e^{-z u_o}(\lambda/u_o)\,d\lambda,\\
\Pi^{r}_{mx} &= \frac{iK_m}{\beta_o}\int_o^\infty J_o(\lambda\rho)\left\{\frac{N^2 u_o - u_1}{N^2 u_o + u_1}\right\} e^{-(z+2h)u_o}(\lambda/u_o)\,d\lambda,\\
\Pi_{mz} &= -\frac{iK_m\cos\theta}{\beta_o}\int_o^\infty J_1(\lambda\rho)\left\{\frac{2(u_o - u_1)}{N^2 u_o + u_1}\right\} e^{-(z+2h)u_o}(\lambda^2/\beta_o^2)\,d\lambda,
\end{aligned}\right\} \tag{A-9}$$

where u_o, u_1, N^2, K_e, and K_m are defined in (A-5) and (A-6).

With the Hertz vector $\vec{\Pi}$ determined, the electromagnetic field in the upper medium is derived through the following relationships:

$$\vec{E} = \text{grad div } \vec{\Pi}_e + \beta_o^2 \vec{\Pi}_e, \qquad \text{(electric dipoles)} \tag{A-10a}$$

$$\vec{B} = \text{grad div } \vec{\Pi}_m + \beta_o^2 \vec{\Pi}_m. \qquad \text{(magnetic dipoles)} \tag{A-10b}$$

The components (in cylindrical coordinates) of interest in this paper are found to be

$$\text{VED: } E_z(\rho, z) = \left(\partial^2/\partial z^2 + \beta_o^2\right)\Pi_{ez} = \left(\partial^2/\partial z^2 + \beta_o^2\right)\left(\Pi_{ez}^d + \Pi_{ez}^r\right)$$

$$= \frac{iK_e}{\beta_o}\int_o^\infty J_o(\lambda\rho)\left[e^{-zu_o} + \left\{\frac{N^2u_o - u_1}{N^2u_o + u_1}\right\}e^{-(z+2h)u_o}\right](\lambda^3/u_o)\,d\lambda, \tag{A-11a}$$

$$\text{HED: } E_\rho(\rho, z) = (\partial/\partial\rho)\,\text{div}\,\vec{\Pi}_e + \beta_o^2\cos\theta\,\Pi_{ex}$$

$$= \frac{iK_e\cos\theta}{\beta_o}\int_o^\infty\left[\left(\beta_o^2 J_o(\lambda\rho) - \lambda^2\left\{J_o(\lambda\rho) - \frac{J_1(\lambda\rho)}{\lambda\rho}\right\}\right)e^{-zu_o}\right.$$

$$+\left(\beta_o^2 J_o(\lambda\rho) - \lambda^2\left\{J_o(\lambda\rho) - \frac{J_1(\lambda\rho)}{\lambda\rho}\right\}\right)\left\{\frac{u_o - u_1}{u_o + u_1}\right\}e^{-(z+2h)u_o}$$

$$\left.+\left(J_o(\lambda\rho) - \frac{J_1(\lambda\rho)}{\lambda\rho}\right)\left\{\frac{2\lambda^2u_o^2(u_o - u_1)}{\beta_o^2(N^2u_o + u_1)}\right\}e^{-(z+2h)u_o}\right](\lambda/u_o)\,d\lambda, \tag{A-11b}$$

$$\text{VMD: } B_z(\rho, z) = \left(\partial^2/\partial z^2 + \beta_o^2\right)\Pi_{mz} = \left(\partial^2/\partial z^2 + \beta_o^2\right)\left(\Pi_{mz}^d + \Pi_{mz}^r\right)$$

$$= \frac{iK_m}{\beta_o}\int_o^\infty J_o(\lambda\rho)\left[e^{-zu_o} + \left\{\frac{u_o - u_1}{u_o + u_1}\right\}e^{-(z+2h)u_o}\right](\lambda^3/u_o)\,d\lambda, \tag{A-11c}$$

$$\text{HMD: } B_\rho(\rho, z) = (\partial/\partial\rho)\,\text{div}\,\vec{\Pi}_m + \beta_o^2\cos\theta\,\Pi_{mx}$$

$$= \frac{iK_m\cos\theta}{\beta_o}\int_o^\infty\left[\left(\beta_o^2 J_o(\lambda\rho) - \lambda^2\left\{J_o(\lambda\rho) - \frac{J_1(\lambda\rho)}{\lambda\rho}\right\}\right)e^{-zu_o}\right.$$

$$+\left(\beta_o^2 J_o(\lambda\rho) - \lambda^2\left\{J_o(\lambda\rho) - \frac{J_1(\lambda\rho)}{\lambda\rho}\right\}\right)\left\{\frac{N^2u_o - u_1}{N^2u_o + u_1}\right\}e^{-(z+2h)u_o}$$

$$\left.+\left(J_o(\lambda\rho) - \frac{J_1(\lambda\rho)}{\lambda\rho}\right)\left\{\frac{2\lambda^2u_o^2(u_o - u_1)}{\beta_o^2(N^2u_o + u_1)}\right\}e^{-(z+2h)u_o}\right](\lambda/u_o)\,d\lambda. \tag{A-11d}$$

To calculate the dipole input impedance using the emf method [Wait, 1953, 1962 d; King, 1956 (p. 258)] requires a knowledge of the axial field at the antenna. This may be obtained by taking the limits of (A-11) as ρ and z approach zero (and with $\theta = 0$ in the case of horizontal dipoles). The impedance Z is then given by

$$\text{VED:}\quad Z = \lim_{\substack{\rho\to o\\ z\to o}} \left\{ E_z(\rho, z)\, d\ell / I_o \right\}$$

$$= \frac{i K_e\, d\ell}{\beta_o I_o} \int_o^\infty \left[1 + \left\{ \frac{N^2 u_o - u_1}{N^2 u_o + u_1} \right\} e^{-2h u_o} \right] (\lambda^3/u_o)\, d\lambda, \qquad \text{(A-12a)}$$

$$\text{HED:}\quad Z = \lim_{\substack{\rho\to o\\ z\to o}} \left\{ E_\rho(\rho, z)\, d\ell / I_o \right\}$$

$$= \frac{i K_e\, d\ell}{\beta_o I_o} \int_o^\infty \left[\left(\beta_o^2 - \lambda^2/2 \right) \left(1 + \left\{ \frac{u_o - u_1}{u_o + u_1} \right\} e^{-2h u_o} \right) \right.$$

$$\left. + \left\{ \frac{\lambda^2 u_o^2 (u_o - u_1)}{\beta_o^2 (N^2 u_o + u_1)} \right\} e^{-2h u_o} \right] (\lambda/u_o)\, d\lambda, \qquad \text{(A-12b)}$$

$$\text{VMD:}\quad Z = \lim_{\substack{\rho\to o\\ z\to o}} \left\{ \omega B_z(\rho, z)\, dA / I_o \right\}$$

$$= \frac{i\omega K_m\, dA}{\beta_o I_o} \int_o^\infty \left[1 + \left\{ \frac{u_o - u_1}{u_o + u_1} \right\} e^{-2h u_o} \right] (\lambda^3/u_o)\, d\lambda, \qquad \text{(A-12c)}$$

$$\text{HMD:}\quad Z = \lim_{\substack{\rho\to o\\ z\to o}} \left\{ \omega B_\rho(\rho, z)\, dA / I_o \right\}$$

$$= \frac{i\omega K_m\, dA}{\beta_o I_o} \int_o^\infty \left[\left(\beta_o^2 - \lambda^2/2 \right) \left(1 + \left\{ \frac{N^2 u_o - u_1}{N^2 u_o + u_1} \right\} e^{-2h u_o} \right) \right.$$

$$\left. + \left\{ \frac{\lambda^2 u_o^2 (u_o - u_1)}{\beta_o^2 (N^2 u_o + u_1)} \right\} e^{-2h u_o} \right] (\lambda/u_o)\, d\lambda. \qquad \text{(A-12d)}$$

Notice that the effect of the ground is contained in terms involving the factor $\exp(-2h u_o)$; thus, the change in impedance ΔZ due to the presence of the ground may be defined as

$$\Delta Z \equiv Z - \lim_{h\to\infty} Z = Z - Z_f \tag{A-13}$$

and the free space antenna resistance r_f is obtained from the relationship:

$$r_f = \mathrm{Re}\left\{\lim_{h\to\infty} Z\right\}. \tag{A-14}$$

With the use of (A-13) and (A-14), one can now derive the expressions for the normalized input impedance change $\Delta Z/r_f$ given by equations (4.2) of section 4; here, the change of variable

$$x = 2h u_o = 2h\sqrt{\lambda^2 - \beta_o^2}$$

has been made and the following relationships used:

$$(\lambda\, d\lambda/u_o) = (dx/2h), \quad \alpha = 2h\beta_o, \quad u_1 = \sqrt{x^2 - \alpha^2(N^2-1)}/2h, \quad \lambda^2 = (\alpha^2 + x^2)/(2h)^2. \tag{A-15}$$

Limiting expressions of (4.2), derived from integrations by parts of the integrals involved, are given by the following equations. For $\alpha N << 1$:

$$\text{VED:}\quad \Delta Z/R_f \simeq \frac{3(N+1)}{4}\left[F_1(D) + \left(\frac{N+1}{2}\right)^2 F_2(D)\right] + i\left\{\frac{3(1+A)\,D}{\alpha^3}\right\} e^{-A}, \tag{A-16a}$$

$$\text{HED:}\quad \Delta Z/R_f \simeq \frac{3(N+1)}{8}\left[F_1(0) + \left(\frac{N+1}{2}\right)^2 F_2(D)\right] + i\left\{\frac{3(1+A)\,D}{2\alpha^3}\right\} e^{-A}, \tag{A-16b}$$

$$\text{VMD:}\quad \Delta Z/R_f \simeq \frac{3(N+1)}{4}\left[F_1(0) + \left(\frac{N+1}{2}\right)^2 F_2(0)\right] + i\left\{\frac{3(N^2+1)\,D}{8\alpha}\right\} e^{-A}, \tag{A-16c}$$

$$\text{HMD:}\quad \Delta Z/R_f \simeq \frac{3(N+1)}{8}\left[F_1(D) + \left(\frac{N+1}{2}\right)^2 F_2(0)\right] + i\left\{\frac{3(N^2+5)\,D}{16\alpha}\right\} e^{-A}, \tag{A-16d}$$

where

$$F_1(X) = X + \{1 - X(1+X)\}\,d + \tfrac{1}{3}(1+X)(1-X^2)\,d^2, \tag{A-17}$$

$$F_2(X) = -\frac{X}{3} + \{1 + X(1-X)\}\,d + \{1 - X(1+X)(2-X)\}\,d^2 + \tfrac{1}{3}\{1 + X(1-X)(2-X^2)\}\,d^3 - \tfrac{1}{5}(1-X)(1-X^2)^2\,d^4, \tag{A-18}$$

$$d \equiv \frac{N-1}{N+1}, \quad D \equiv \frac{N^2-1}{N^2+1}, \quad A \equiv \alpha\sqrt{N^2-1}. \tag{A-19}$$

For $\alpha N >> 1$:

$$\text{VED:}\quad \Delta Z/R_f \sim \frac{3}{\alpha^3}\left\{\frac{N-1}{N+1}\right\}\left[(1+4/N)+i\left\{\alpha+\frac{6}{\alpha N}\left(1-\frac{2N-3}{N^2}\right)\right\}\right] i e^{-i\alpha}, \tag{A-20a}$$

$$\text{HED:}\quad \Delta Z/R_f \sim \frac{3}{2\alpha^3}\left\{\frac{N-1}{N+1}\right\}\left[(1-\alpha^2+2/N)+i\left\{\alpha+\frac{6}{\alpha N}\left(1-\frac{2N-3}{N^2}\right)\right\}\right] i e^{-i\alpha}, \tag{A-20b}$$

$$\text{VMD:}\quad \Delta Z/R_f \sim -\frac{3}{\alpha^3}\left\{\frac{N-1}{N+1}\right\}\left[(1-4/N)+i\left\{\alpha+\frac{6}{\alpha N}\left(1-\frac{2N+1}{N^2}\right)\right\}\right] i e^{-i\alpha}, \tag{A-20c}$$

$$\text{HMD:}\quad \Delta Z/R_f \sim -\frac{3}{2\alpha^3}\left\{\frac{N-1}{N+1}\right\}\left[(1-\alpha^2-6/N)+i\left\{\alpha+\frac{6}{\alpha N}\left(1-\frac{2N+1}{N^2}\right)\right\}\right] i e^{-i\alpha}. \tag{A-20d}$$

For the case of dipoles above a perfectly conducting plane ($N\to\infty$), equations (A-20) reduce to the well-known expressions:

$$\text{VED:}\quad \Delta Z/R_f \to \left(\frac{3}{\alpha^3}\right)\left[\{\sin\alpha-\alpha\cos\alpha\}+i\{\cos\alpha+\alpha\sin\alpha\}\right], \tag{A-21a}$$

$$\text{HED:}\quad \Delta Z/R_f \to \left(\frac{3}{2\alpha^3}\right)\left[\{(1-\alpha^2)\sin\alpha-\alpha\cos\alpha\}+i\{(1-\alpha^2)\cos\alpha+\alpha\sin\alpha\}\right], \tag{A-21b}$$

$$\text{VMD:}\quad \Delta Z/R_f \to -\left(\frac{3}{\alpha^3}\right)\left[\{\sin\alpha-\alpha\cos\alpha\}+i\{\cos\alpha+\alpha\sin\alpha\}\right], \tag{A-21c}$$

$$\text{HMD:}\quad \Delta Z/R_f \to -\left(\frac{3}{2\alpha^3}\right)\left[\{(1-\alpha^2)\sin\alpha-\alpha\cos\alpha\}+i\{(1-\alpha^2)\cos\alpha+\alpha\sin\alpha\}\right]. \tag{A-21d}$$

11. REFERENCES

Beverage, H. H., C. W. Rice, and E. W. Kellogg (1923), The wave antenna, Trans. AIEE 42, 215.

Bremmer, H. (1949), Terrestrial radio waves, (Elsevier Publishing Co., Amsterdam).

Brown, W. E. (1960), A lunar and planetary echo theory, J. Geophys. Res. 65, 3087.

Burrows, C. R., and S. S. Atwood (1949), Radio wave propagation, (Academic Press Inc., New York, N. Y.).

Carson, J. R. (1926), Wave propagation in overhead wires with ground return, Bell System Tech. J. 5, 539.

CCIR (1951), Bandwidths and signal-to-noise ratios in complete systems, VI Plenary Assembly, International Radio Consultative Committee 1, 30, Geneva.

CCIR (1963), The concept of transmission loss in studies of radio systems, Documents of the Xth Plenary Assembly, Recommendation 341, ITU Vol. III, Geneva.

Coleman, B. L. (1950), Propagation of electromagnetic disturbances along a thin wire in a horizontally stratified medium, Phil. Mag. 41, 276.

Crichlow, W. Q., D. F. Smith, R. N. Morton, and W. R. Corliss (1955), Worldwide radio noise levels expected in the frequency band 10 kc to 100 Mc, NBS Circ. 557.

Daniels, F. B. (1961), A theory of radar reflection from the moon and planets, J. Geophys. Res. 66, 1781.

Elsmore, B. (1957), Radio observations of the lunar atmosphere, Phil. Mag. 2, Series 8, No. 20, 1040-1046.

Hartz, T. R. (1963), Satellite measurements of cosmic radio intensities at frequencies less than 12 Mc/s, talk given at the 1963 Spring URSI Meeting, Washington, D. C.

King, R. W. P. (1956), The theory of linear antennas, (Harvard University Press, Cambridge, Mass.).

Martin, C. A., and G. S. Wickizer (1949), Study of Beverage wave antenna for use with low-frequency Loran, RCA, Final Engineering Report on Contract W-28-099-ac-315.

Menzel, D. H. (1961), Cosmic noise survey, Harvard College Observatory, Cambridge 38, Mass.

Norton, K. A. (1941), The calculation of ground-wave field intensity over a finitely conducting spherical earth, Proc. IRE 29, No. 12, 623-639.

Norton, K. A. (1959), System loss in radio wave propagation, J. Res. NBS 63D (Radio Prop.), No. 1, 53-73.

Norton, K. A. (1962), Efficient use of the radio spectrum, NBS Tech. Note No. 158.

Page (1962), Utility of lunar groundwave propagation, Report PCE-R-4541-0001A, Page Communications Engineers, Inc., Washington, D. C.

Senior, T. B. A., and K. M. Siegel (1960), A theory of radar scattering by the moon, J. Res. NBS 64D (Radio Prop.), No. 3, 217.

Vogler, L. E. (1963a), Point-to-point communication on the moon, J. Res. NBS 67D (Radio Prop.), No. 1, 5-21.

Vogler, L. E. (1963b), Lunar point-to-point communication, chapter (pp. 533-559) in Technology of lunar exploration, edited by C. I. Cummings and H. R. Lawrence, (Academic Press, New York, N. Y.).

Vogler, L. E. (1964), The calculation of ground wave attenuation in the far diffraction region Radio Sci. J. Res. NBS/ USNC-URSI 68D, No. 7, 819-826.

Vogler, L. E., and J. L. Noble (1963), Curves of ground proximity loss for dipole antennas, NBS Tech. Note No. 175.

Vogler, L. E., and J. L. Noble (1964), Curves of input impedance change due to ground for dipole antennas, NBS Monograph 72.

Wait, J. R. (1953), Radiation resistance of a small circular loop in the presence of a conducting ground, J. Appl. Phys. 24, No. 5, 646-649.

Wait, J. R. (1954), Radiation from a ground antenna, Can. J. Technol. 32, 1.

Wait, J. R. (1956), Effect of the ground screen on the field radiated from a monopole, IRE Trans. Ant. Prop. AP-4, 179.

Wait, J. R. (1959), Transmission of power in radio propagation, Electronic and Radio Engineer 36, No. 4, 146.

Wait, J. R. (1961), Private communication.

Wait, J. R. (1962a), Electromagnetic waves in stratified media, (Pergamon Press, Oxford).

Wait, J. R. (1962b), The propagation of electromagnetic waves along the earth's surface, chapter (pp. 243-290) in Electromagnetic waves, edited by R. E. Langer, (University of Wisconsin Press, Madison, Wis.).

Wait, J. R. (1962c), Introduction to the theory of VLF propagation, Proc. IRE 50, 1624-1647.

Wait, J. R. (1962d), Possible influence of the ionosphere on the impedance of a ground-based antenna, J. Res. NBS 66D (Radio Prop.), No. 5, 563-569.

Wait, J. R., and W. J. Surtees (1954), Impedance of a top-loaded antenna of arbitrary length over a circular grounded screen, J. Appl. Phys. 25, 553.

Weil, H., and M. L. Barasch (1963), A theoretical lunar ionosphere, Icarus 1, No. 4, 346-356.

12. GRAPHS OF GROUND PROXIMITY LOSS, $L_{t,r} = 10 \log (r/r_f)$

for

Vertical Electric Dipoles (VED)

Horizontal Electric Dipoles (HED)

Vertical Magnetic Dipoles (VMD)

Horizontal Magnetic Dipoles (HMD)

$s = 60 \lambda \sigma$(mhos/m), $\alpha = (2h)(2\pi/\lambda)$,

ϵ_r: relative dielectric constant of ground

σ(mhos/m): conductivity of ground

h: height in meters of antenna above ground

λ: wavelength in meters

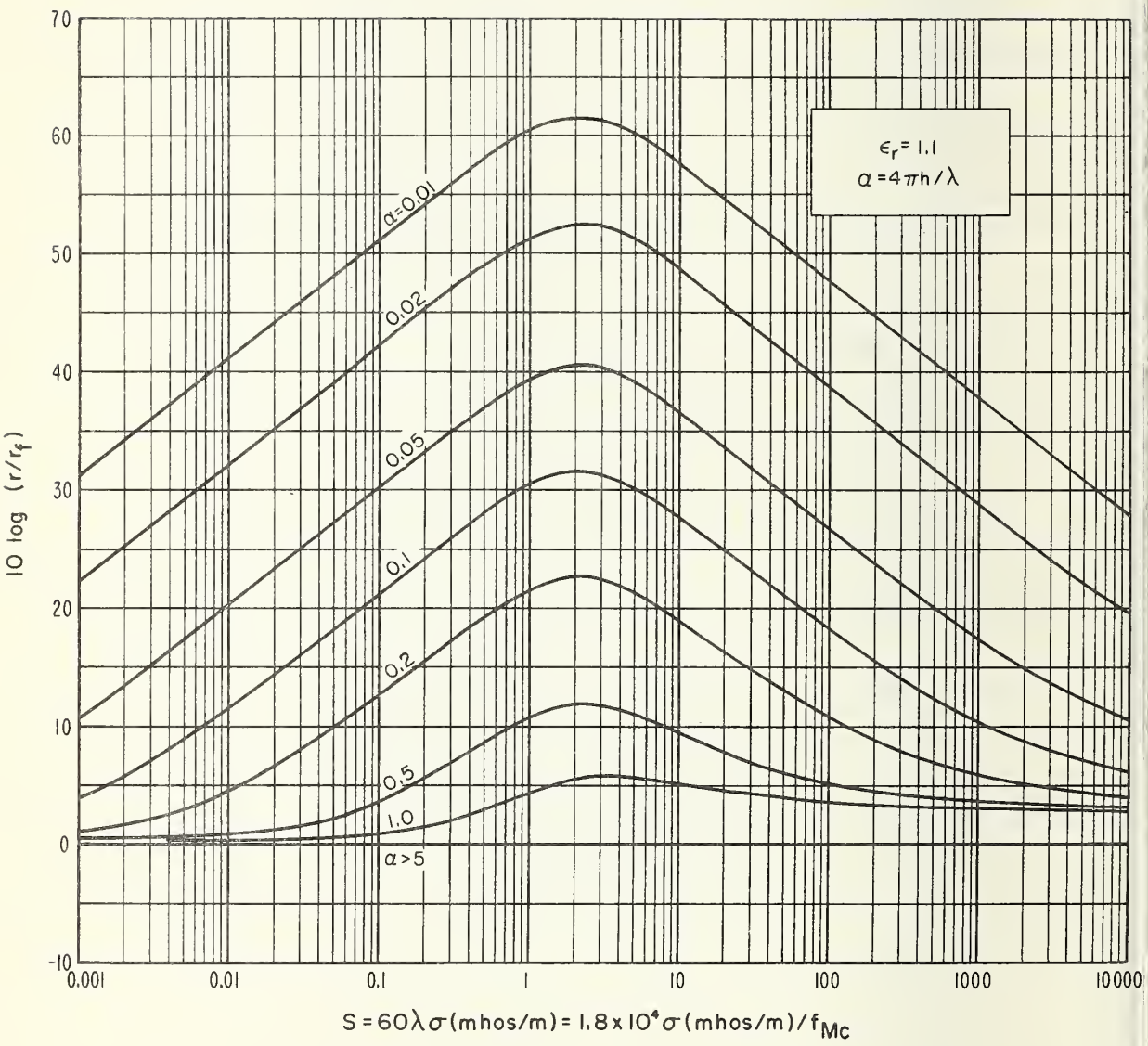

Figure A-1. Ground proximity loss $L_{t,r}$ for VED, $\epsilon_r = 1.1$.

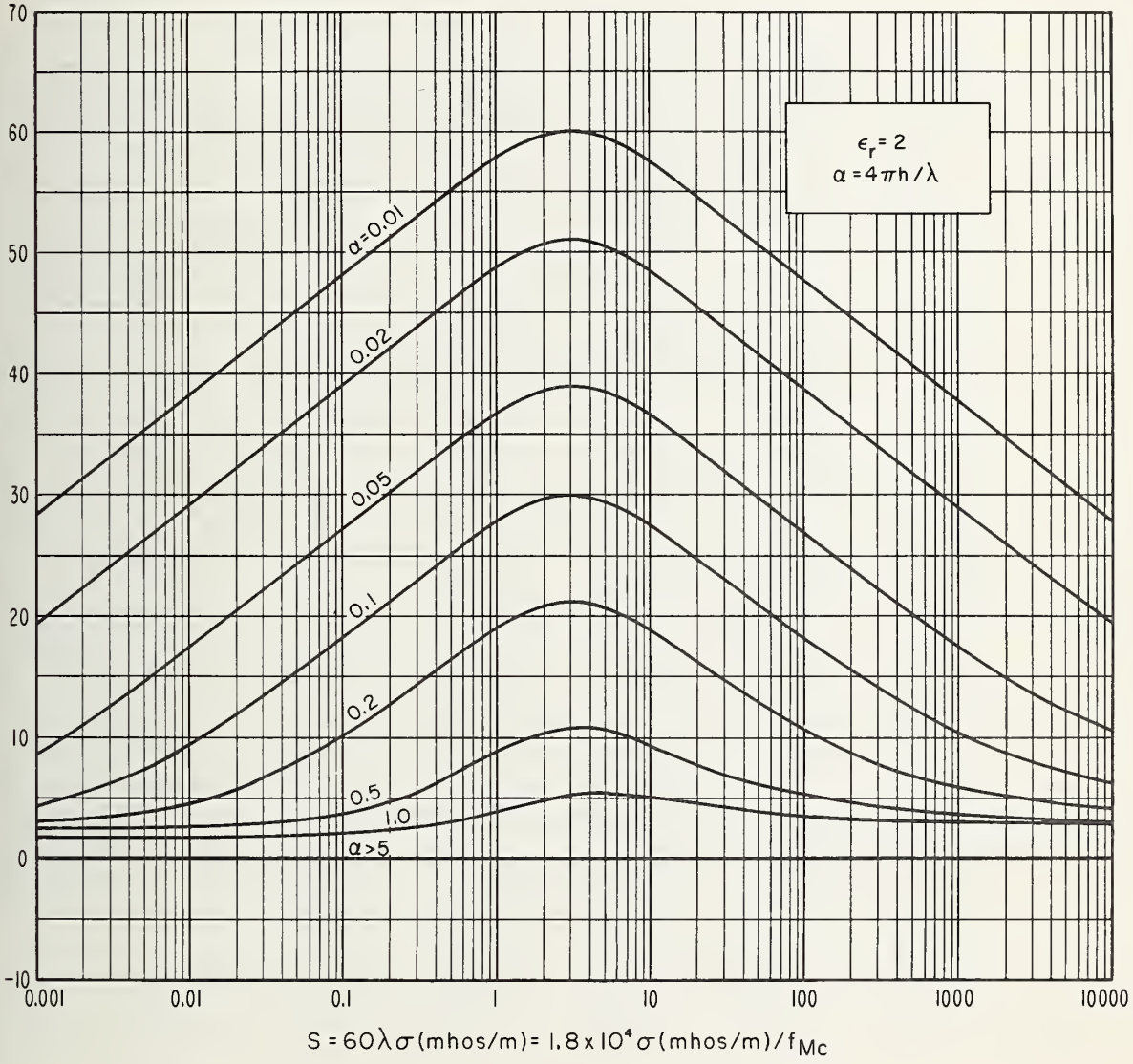

Figure A-2. Ground proximity loss $L_{t,r}$ for VED, $\epsilon_r = 2$.

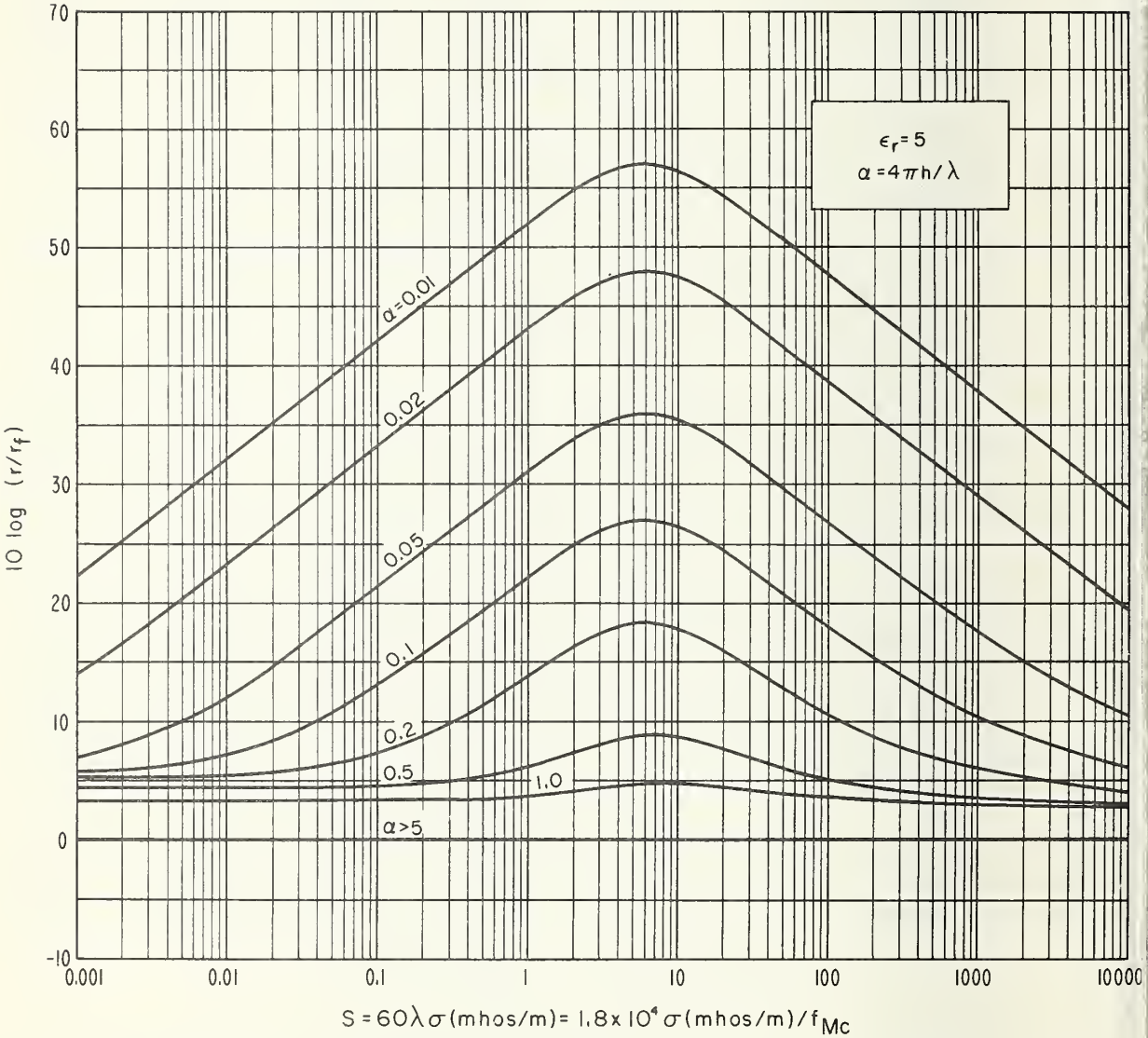

Figure A-3. Ground proximity loss $L_{t,r}$ for VED, $\epsilon_r = 5$.

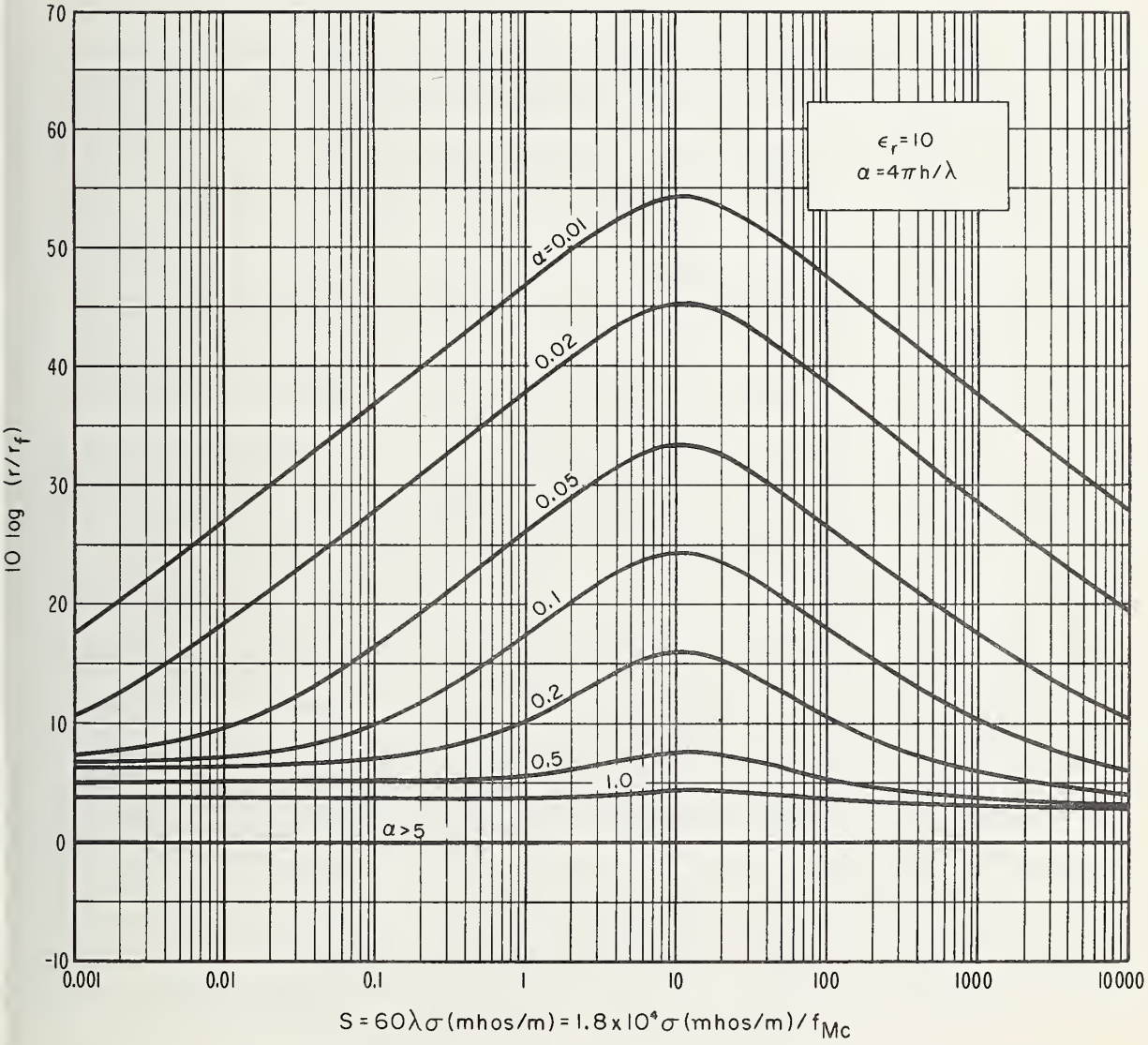

Figure A-4. Ground proximity loss $L_{t,r}$ for VED, $\epsilon_r = 10$.

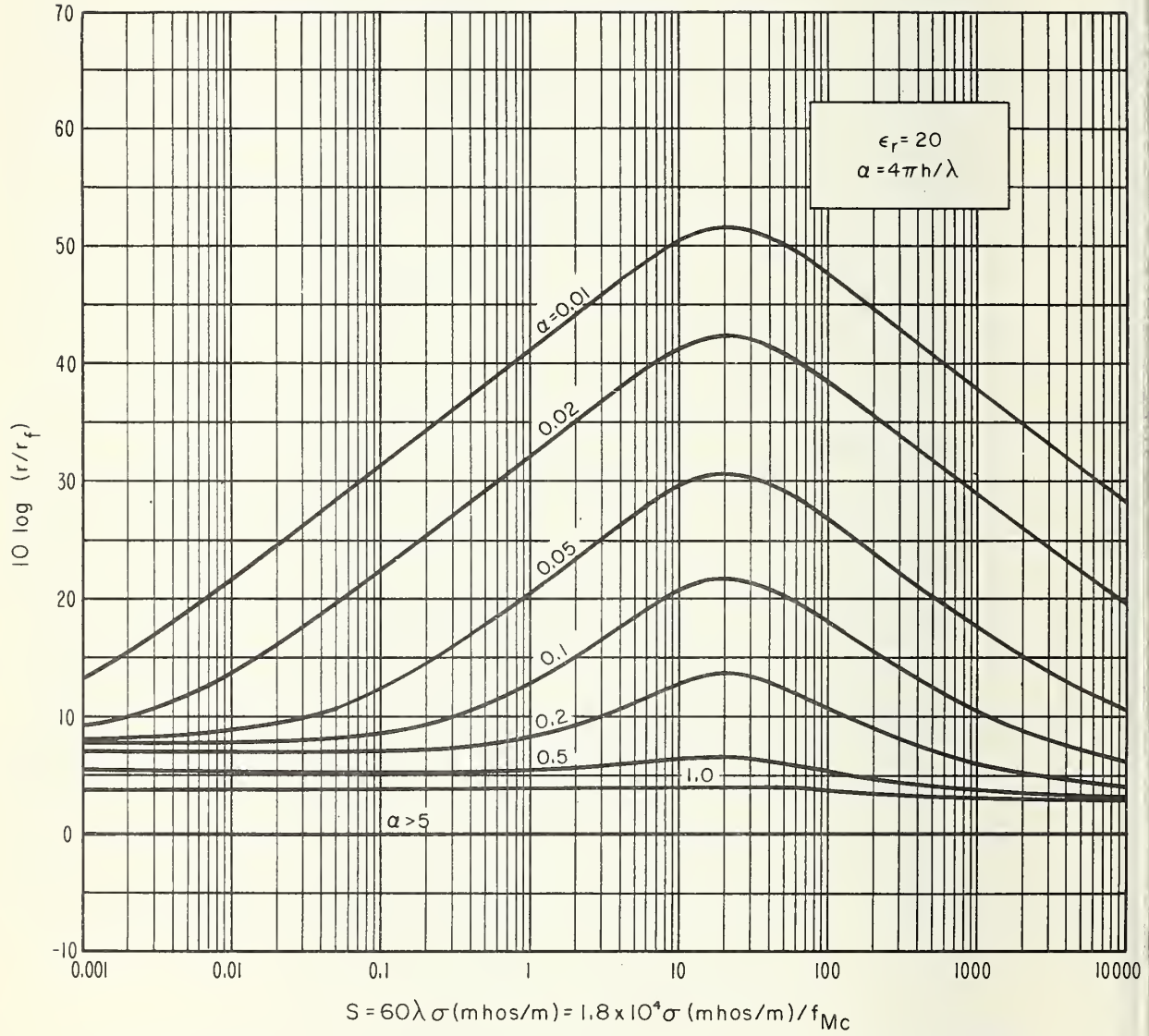

Figure A-5. Ground proximity loss $L_{t,r}$ for VED, $\epsilon_r = 20$.

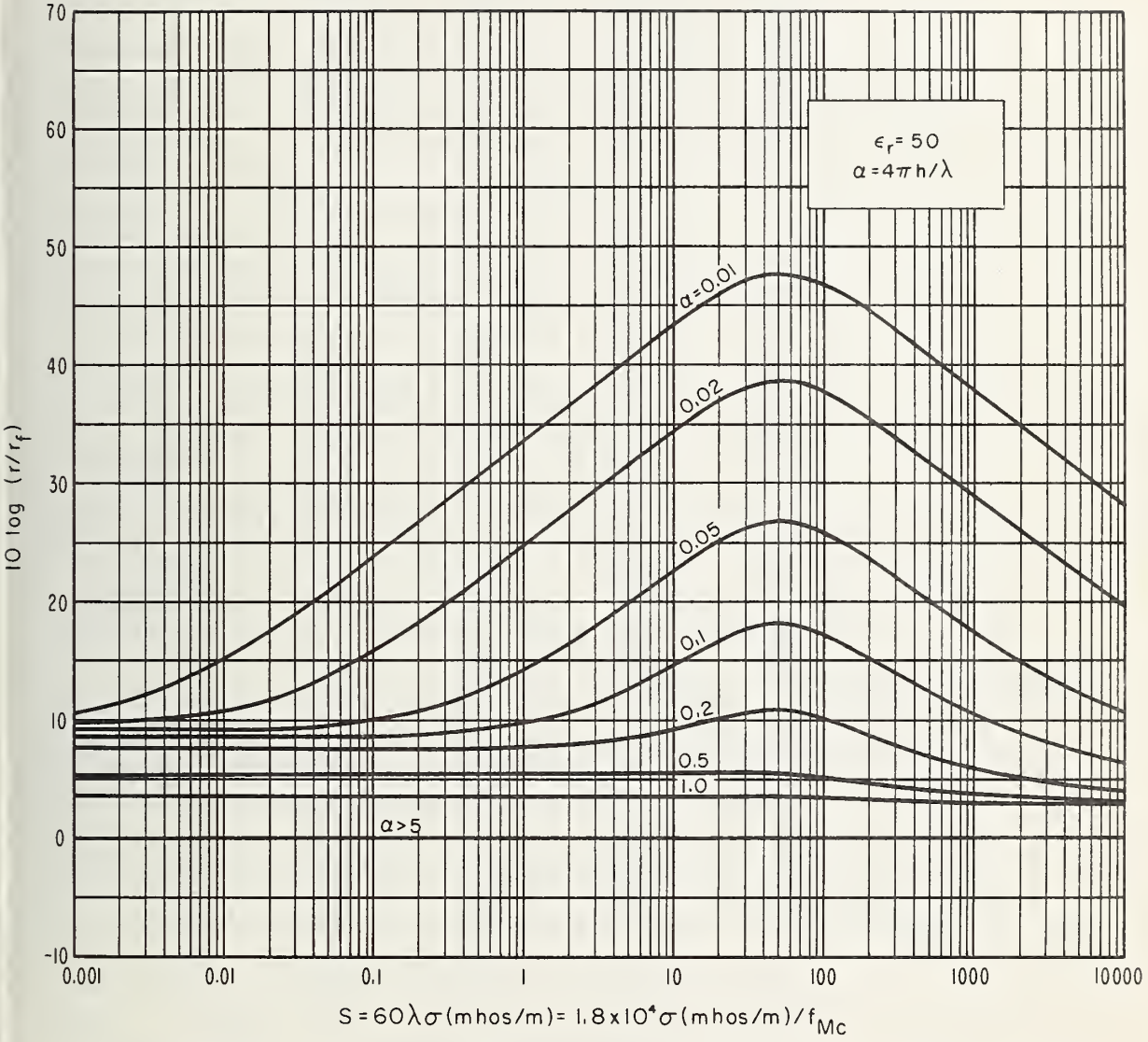

Figure A-6. Ground proximity loss $L_{t,r}$ for VED, $\epsilon_r = 50$.

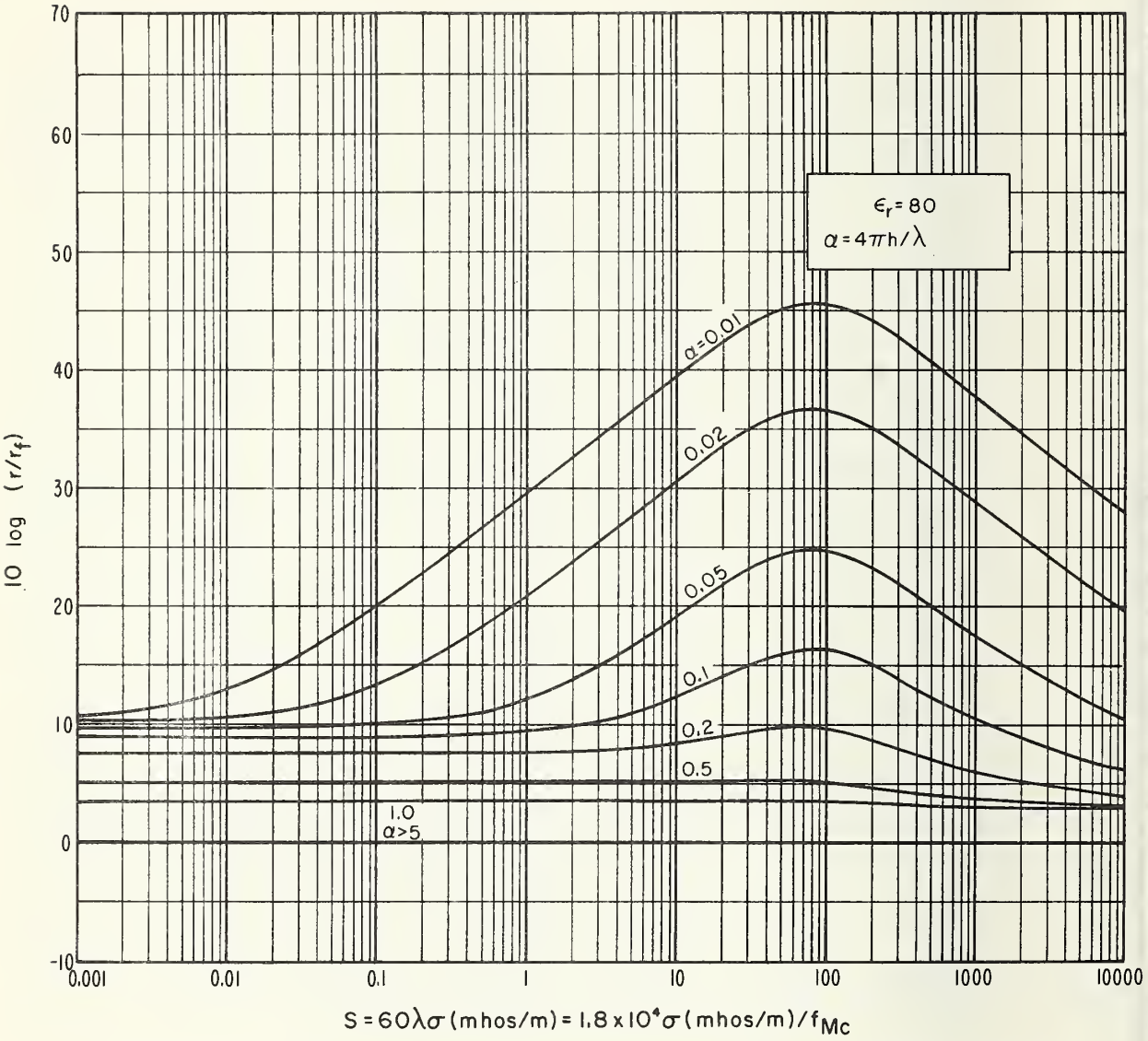

Figure A-7. Ground proximity loss $L_{t,r}$ for VED, $\epsilon_r = 80$.

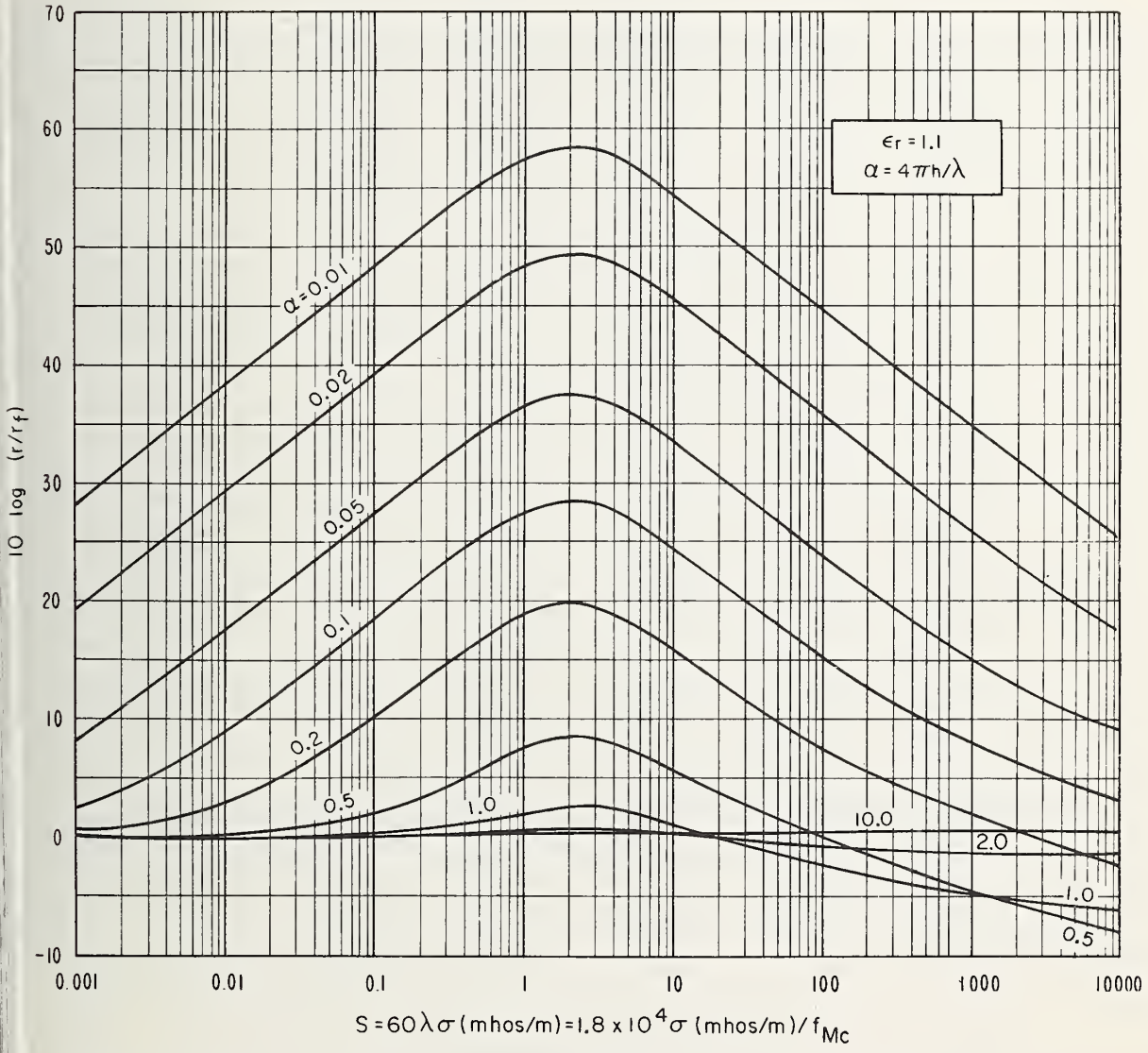

Figure A-8. Ground proximity loss $L_{t,r}$ for HED, $\epsilon_r = 1.1$.

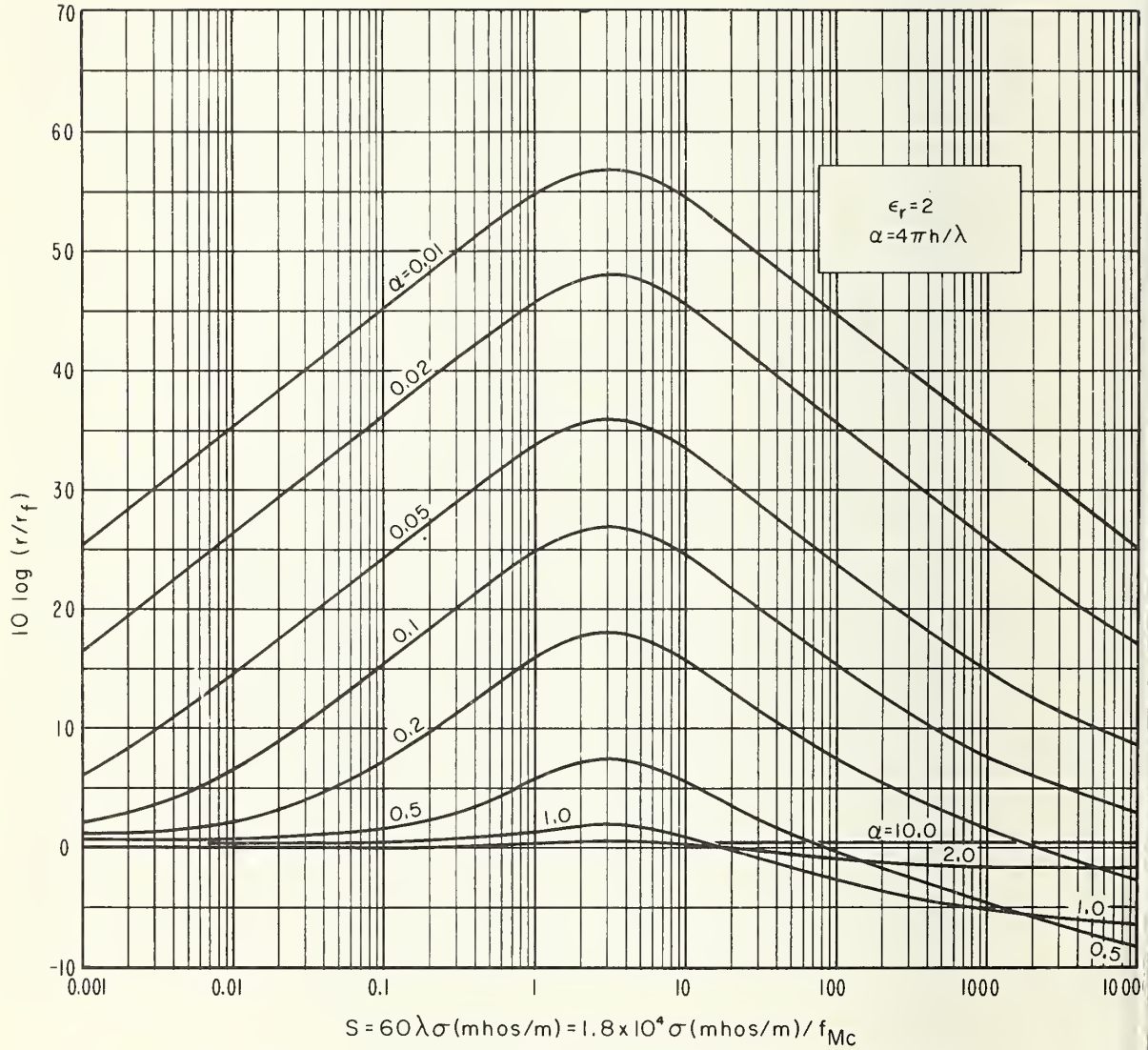

Figure A-9. Ground proximity loss $L_{t,r}$ for HED, $\epsilon_r = 2$.

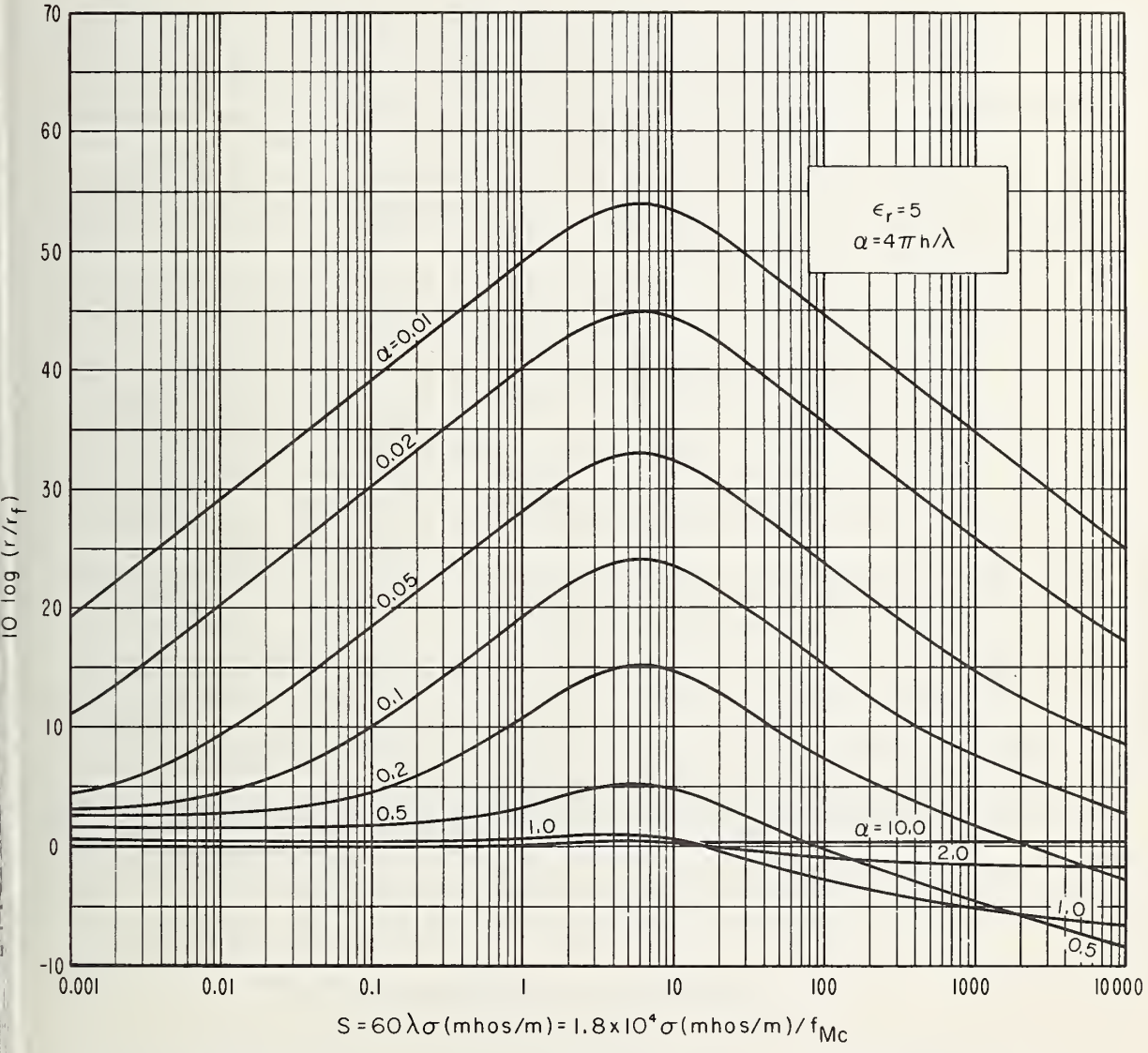

Figure A-10. Ground proximity loss $L_{t,r}$ for HED, $\epsilon_r = 5$.

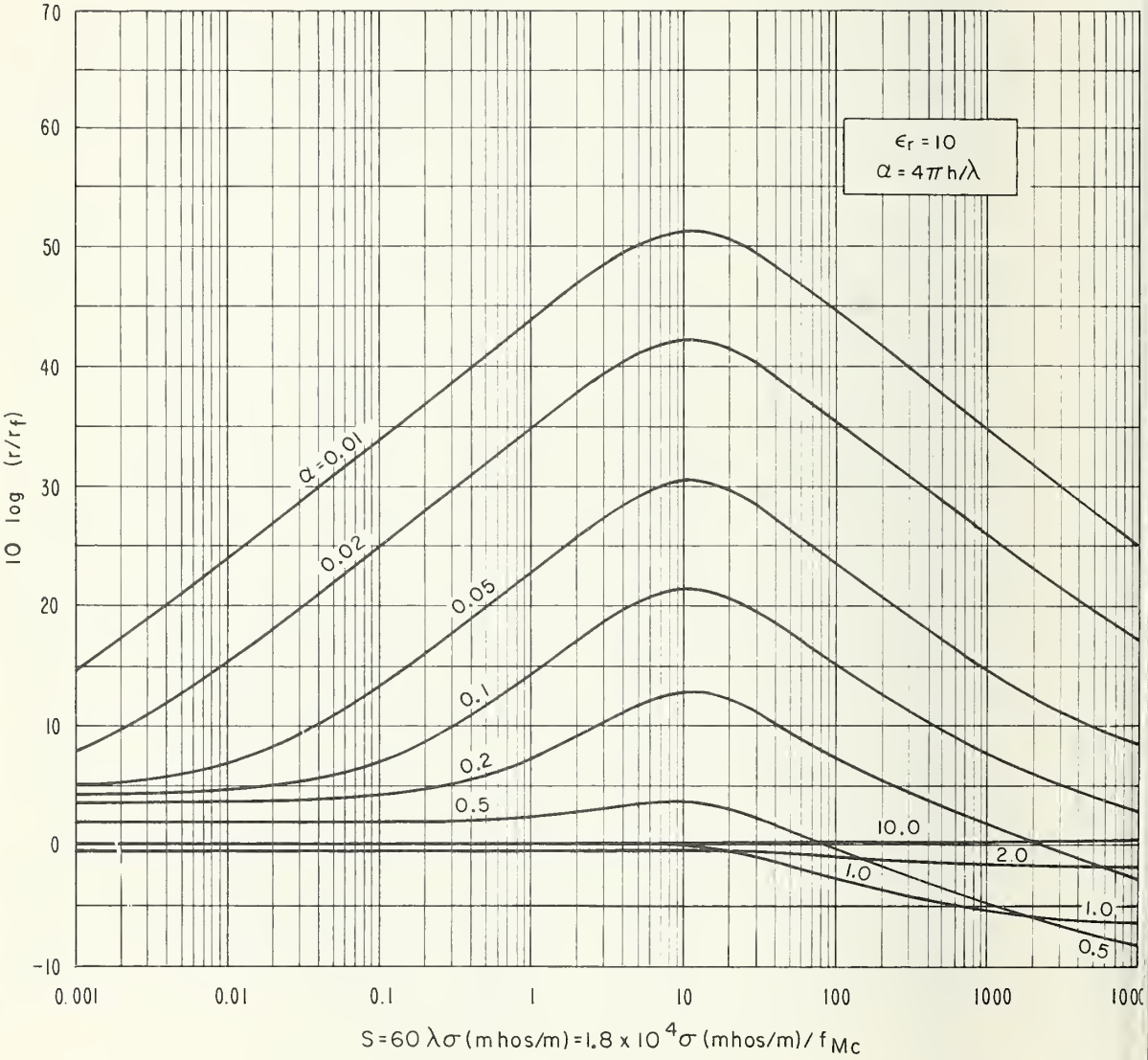

Figure A-11. Ground proximity loss $L_{t,r}$ for HED, $\epsilon_r = 10$.

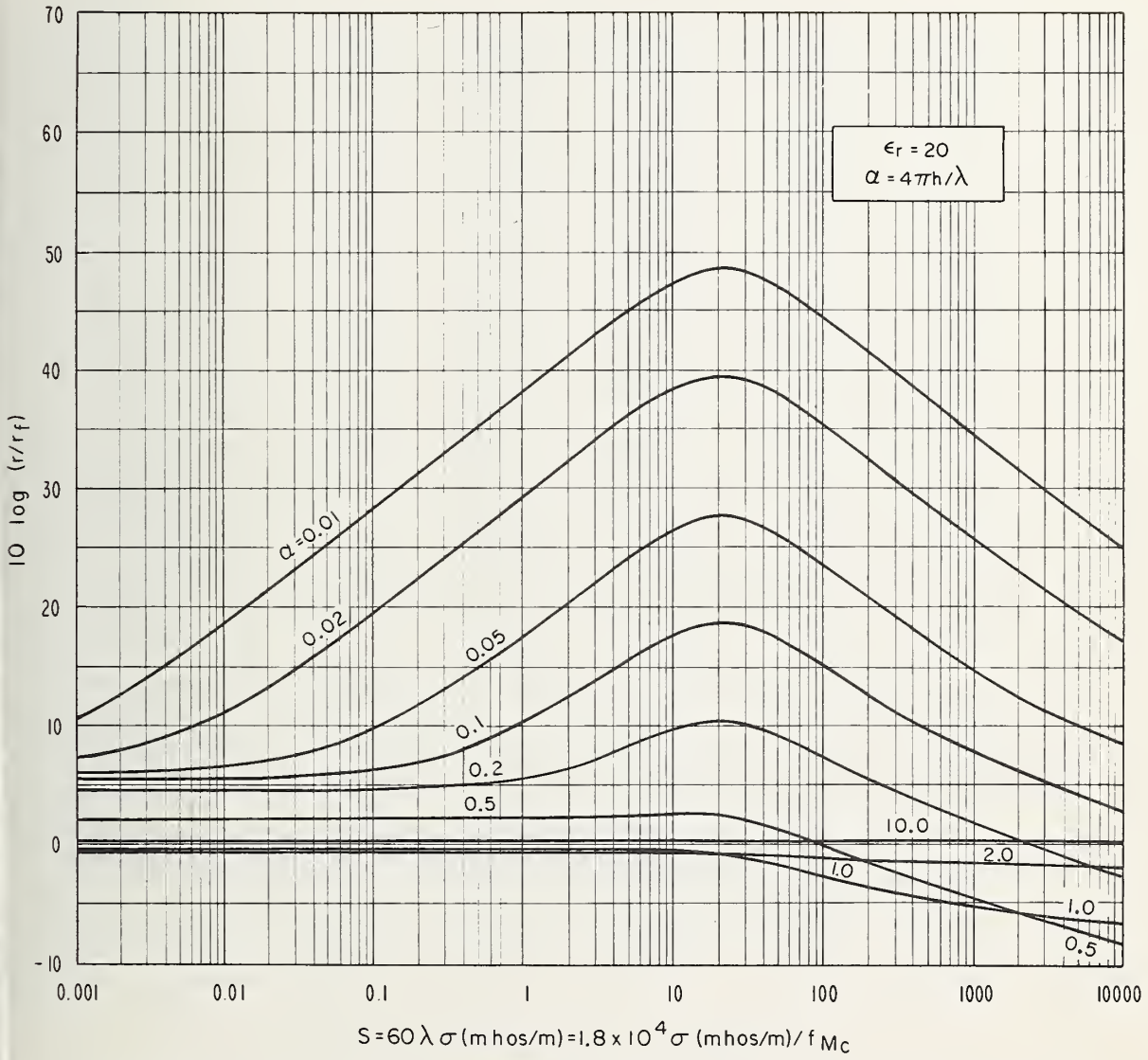

Figure A-12. Ground proximity loss $L_{t,r}$ for HED, $\epsilon_r = 20$.

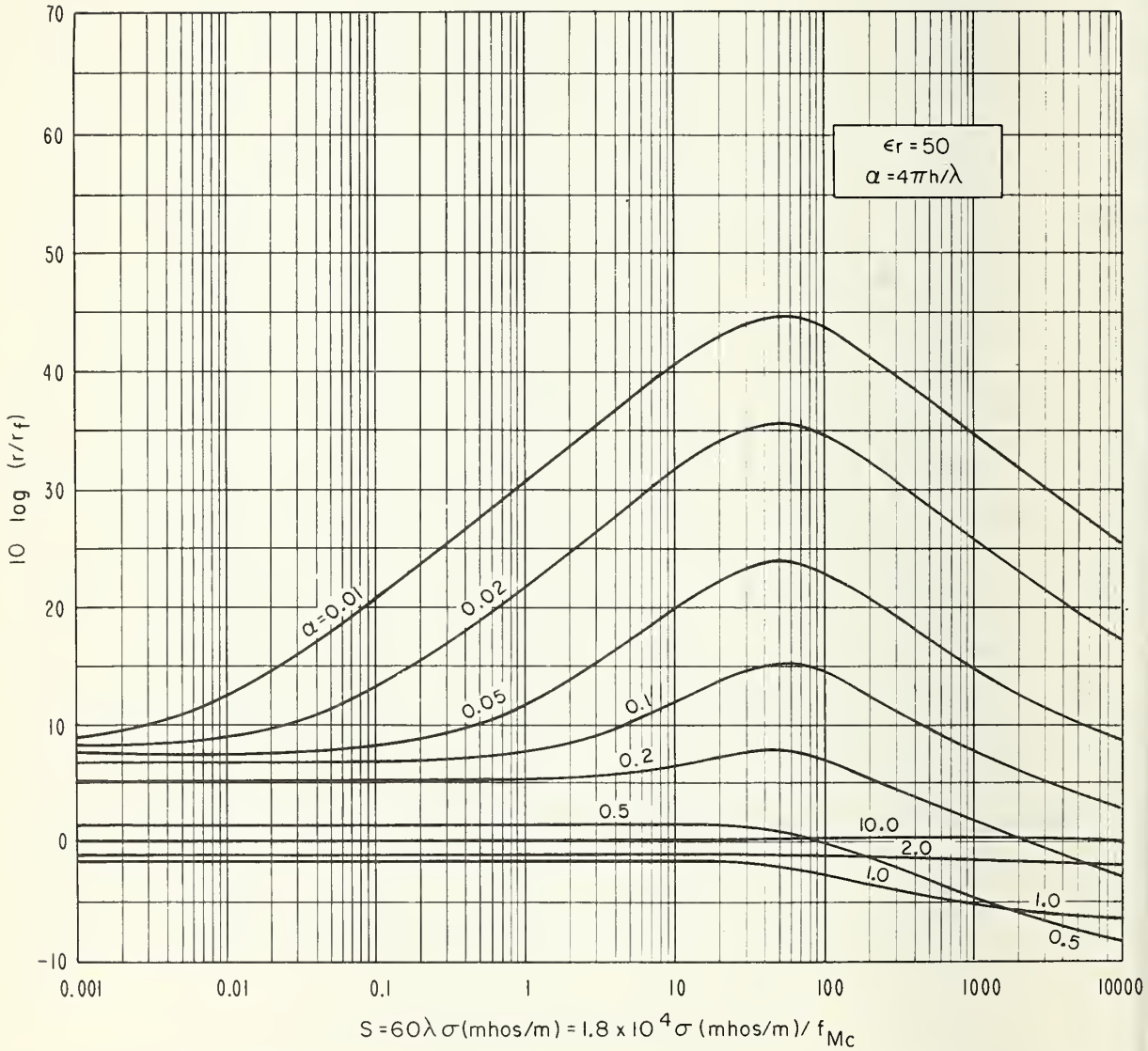

Figure A-13. Ground proximity loss $L_{t,r}$ for HED, $\epsilon_r = 50$.

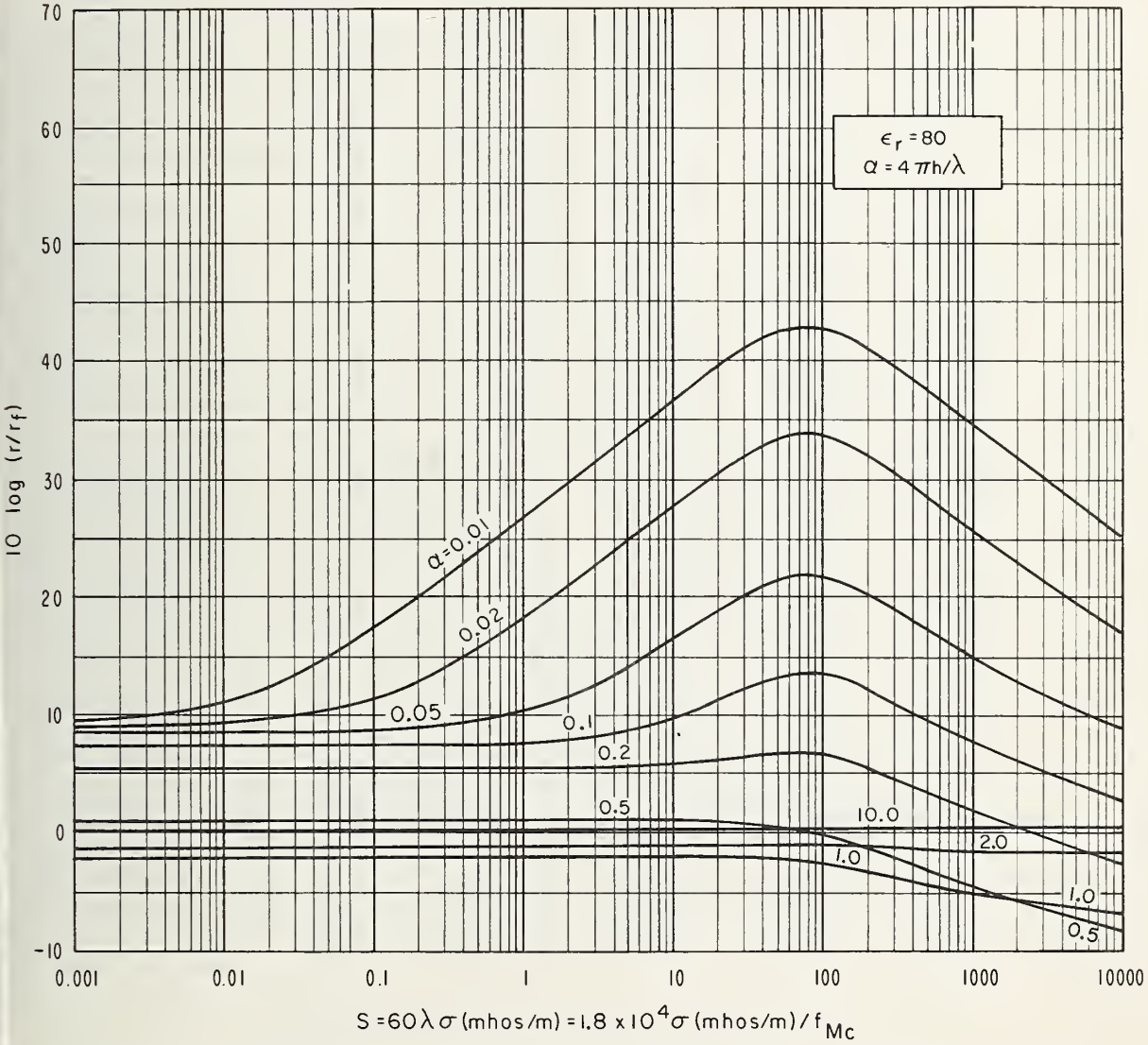

Figure A-14. Ground proximity loss $L_{t,r}$ for HED, $\epsilon_r = 80$.

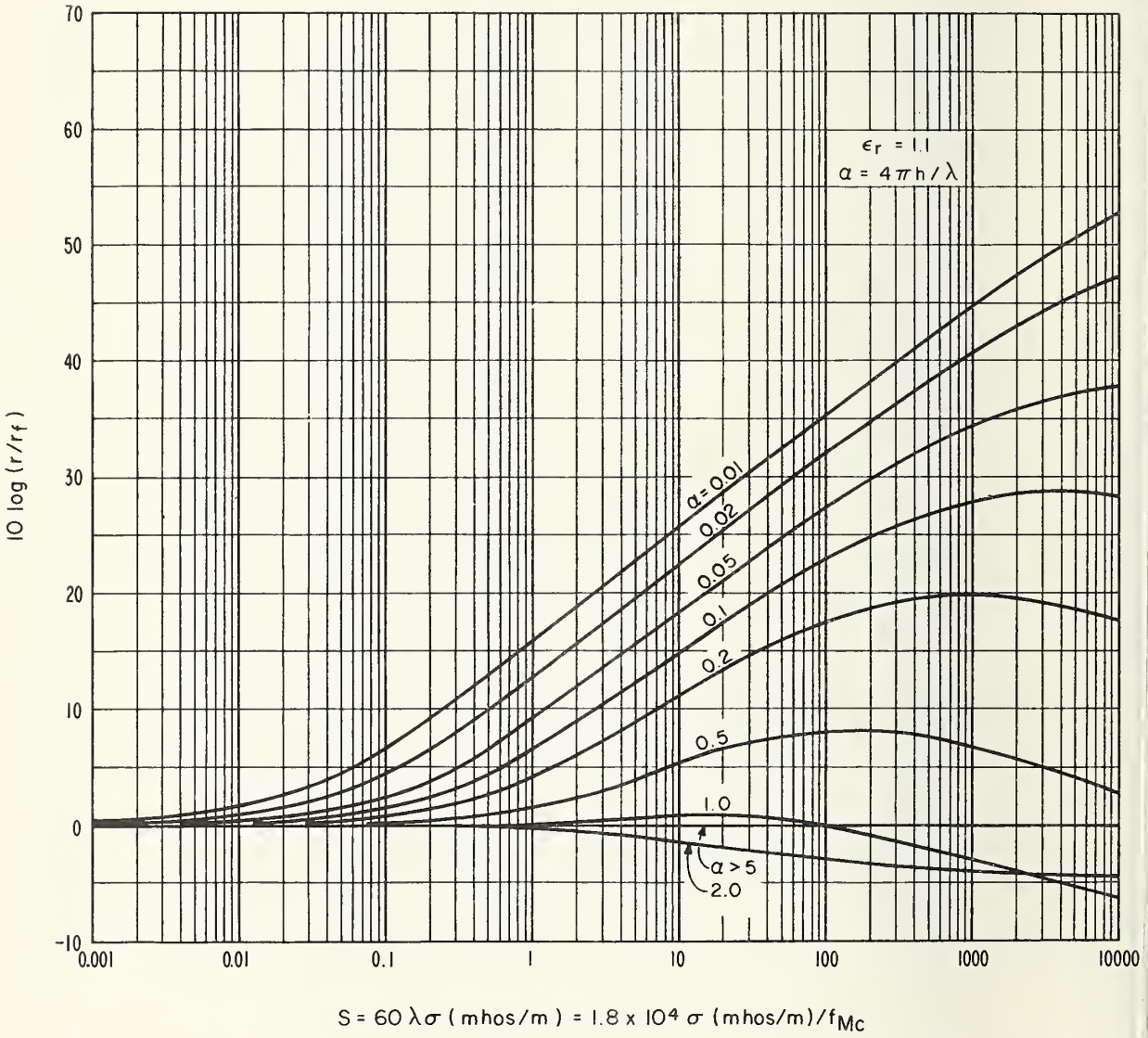

Figure A-15. Ground proximity loss $L_{t,r}$ for VMD, $\epsilon_r = 1.1$.

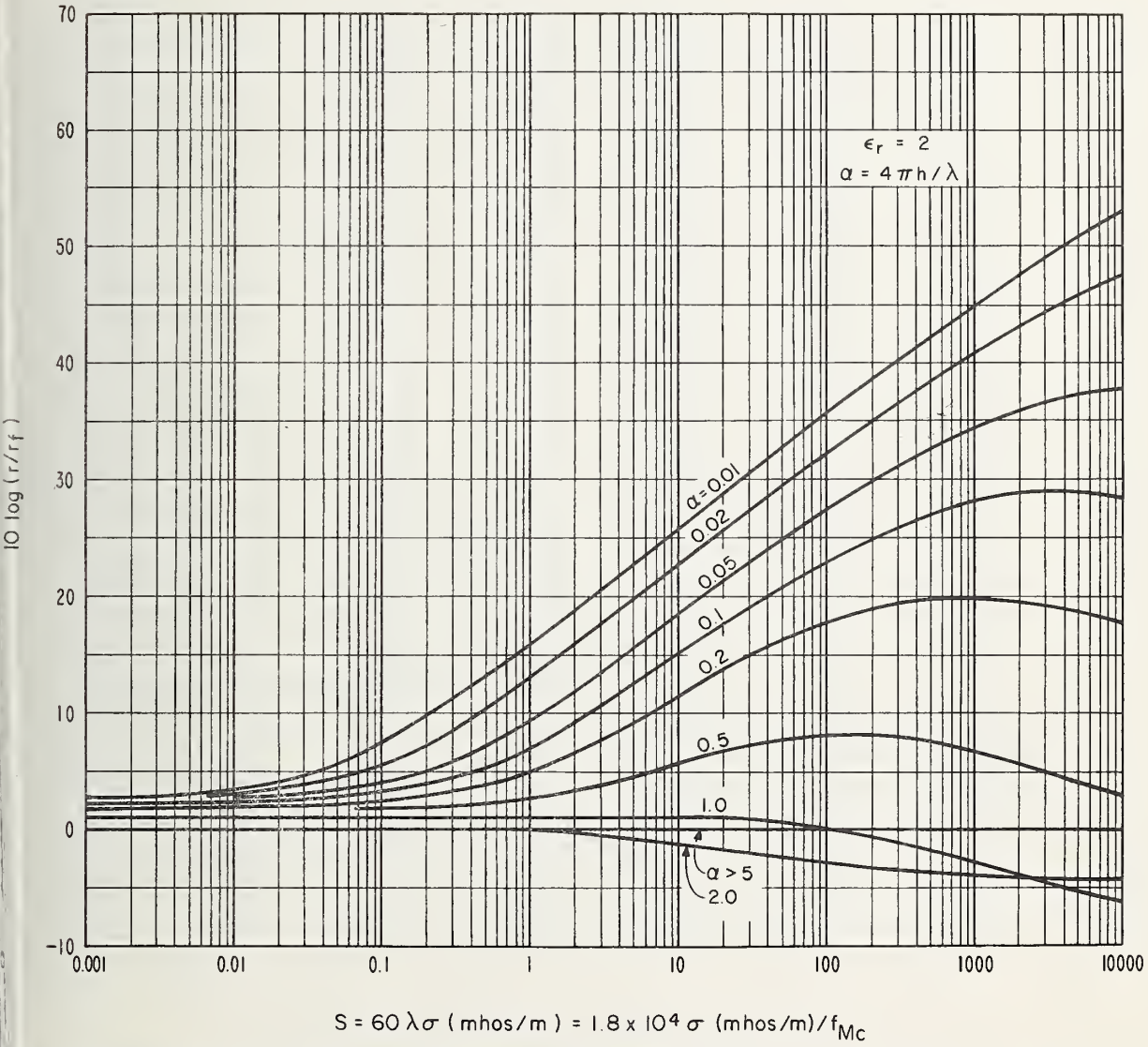

Figure A-16. Ground proximity loss $L_{t,r}$ for VMD, $\epsilon_r = 2$.

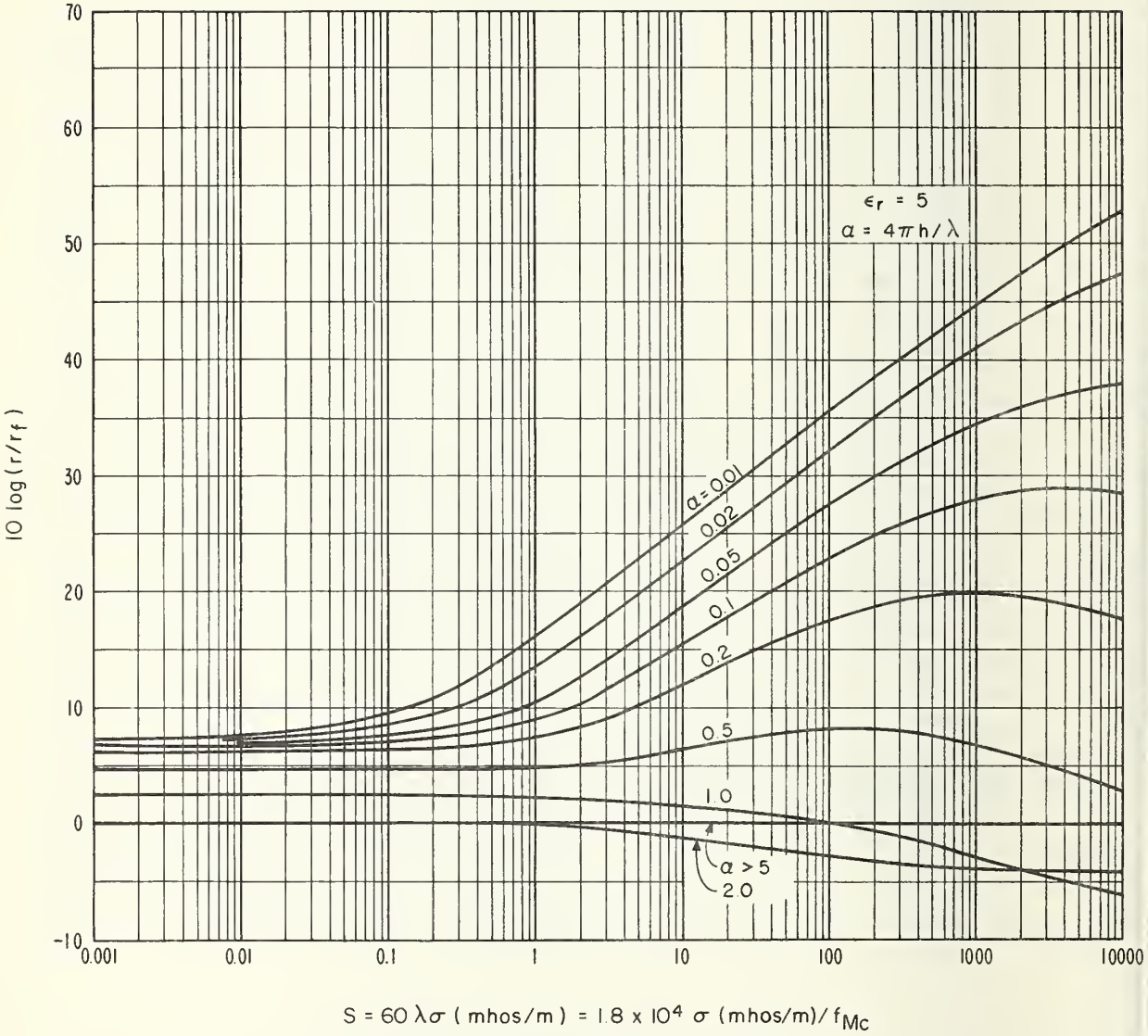

Figure A-17. Ground proximity loss $L_{t,r}$ for VMD, $\epsilon_r = 5$.

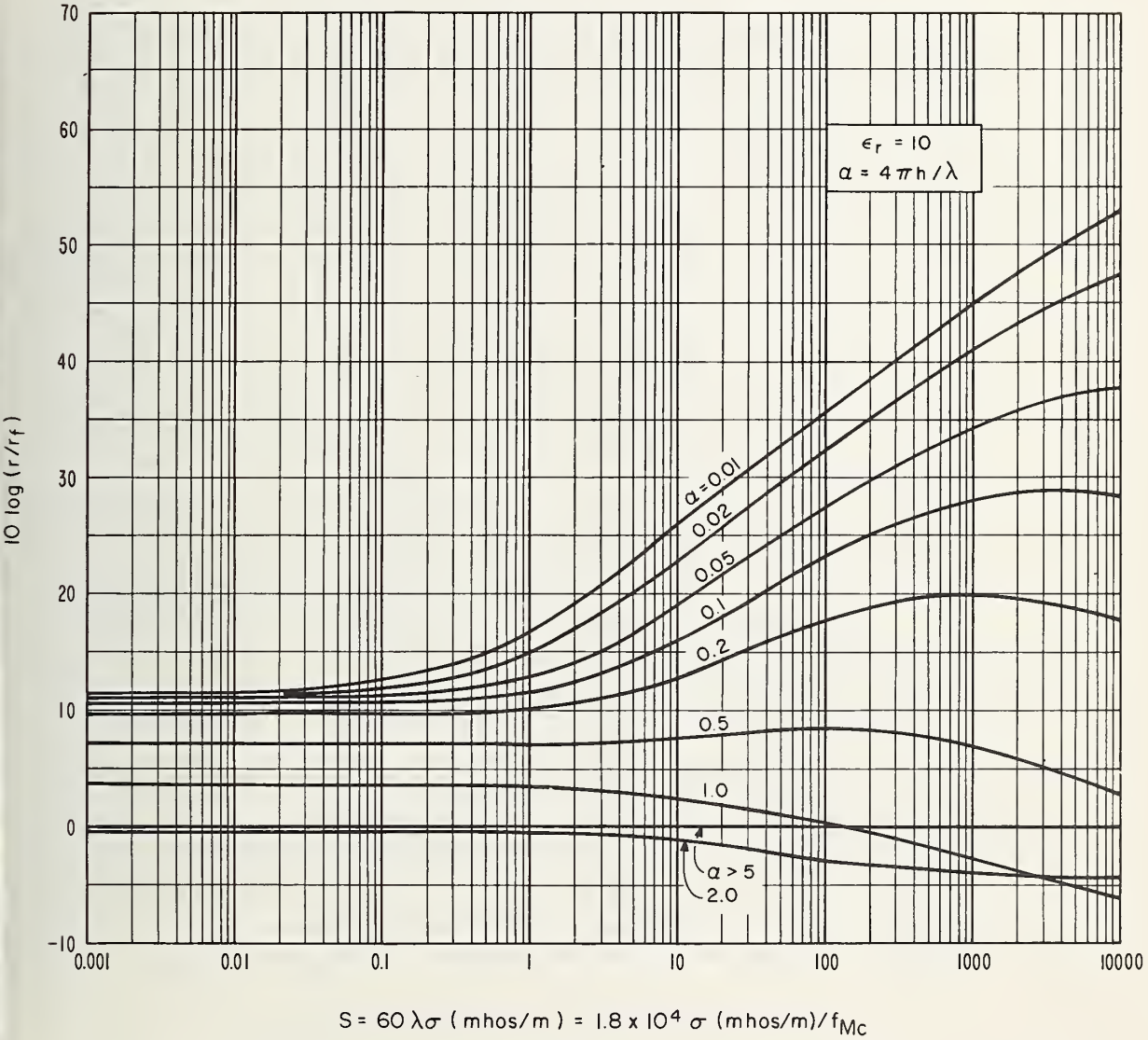

Figure A-18. Ground proximity loss $L_{t,r}$ for VMD, $\epsilon_r = 10$.

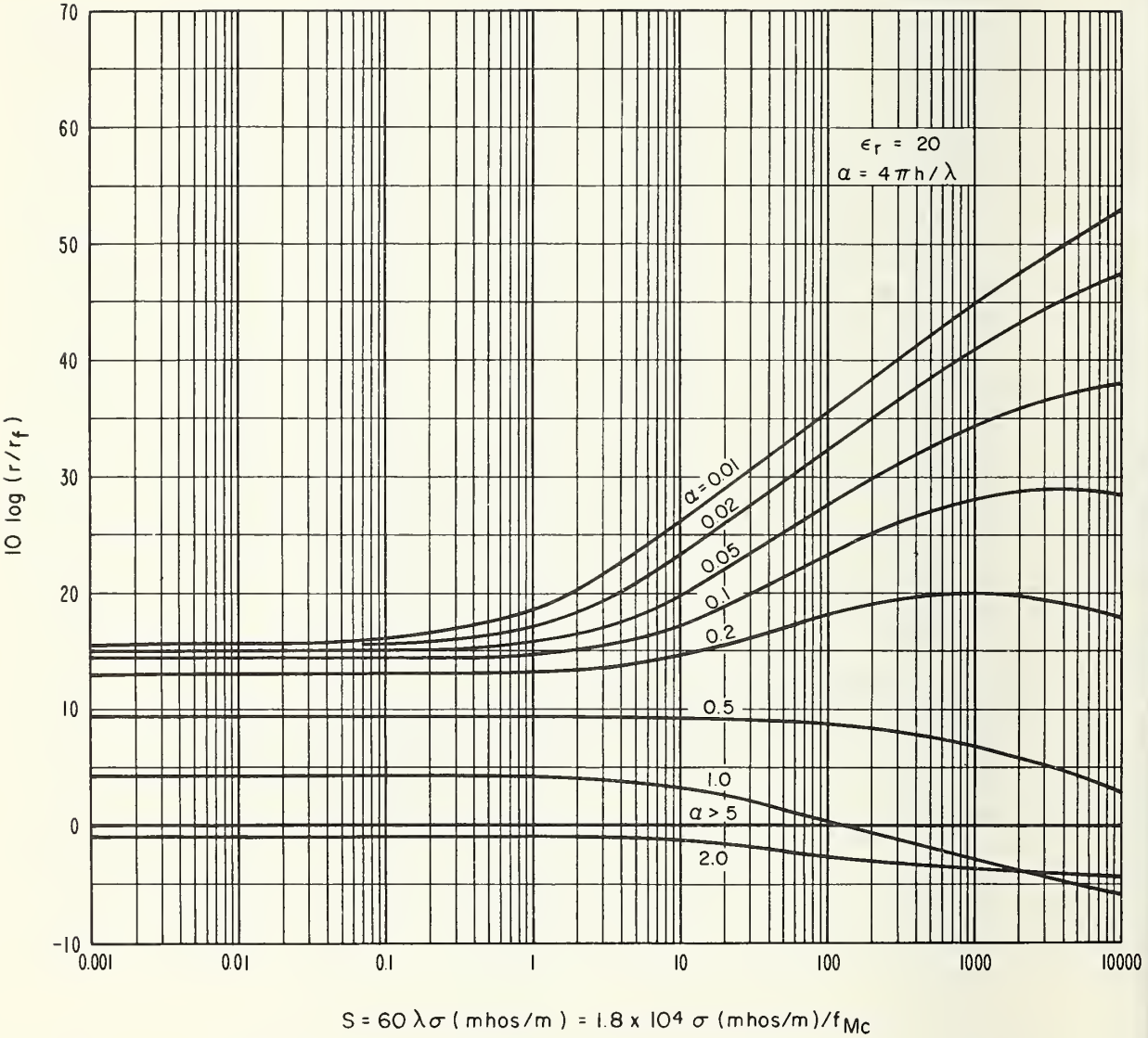

Figure A-19. Ground proximity loss $L_{t,r}$ for VMD, $\epsilon_r = 20$.

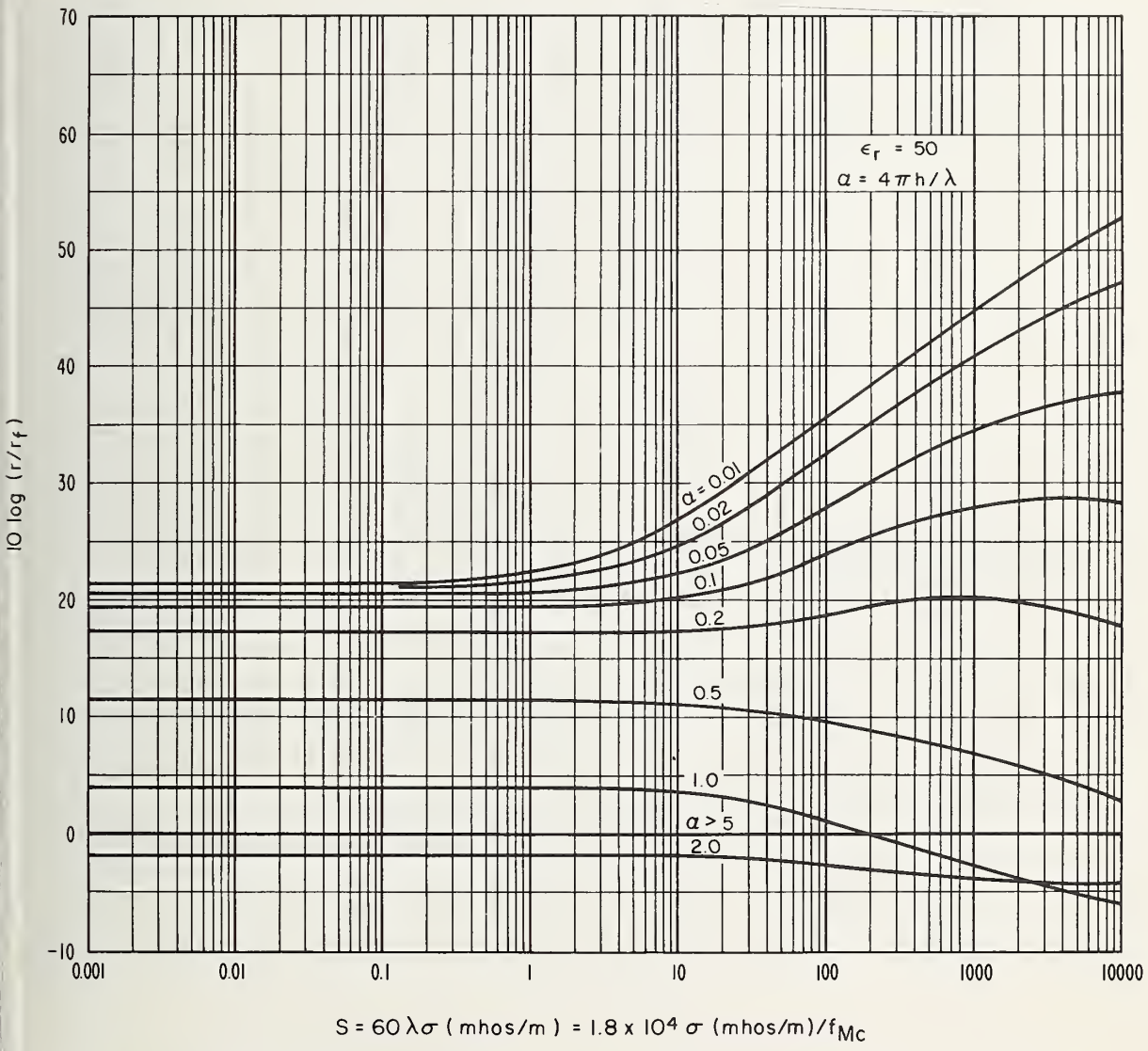

Figure A-20. Ground proximity loss $L_{t,r}$ for VMD, $\epsilon_r = 50$.

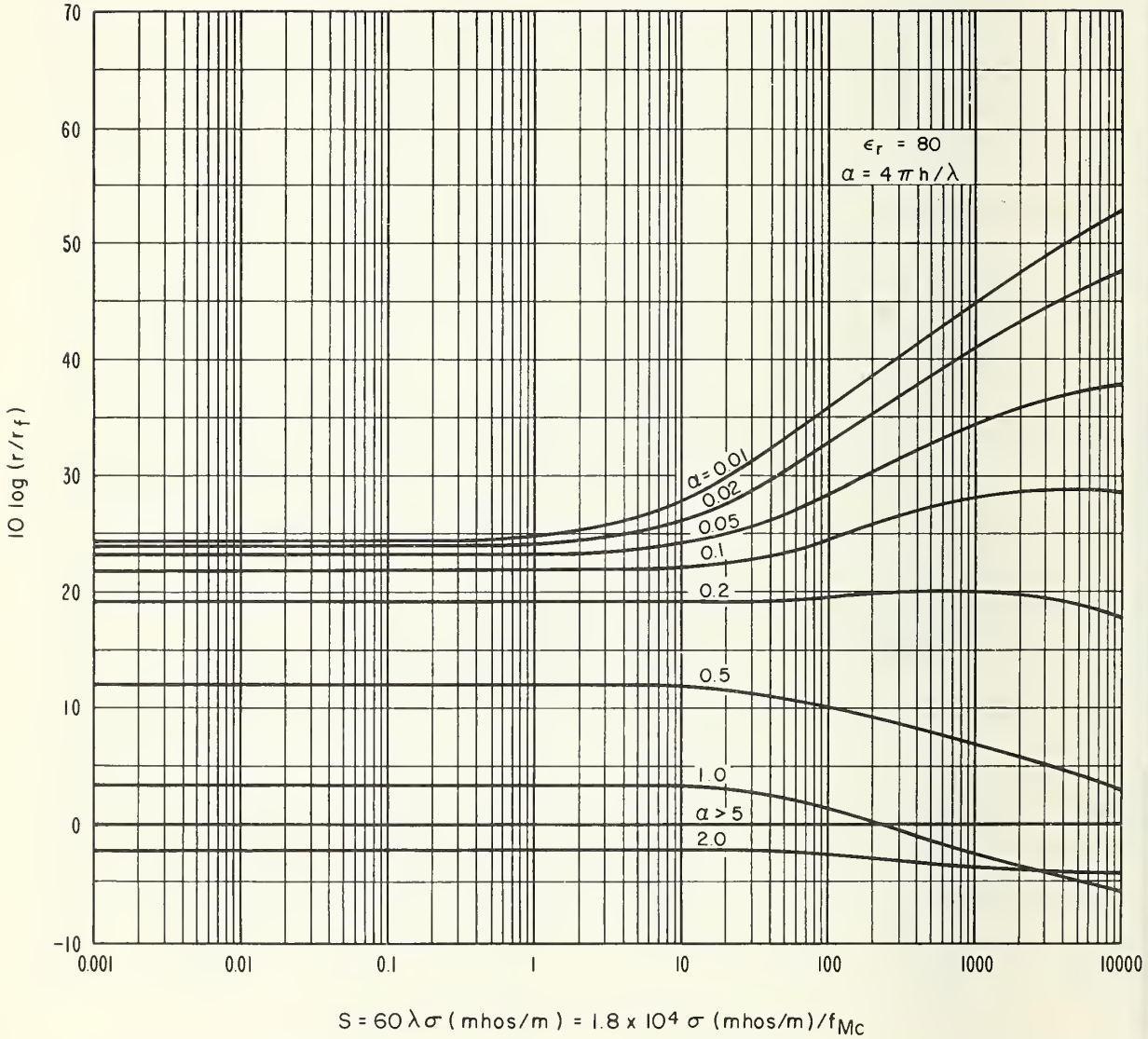

Figure A-21. Ground proximity loss $L_{t,r}$ for VMD, $\epsilon_r = 80$.

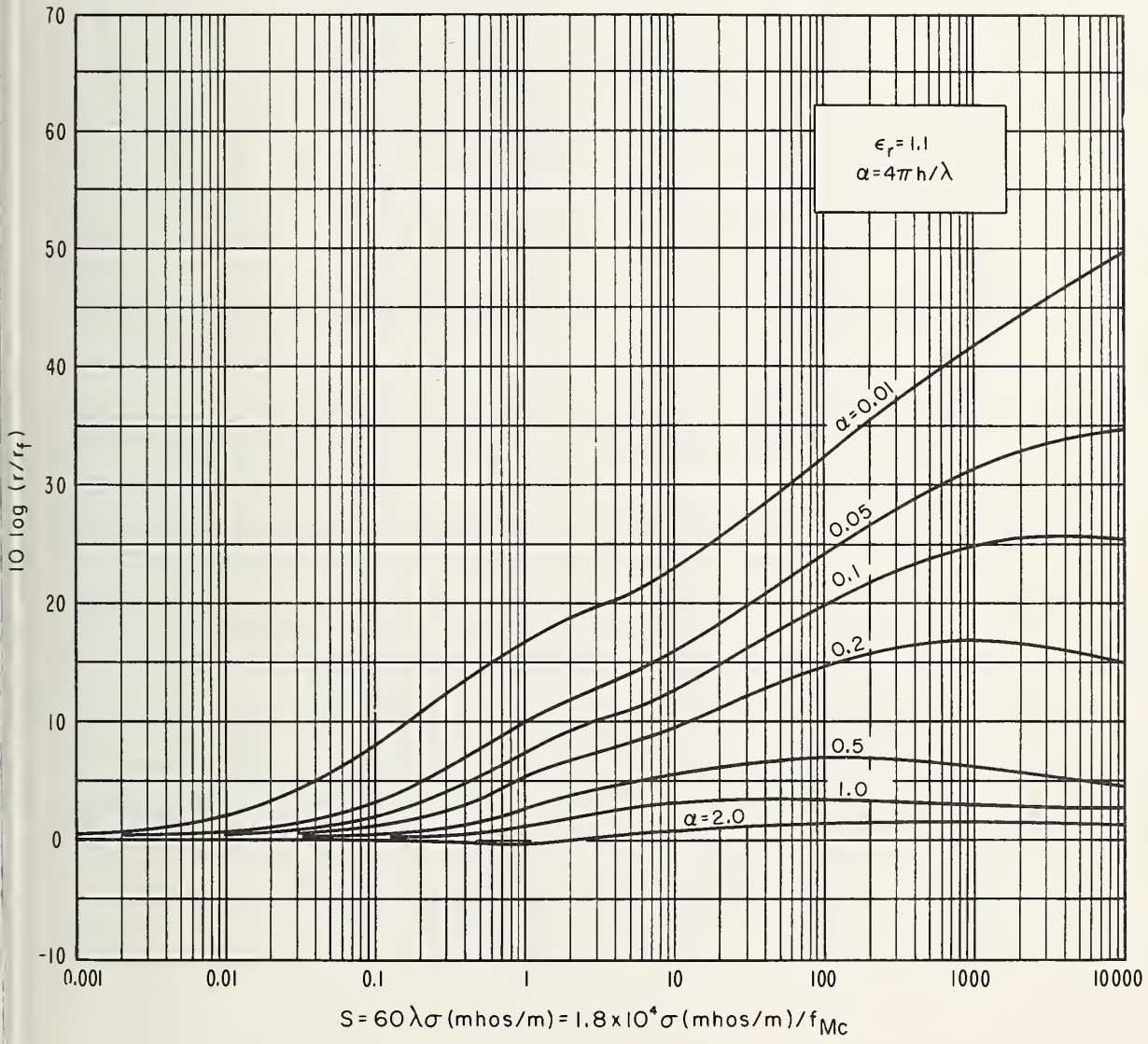

Figure A-22. Ground proximity loss $L_{t,r}$ for HMD, $\epsilon_r = 1.1$.

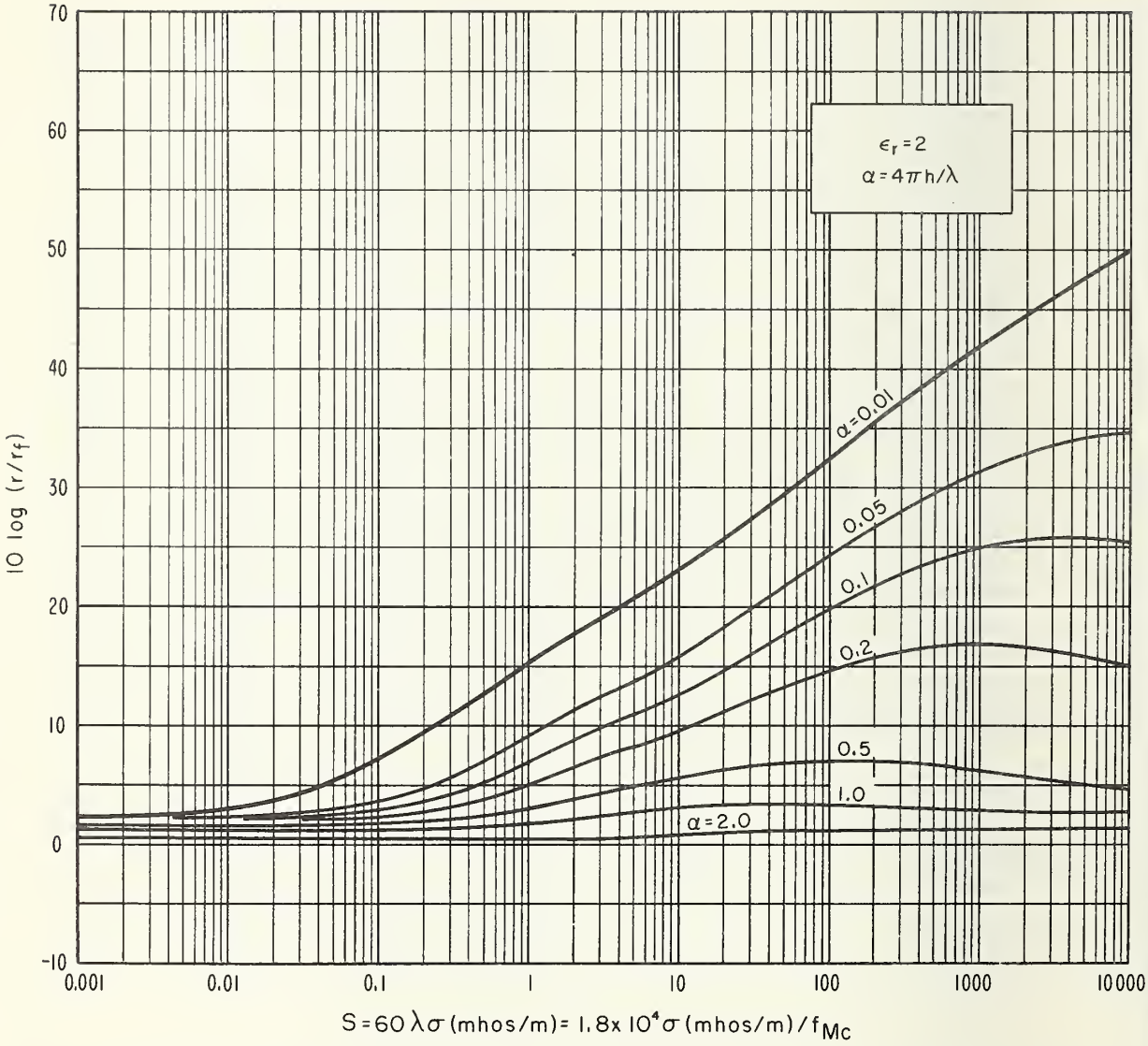

Figure A-23. Ground proximity loss $L_{t.r}$ for HMD, $\epsilon_r = 2$.

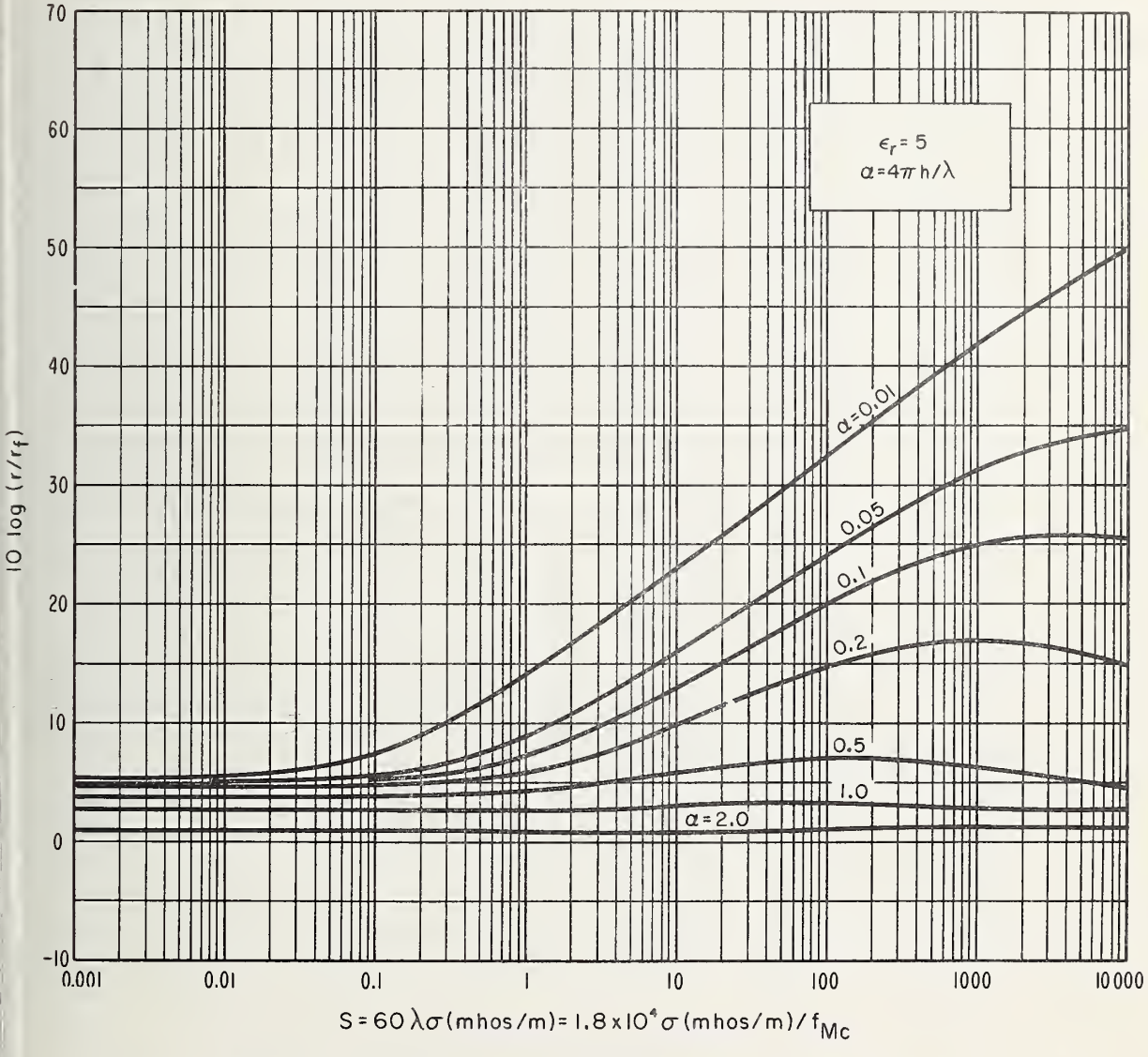

Figure A-24. Ground proximity loss $L_{t,r}$ for HMD, $\epsilon_r = 5$.

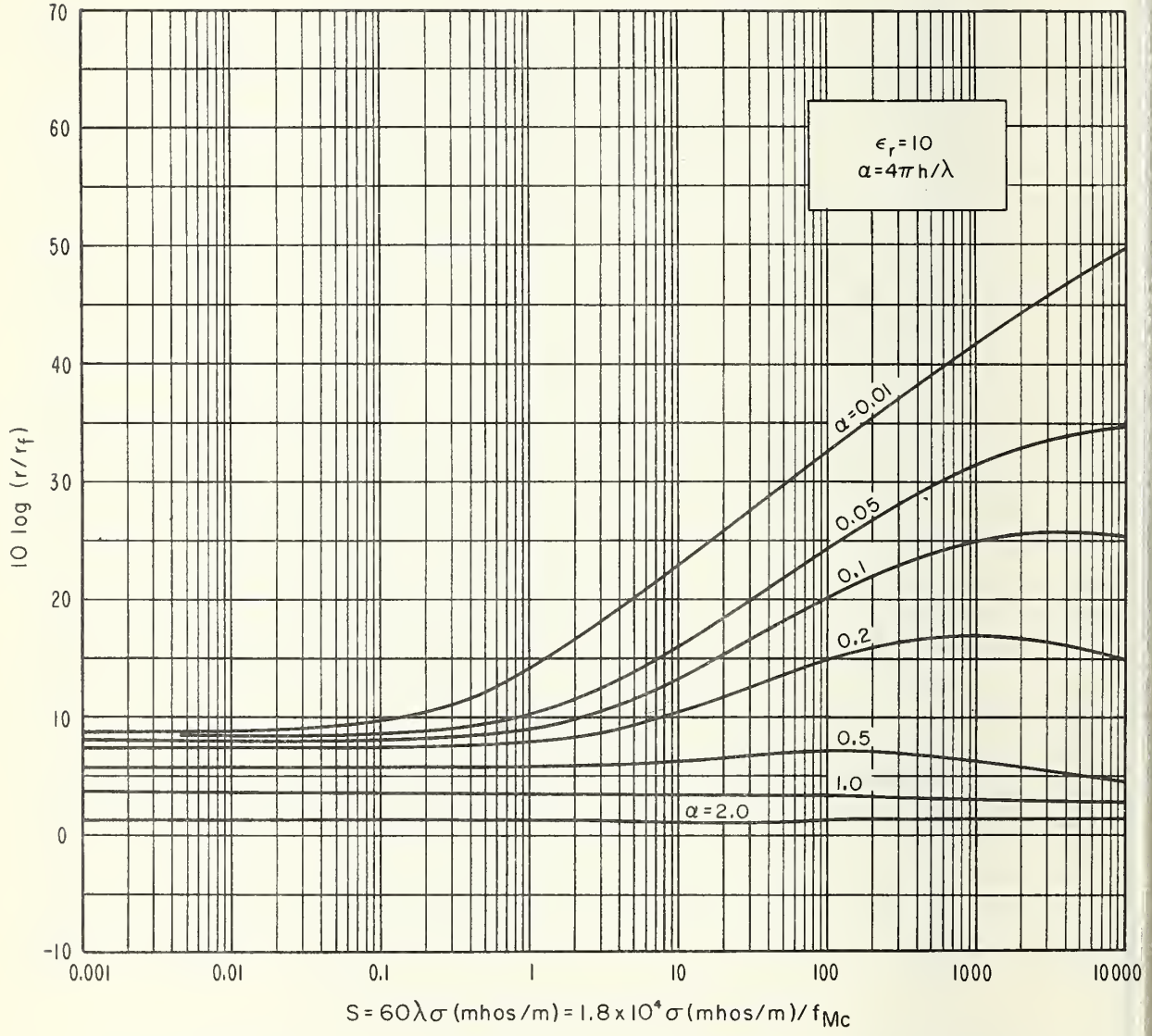

Figure A-25. Ground proximity loss $L_{t,r}$ for HMD, $\epsilon_r = 10$.

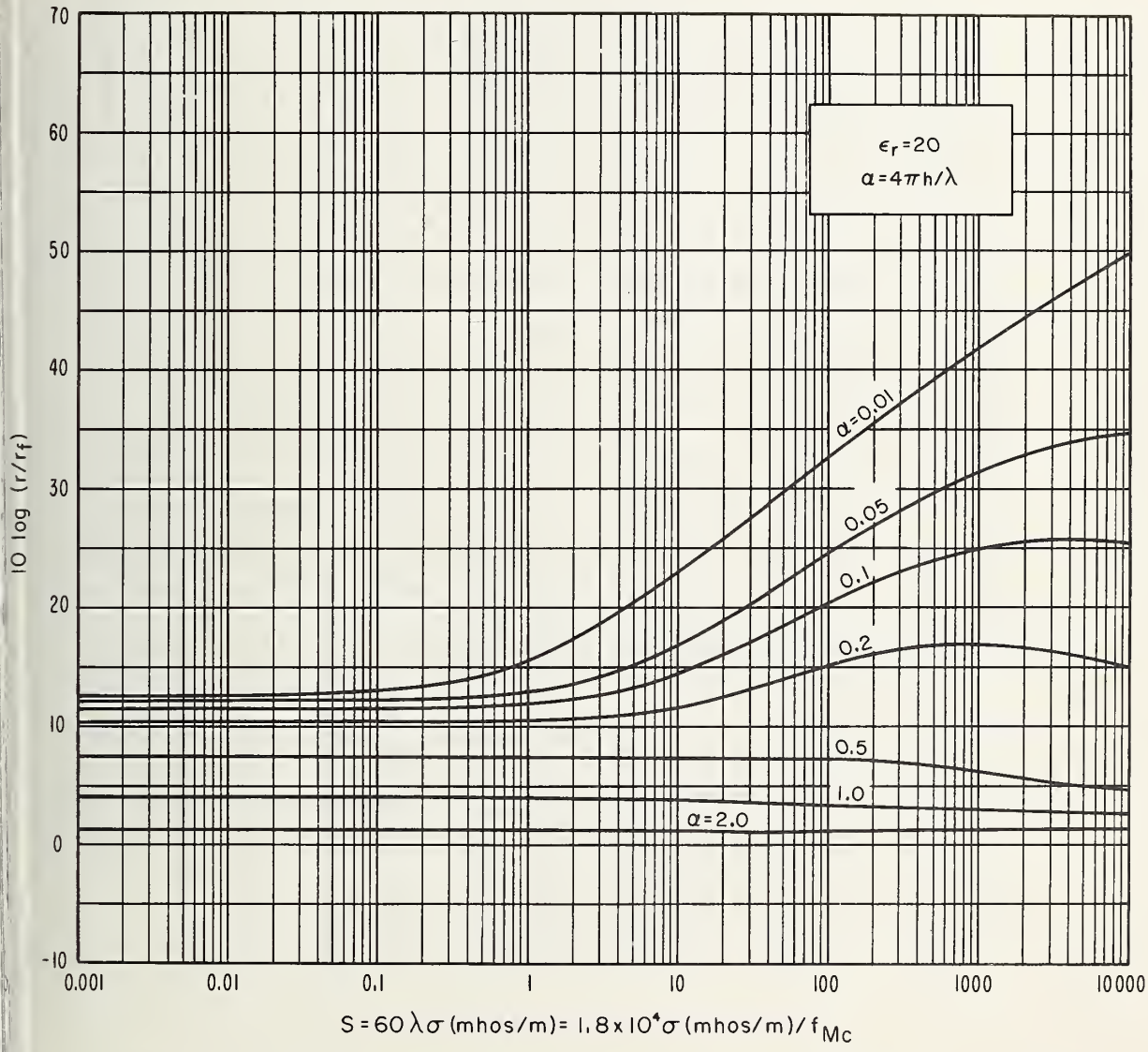

Figure A-26. Ground proximity loss $L_{t,r}$ for HMD, $\epsilon_r = 20$.

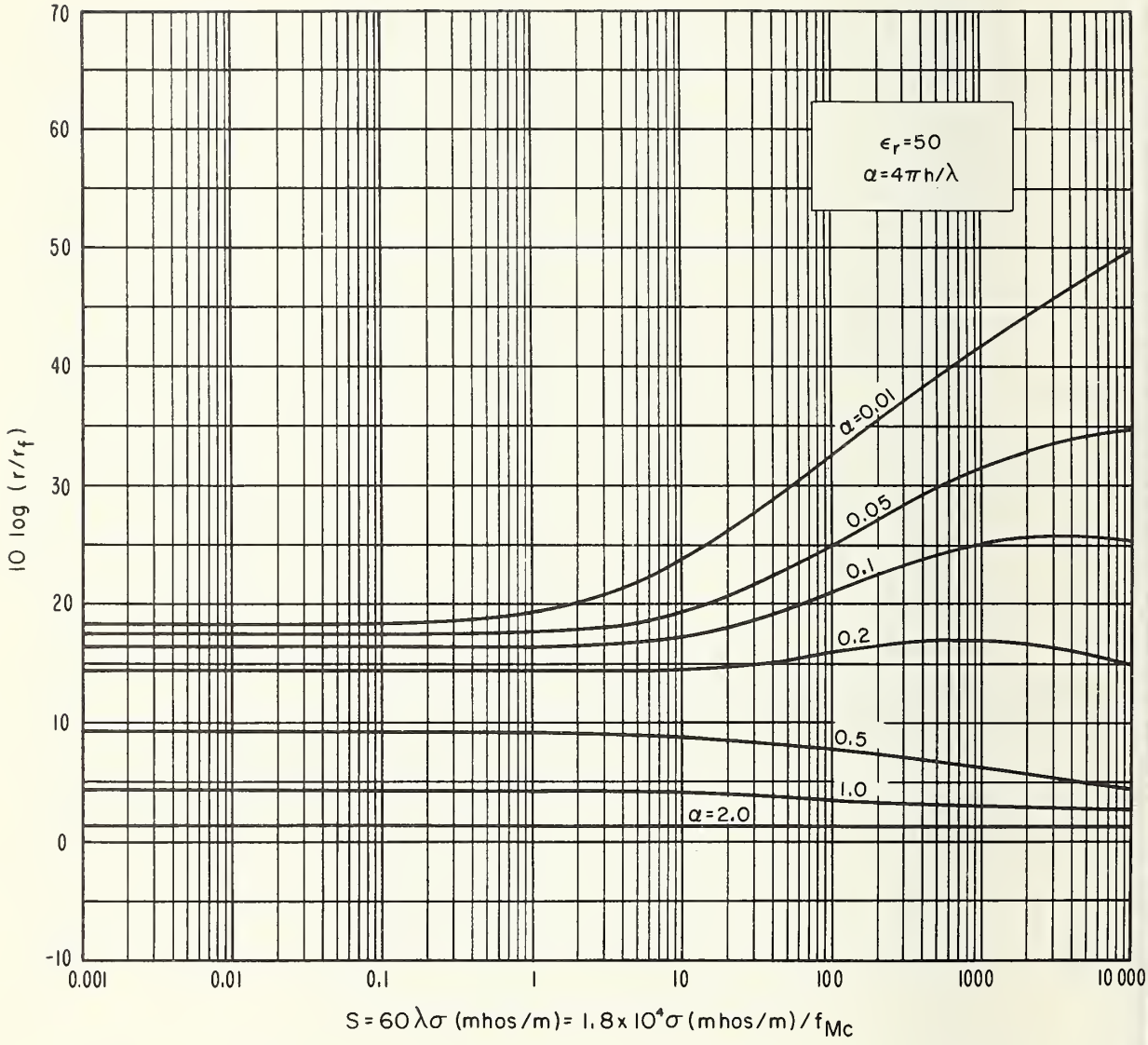

Figure A-27. Ground proximity loss $L_{t,r}$ for HMD, $\epsilon_r = 50$.

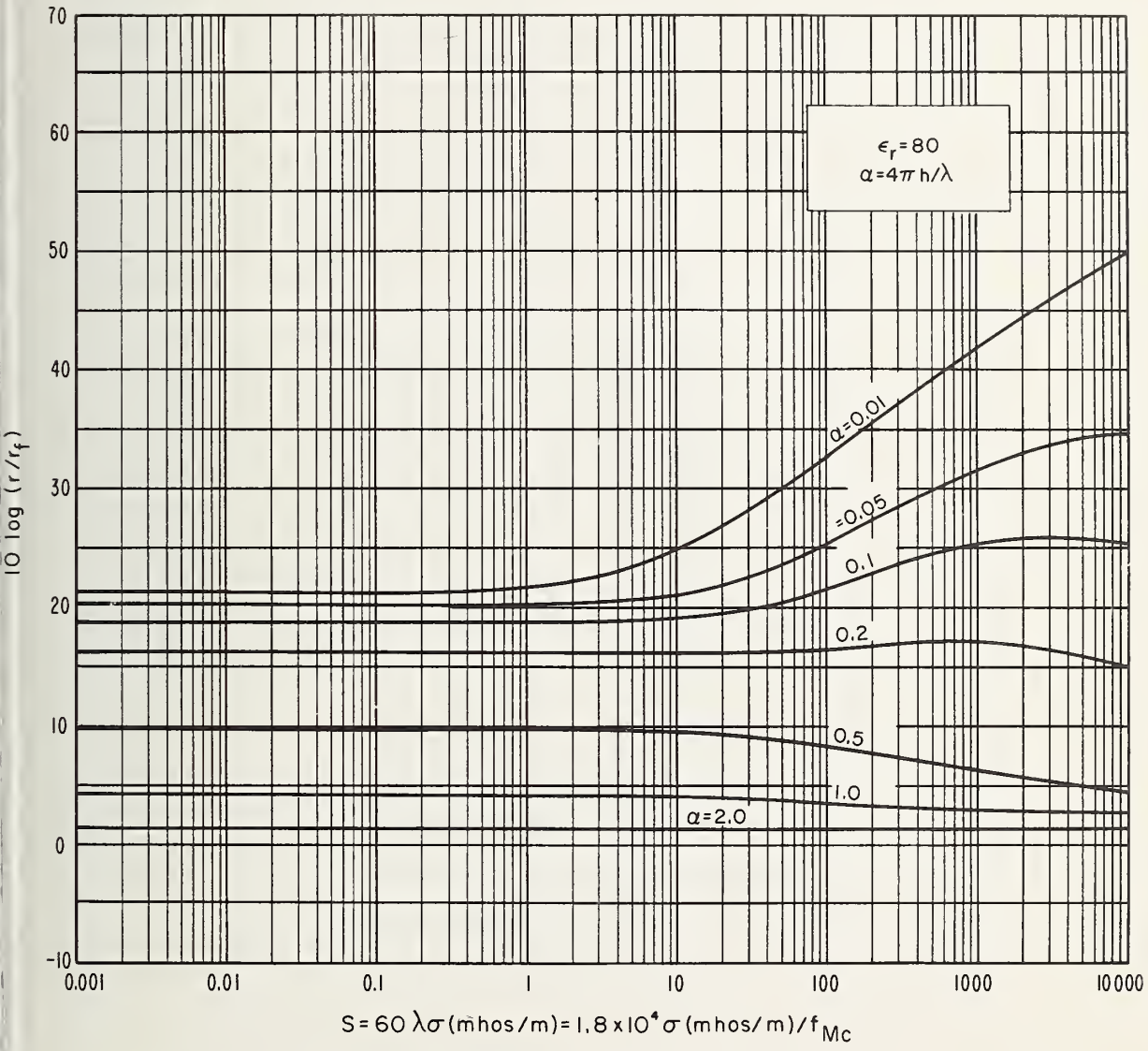

Figure A-28. Ground proximity loss $L_{t,r}$ for HMD, $\epsilon_r = 80$.

13. GRAPHS OF NORMALIZED INPUT IMPEDANCE CHANGE, $\Delta Z/r_f$

for

Vertical Electric Dipoles (VED)

Horizontal Electric Dipoles (HED)

Vertical Magnetic Dipoles (VMD)

Horizontal Magnetic Dipoles (HMD)

$$|N| = \left[\epsilon_r^2 + s^2\right]^{1/4}, \quad \phi/2 = (1/2)\tan^{-1}(s/\epsilon_r) ,$$

$s = 60\lambda\sigma$(mhos/m), $\alpha = (2h)(2\pi/\lambda)$,

ϵ_r: relative dielectric constant of ground

σ(mhos/m): conductivity of ground

h: height in meters of antenna above ground

λ: wavelength in meters

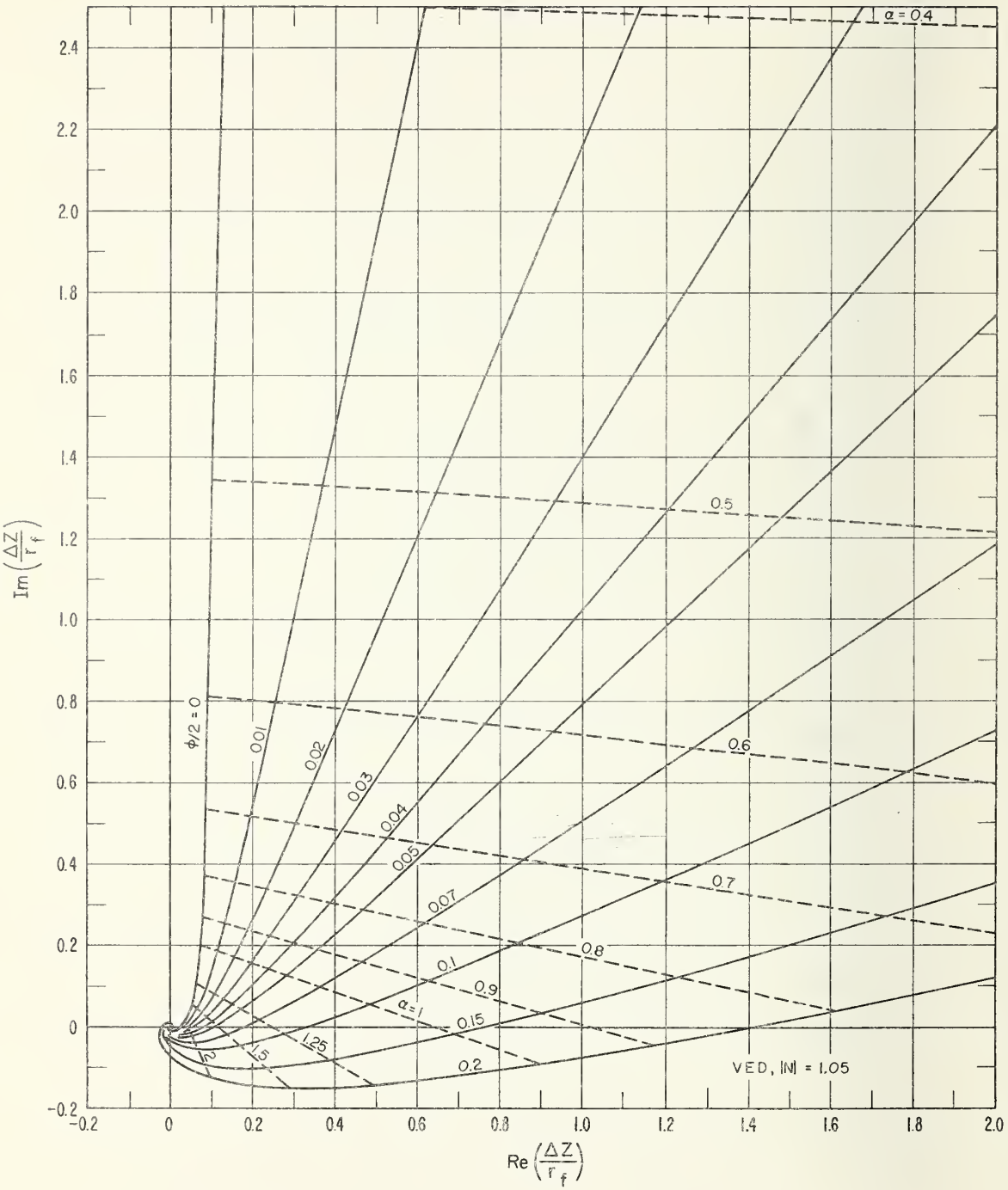

Figure A-29. Normalized input impedance change for VED, $|N| = 1.05$.

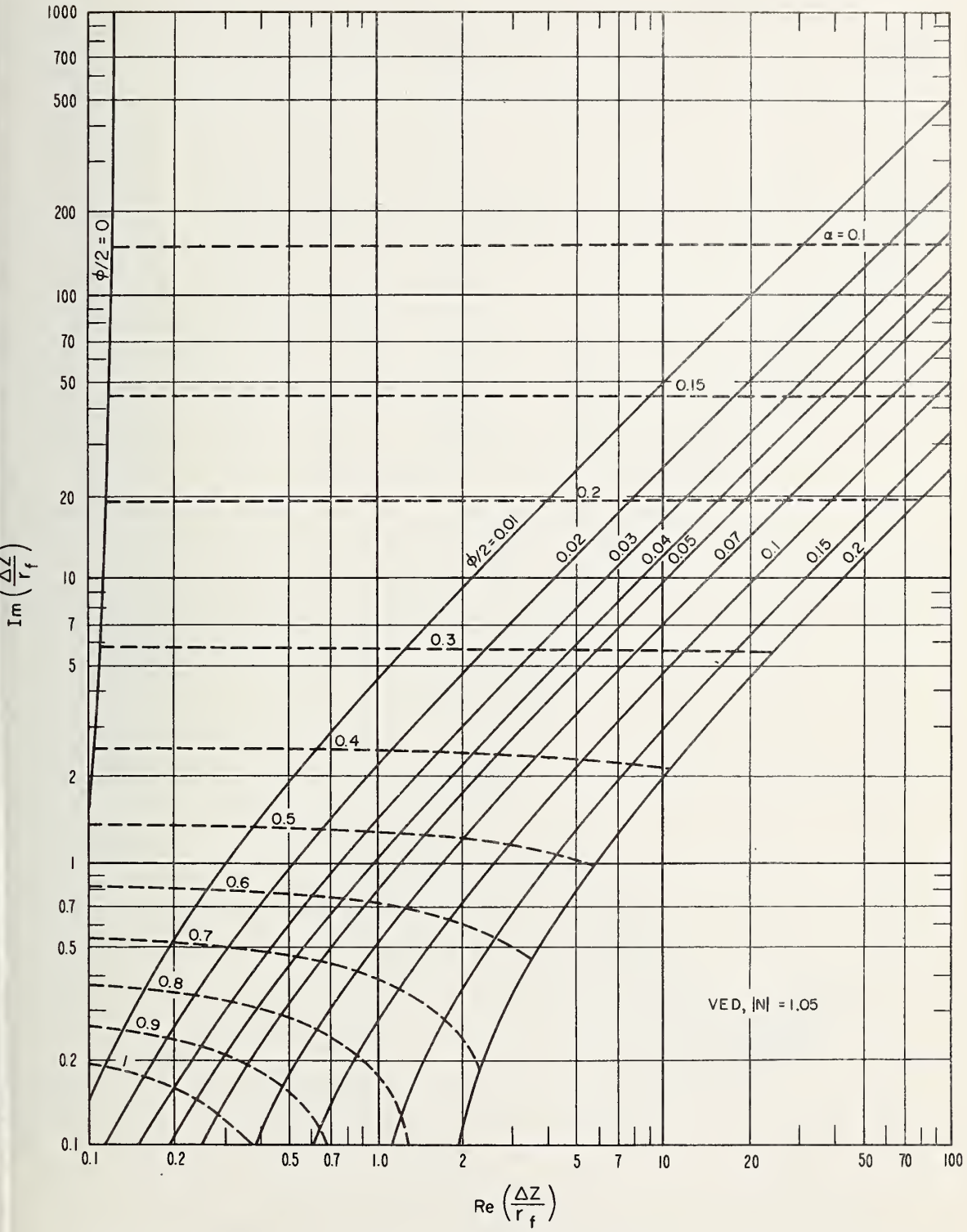

Figure A-30. Normalized input impedance change for VED, $|N| = 1.05$.

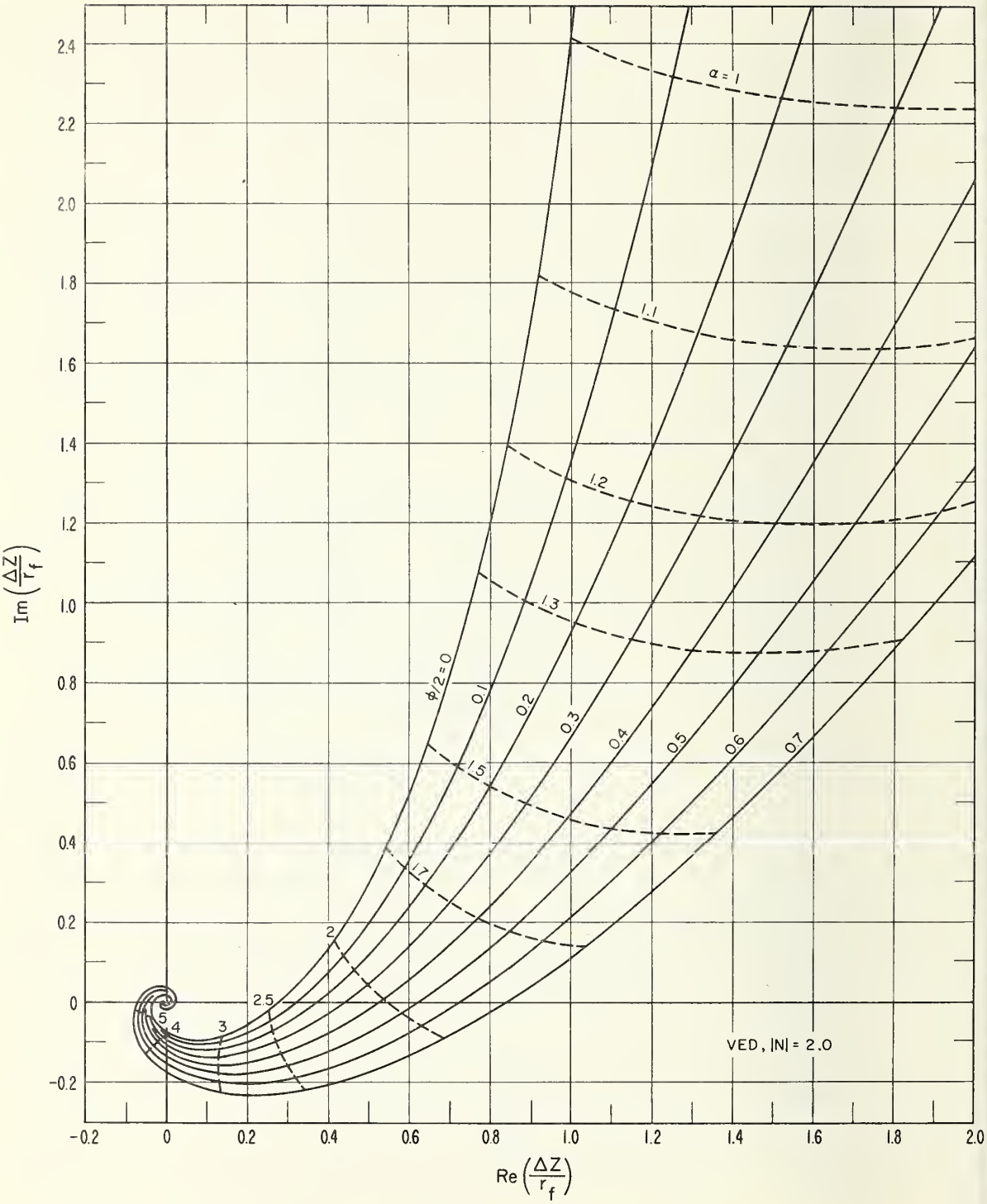

Figure A-31. Normalized input impedance change for VED, $|N| = 2$.

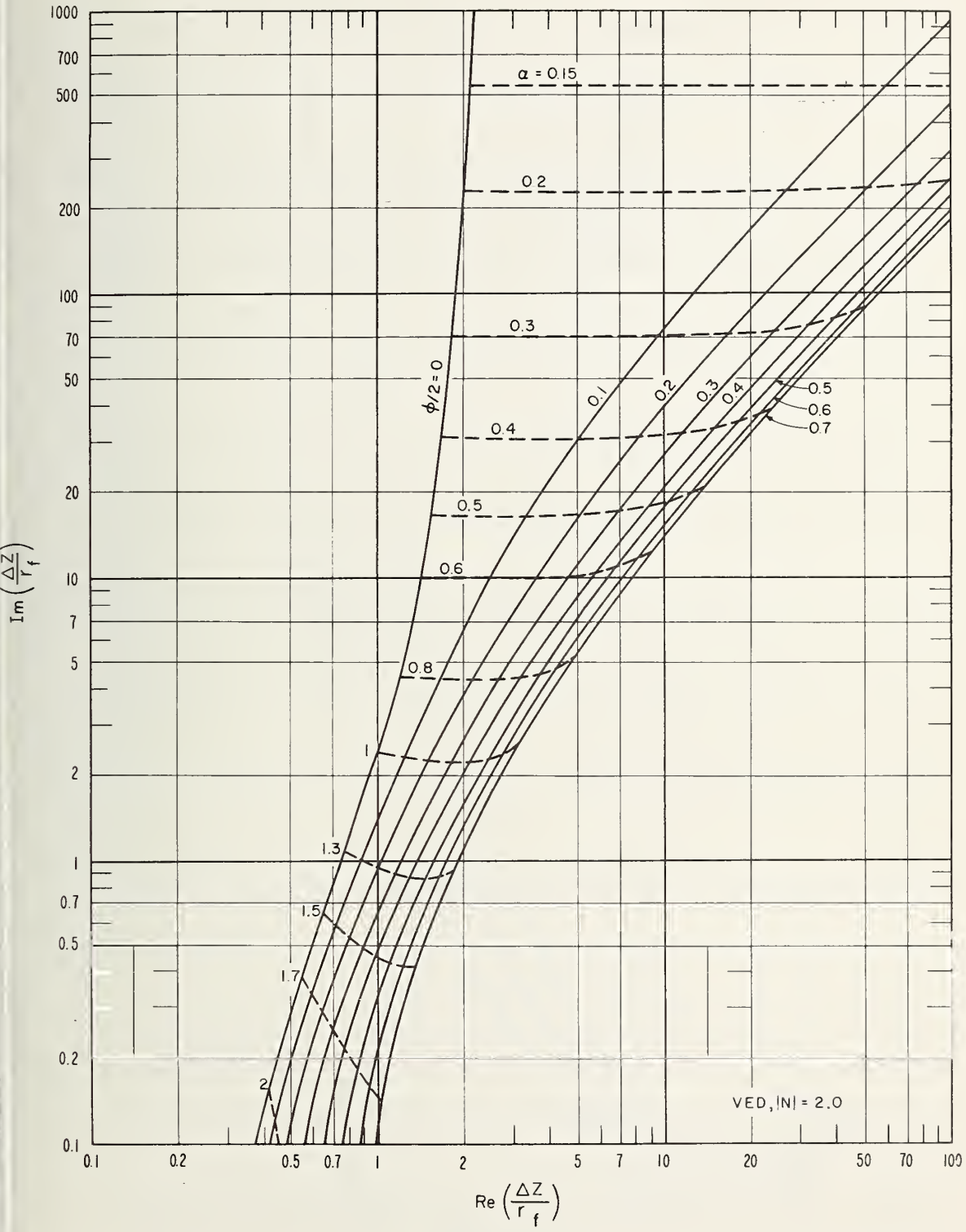

Figure A-32. Normalized input impedance change for VED, $|N| = 2$.

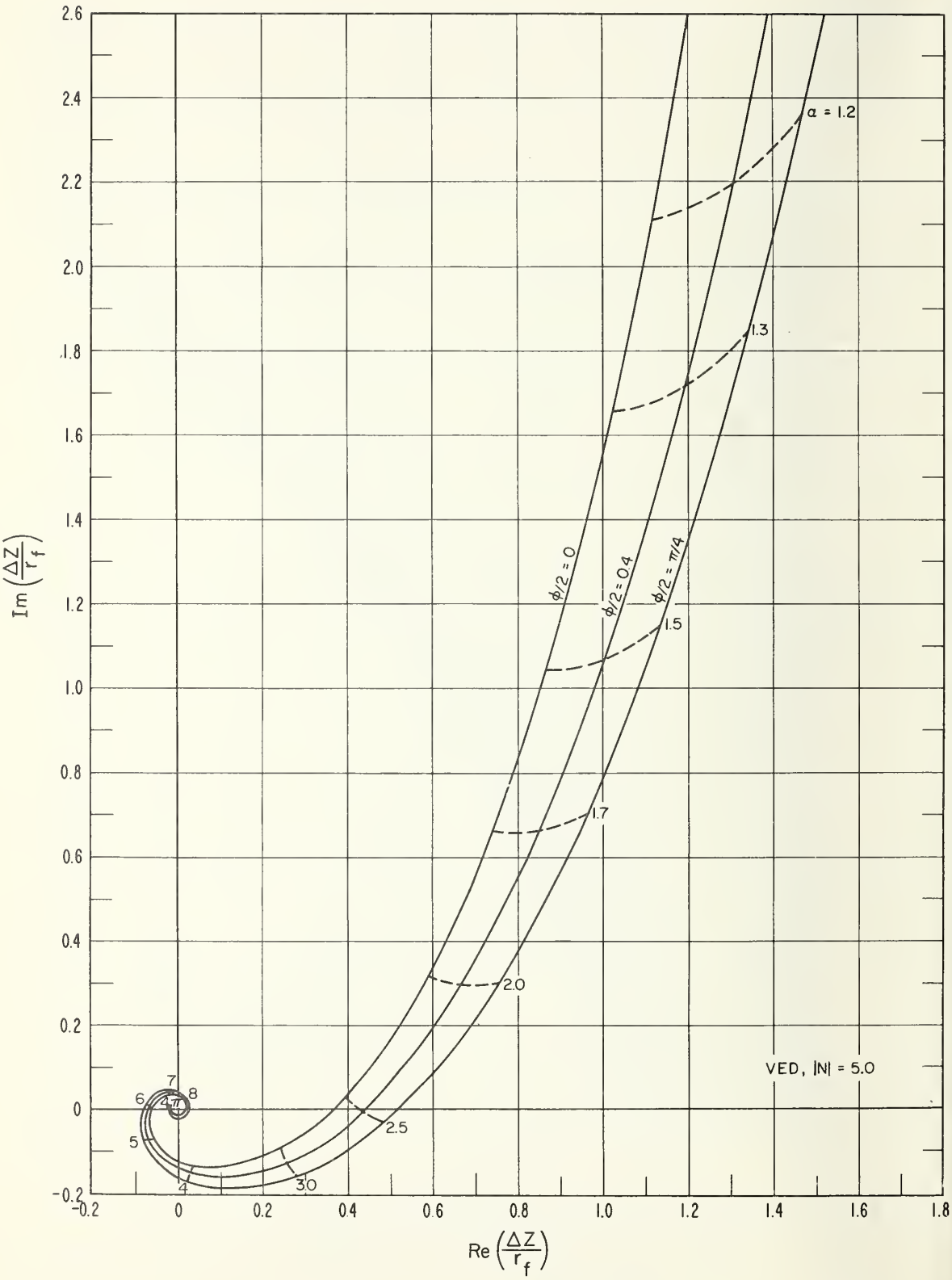

Figure A-33. Normalized input impedance change for VED, $|N| = 5$.

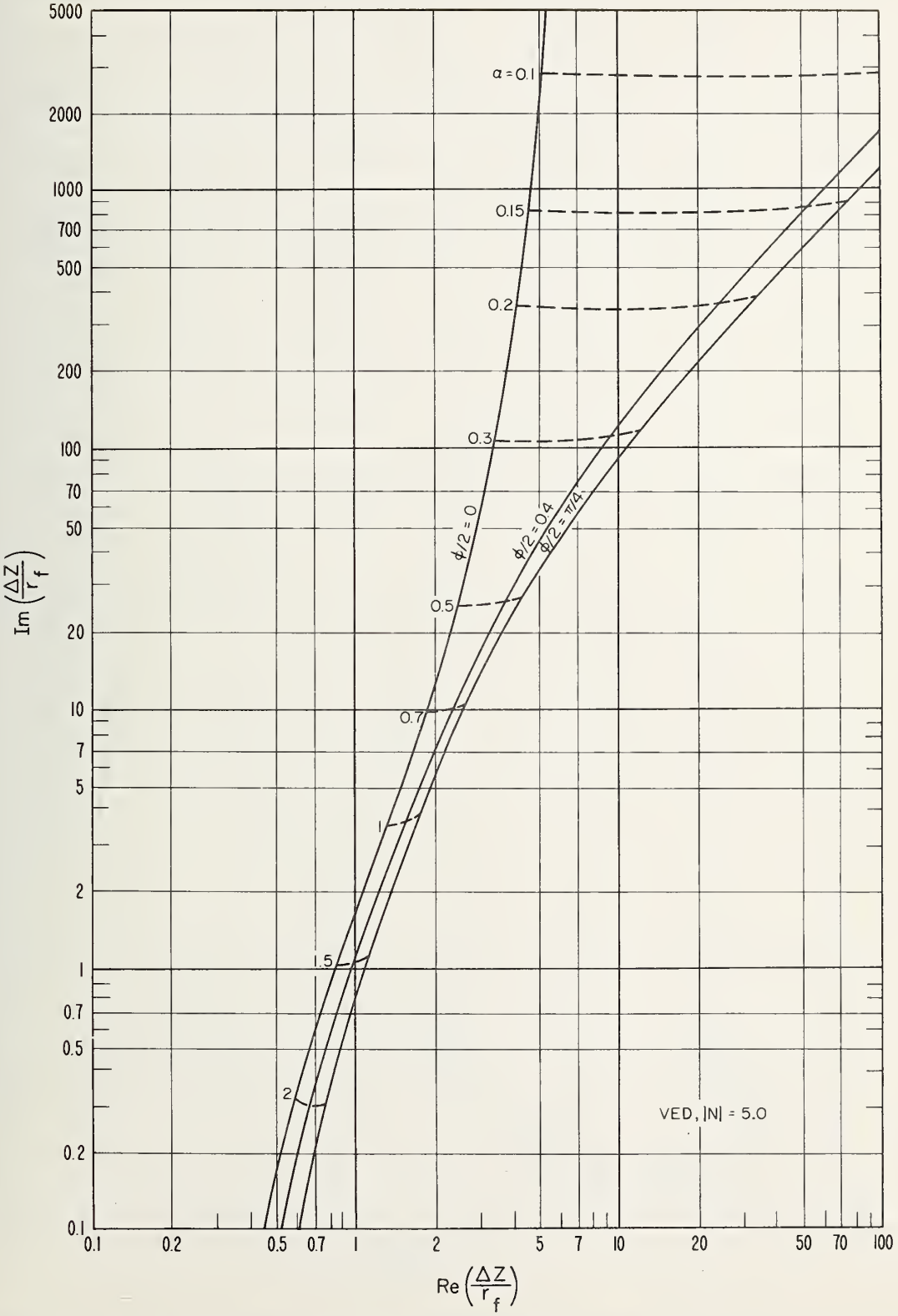

Figure A-34. Normalized input impedance change for VED, $|N| = 5$.

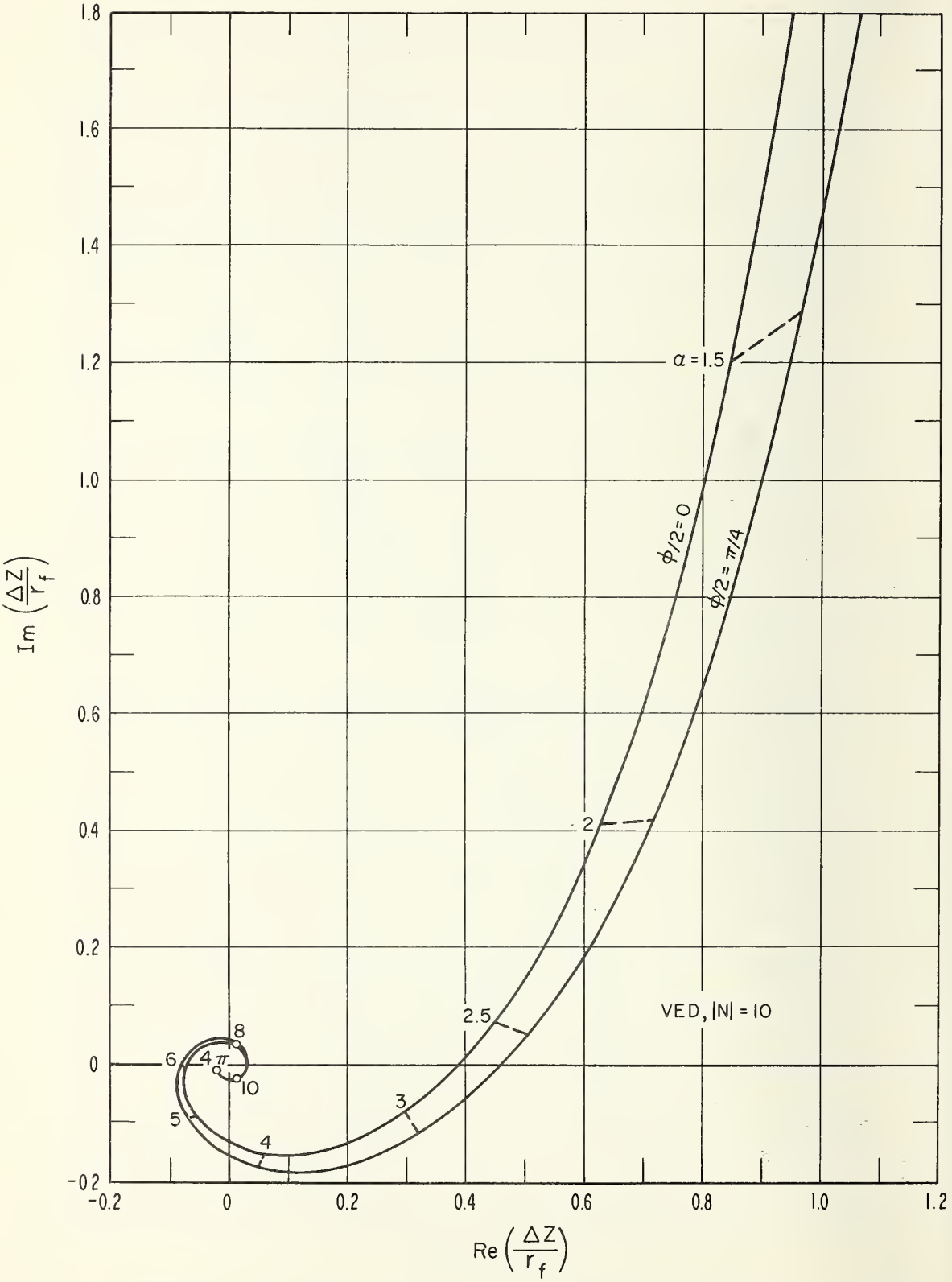

Figure A-35. Normalized input impedance change for VED, $|N| = 10$.

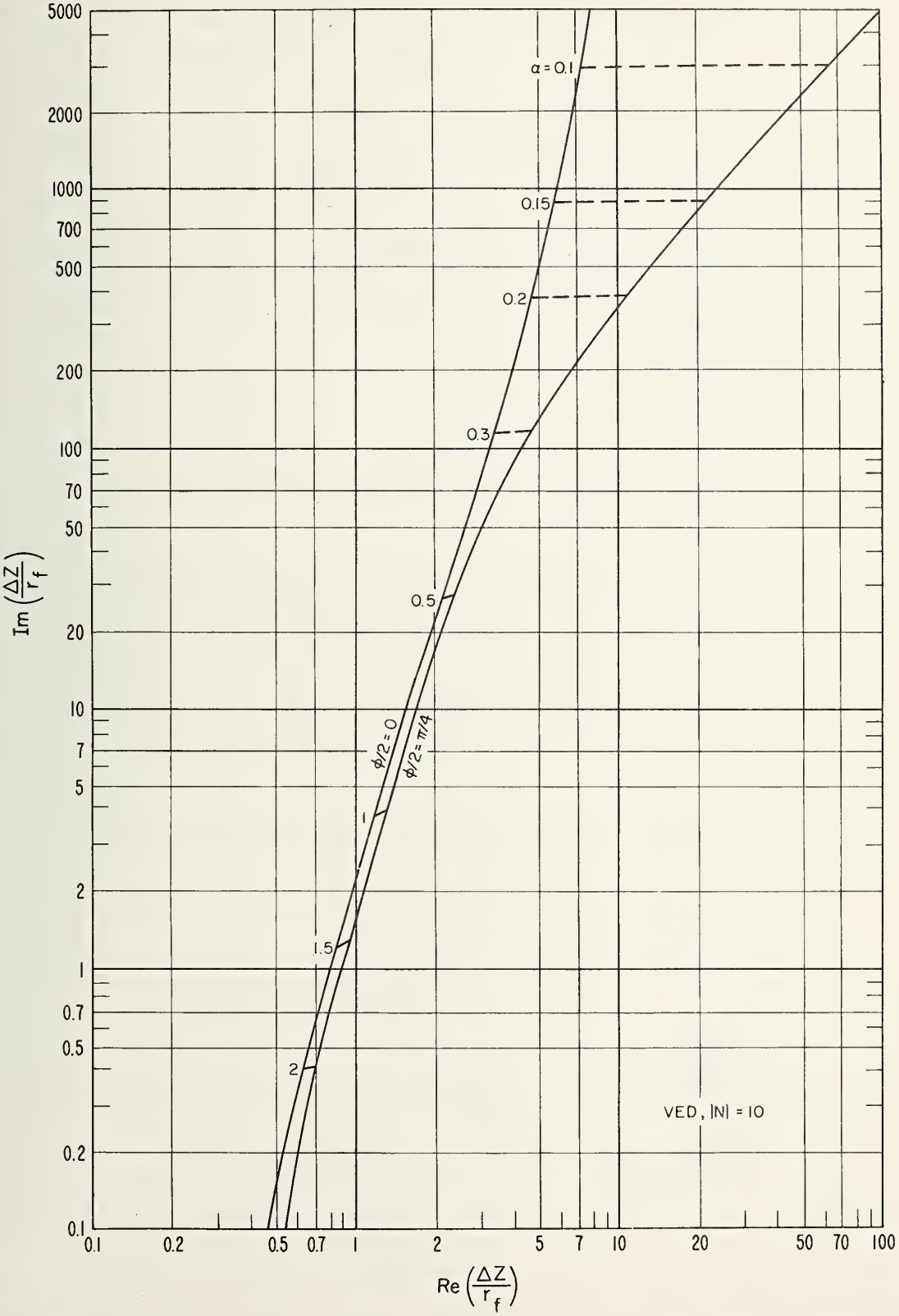

Figure A-36. Normalized input impedance change for VED, $|N| = 10$.

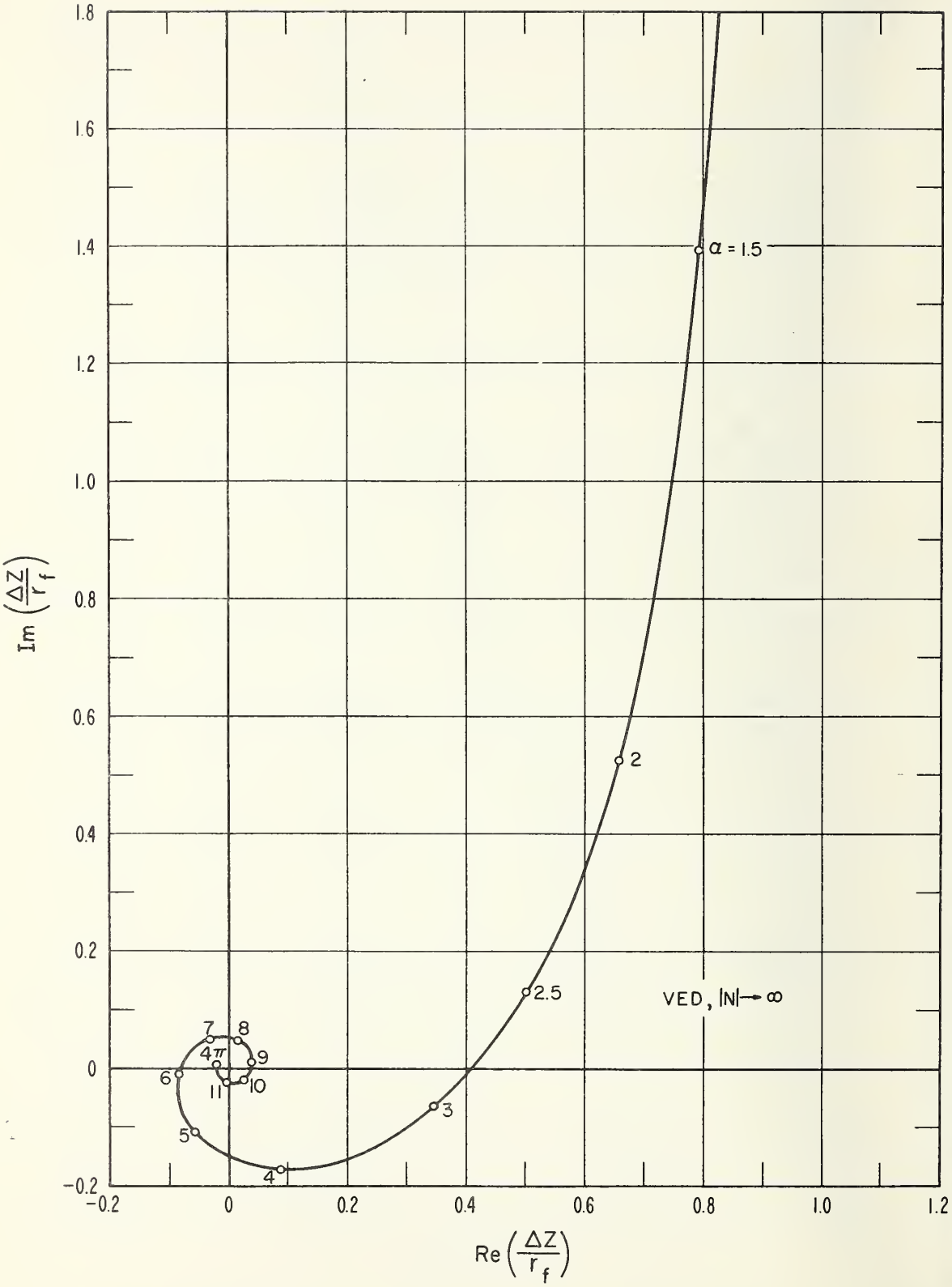

Figure A-37. Normalized input impedance change for VED, $|N| \to \infty$.

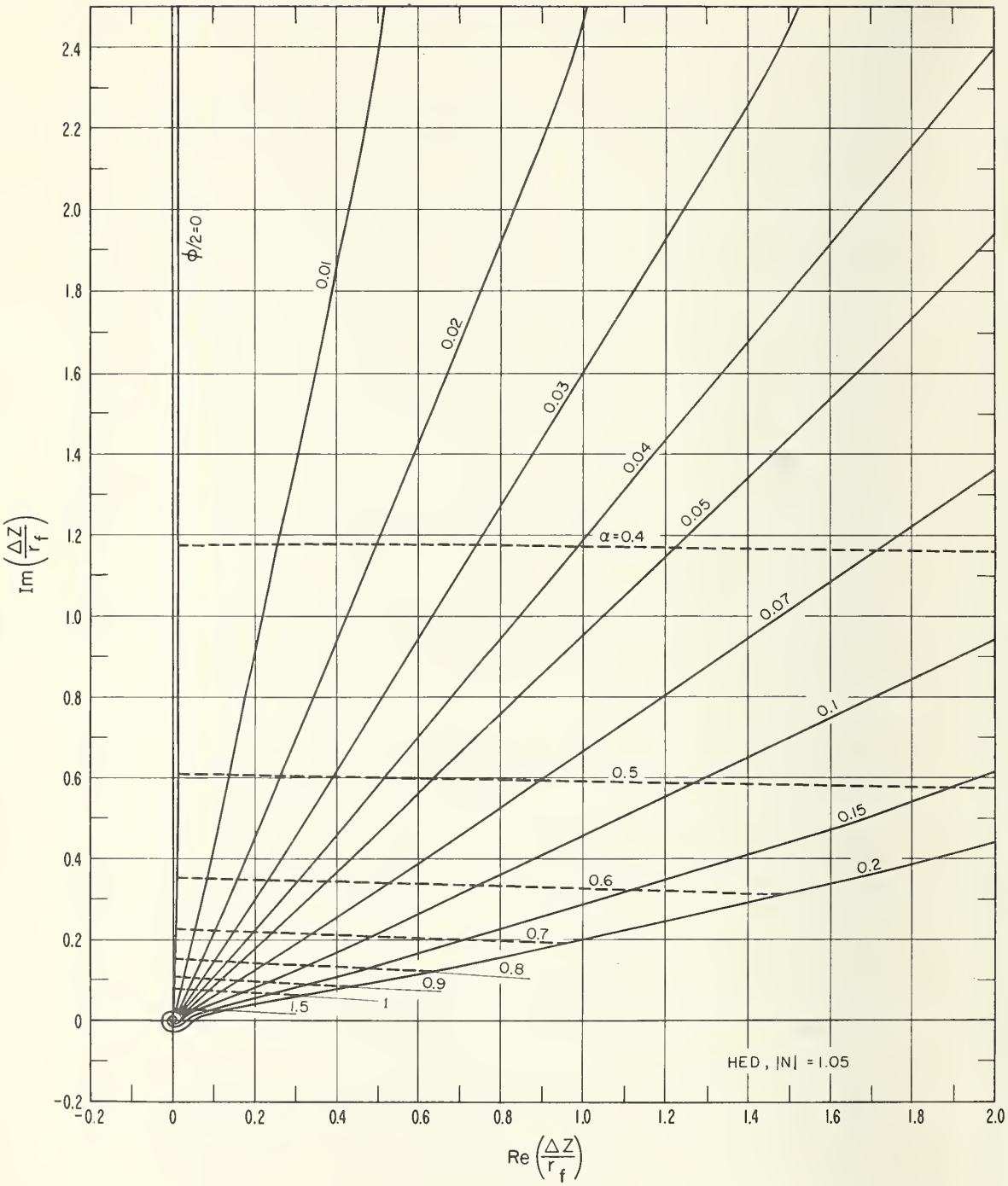

Figure A-38. Normalized input impedance change for HED, $|N| = 1.05$.

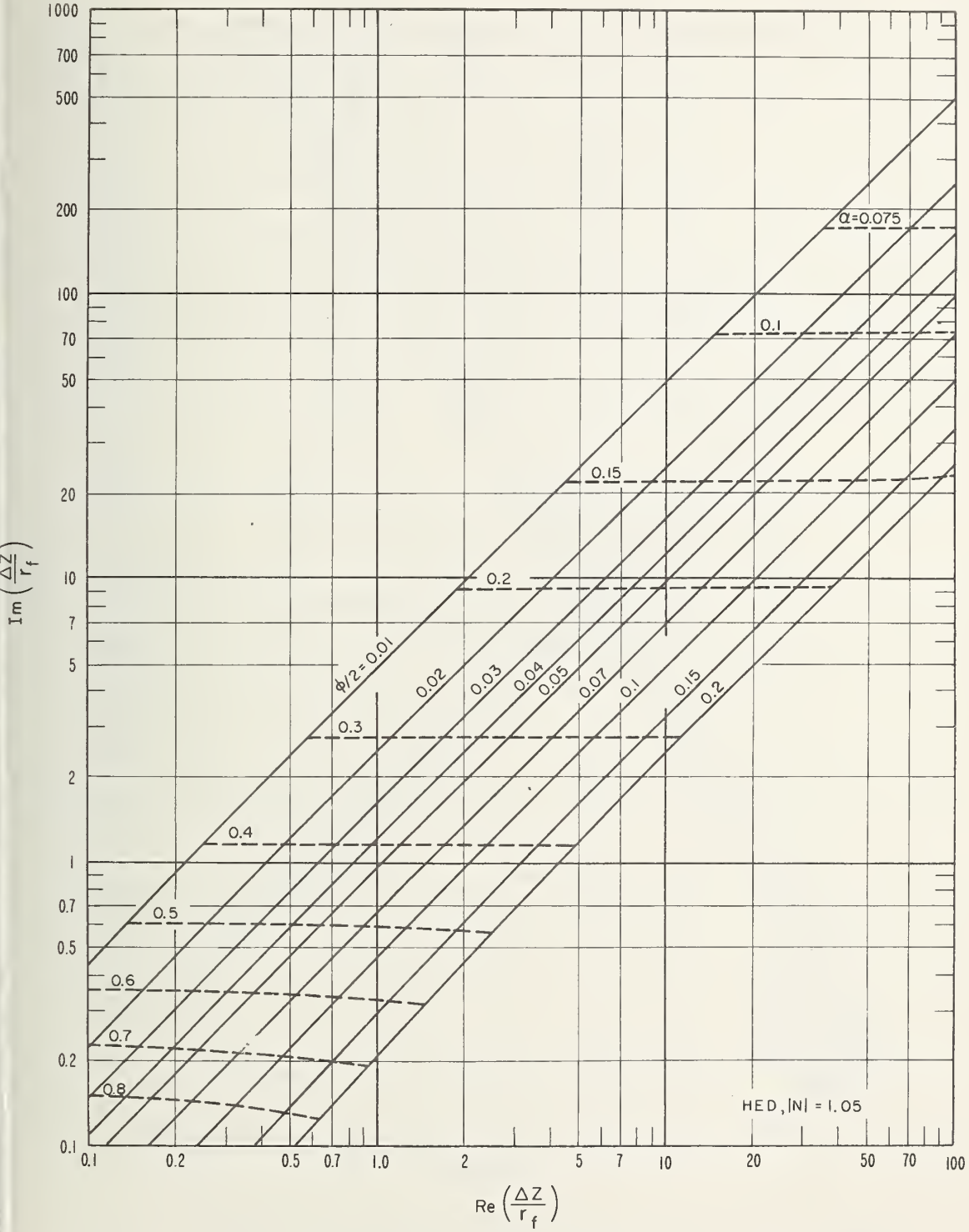

Figure A-39. Normalized input impedance change for HED, $|N| = 1.05$.

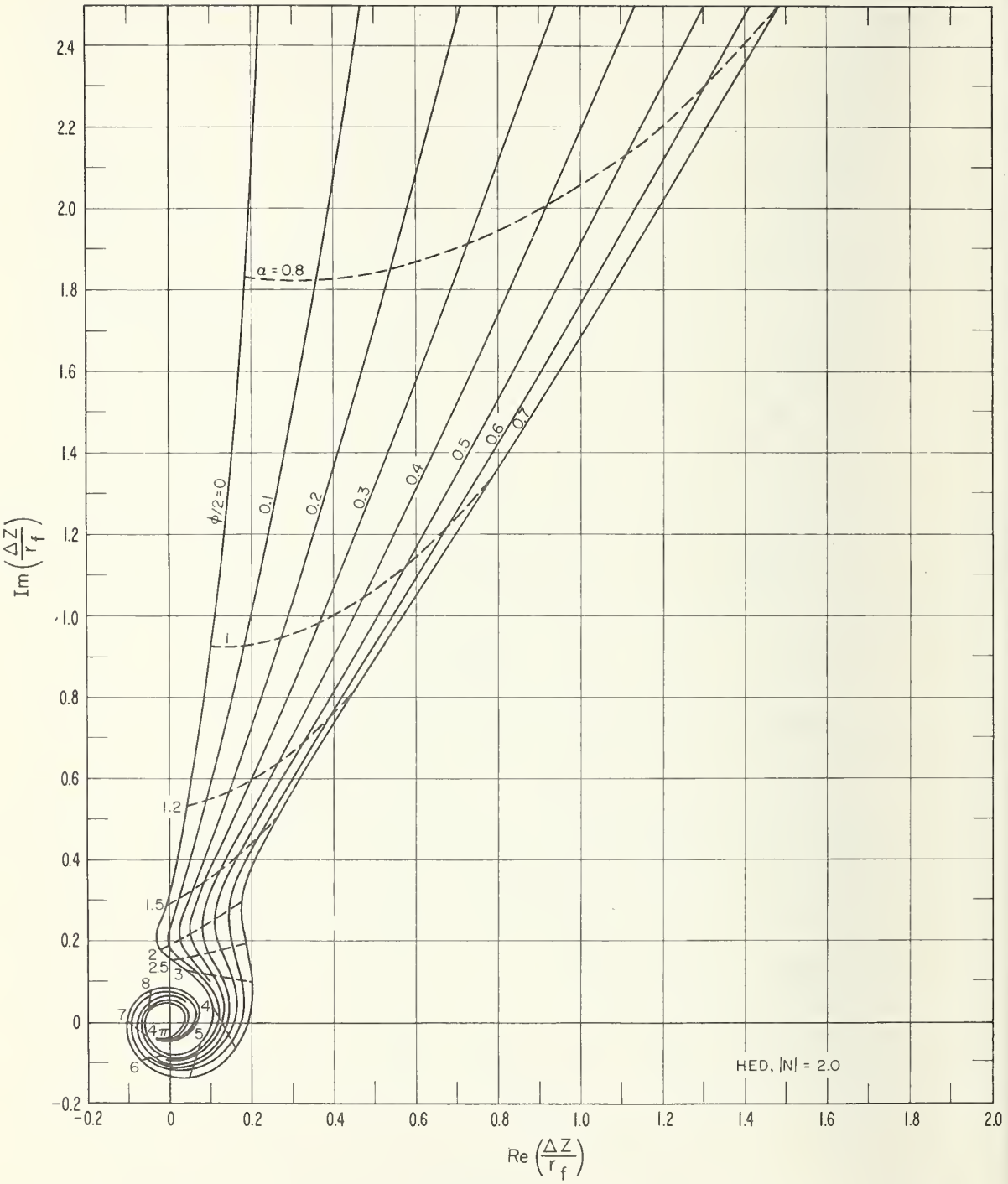

Figure A-40. Normalized input impedance change for HED, $|N| = 2$.

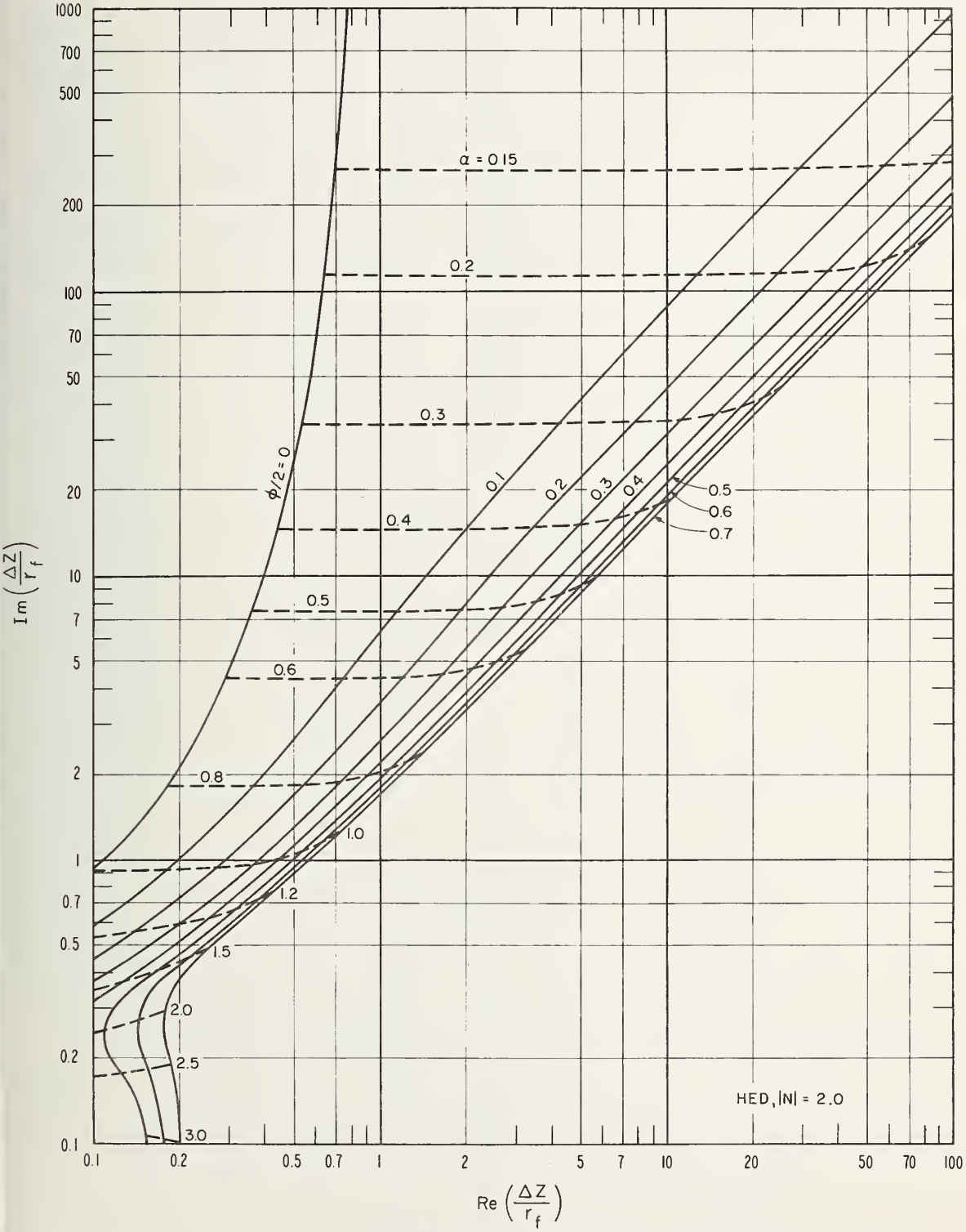

Figure A-41. Normalized input impedance change for HED, $|N| = 2$.

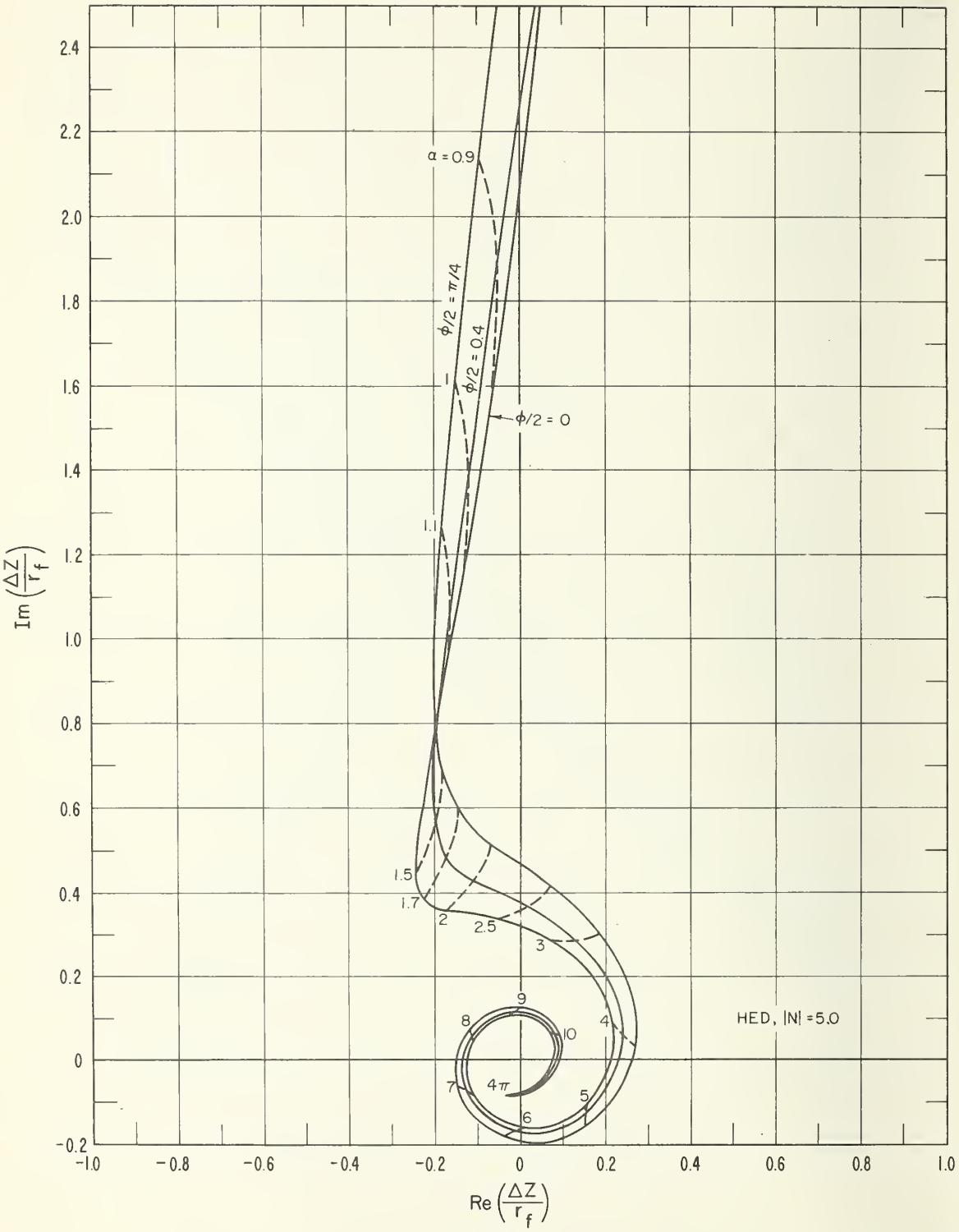

Figure A-42. Normalized input impedance change for HED, $|N| = 5$.

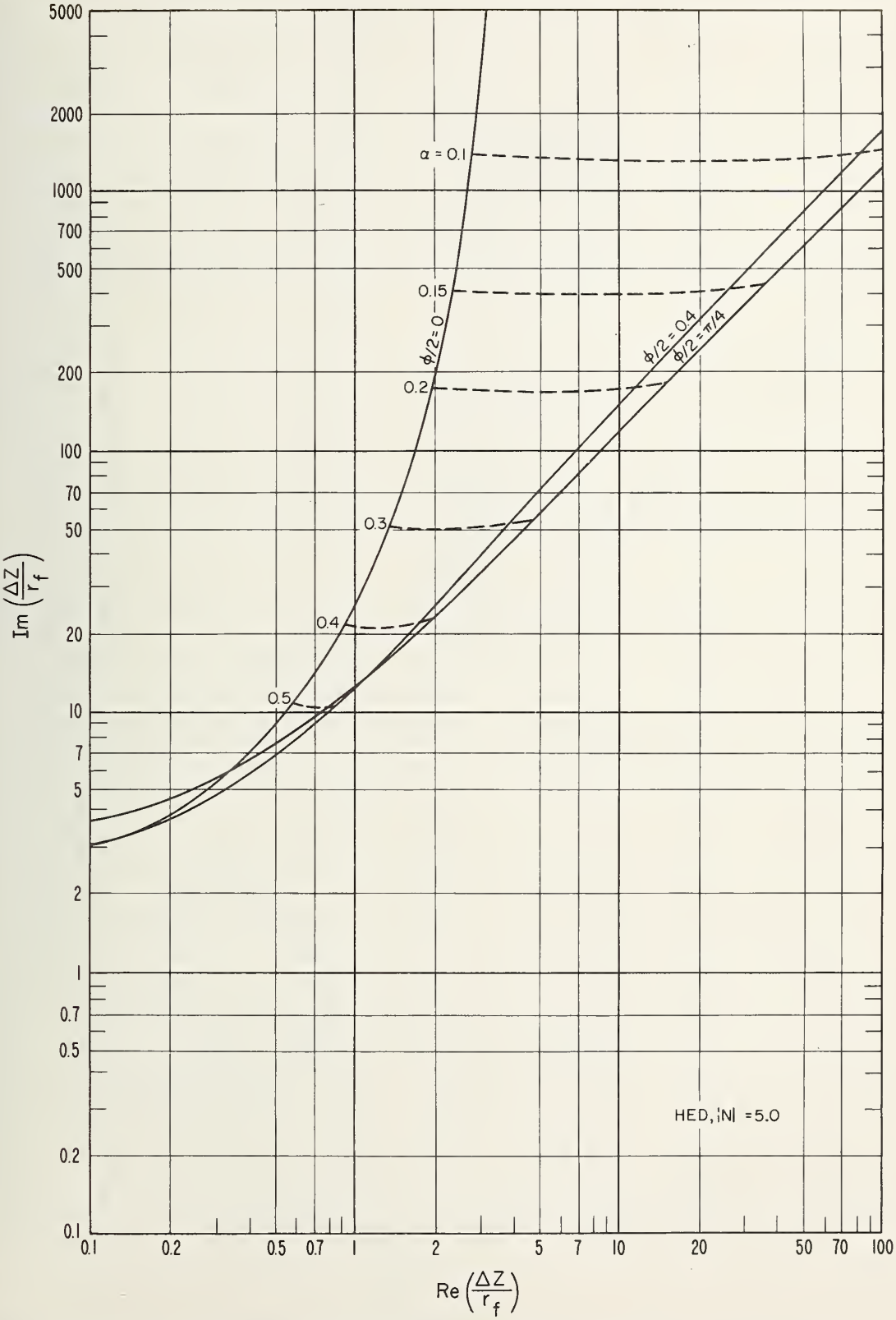

Figure A-43. Normalized input impedance change for HED, $|N| = 5$.

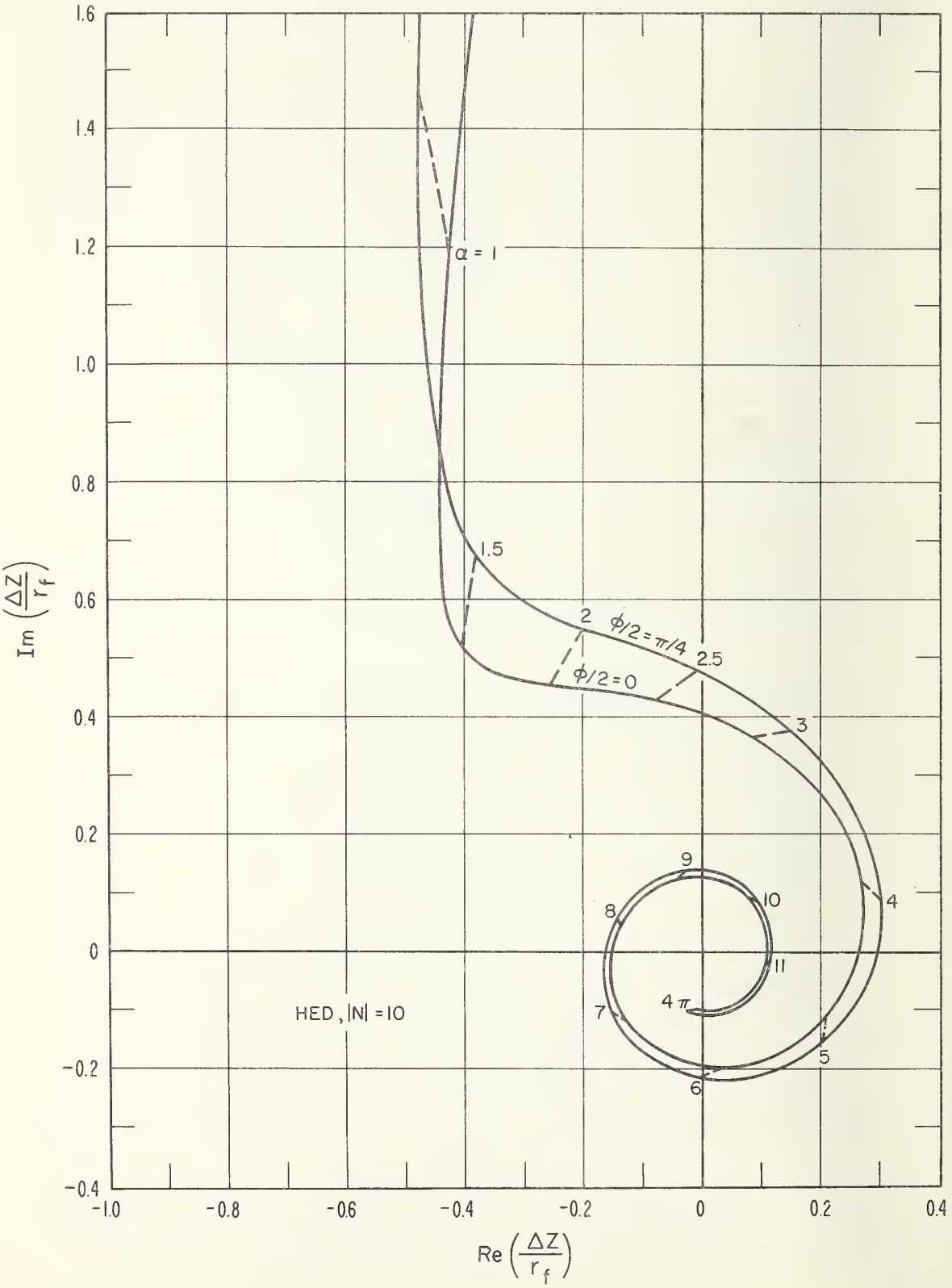

Figure A-44. Normalized input impedance change for HED, $|N| = 10$.

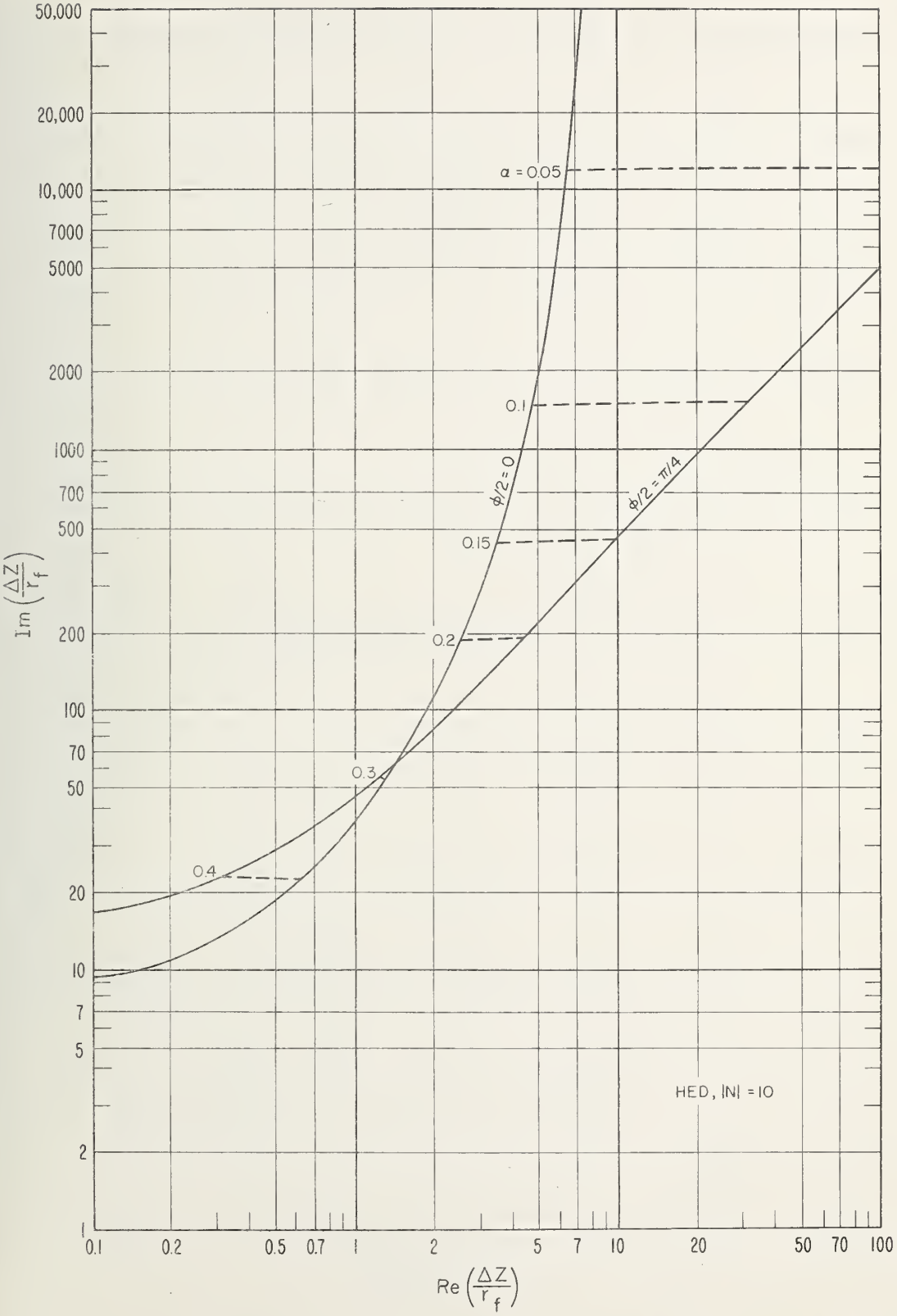

Figure A-45. Normalized input impedance change for HED, $|N| = 10$.

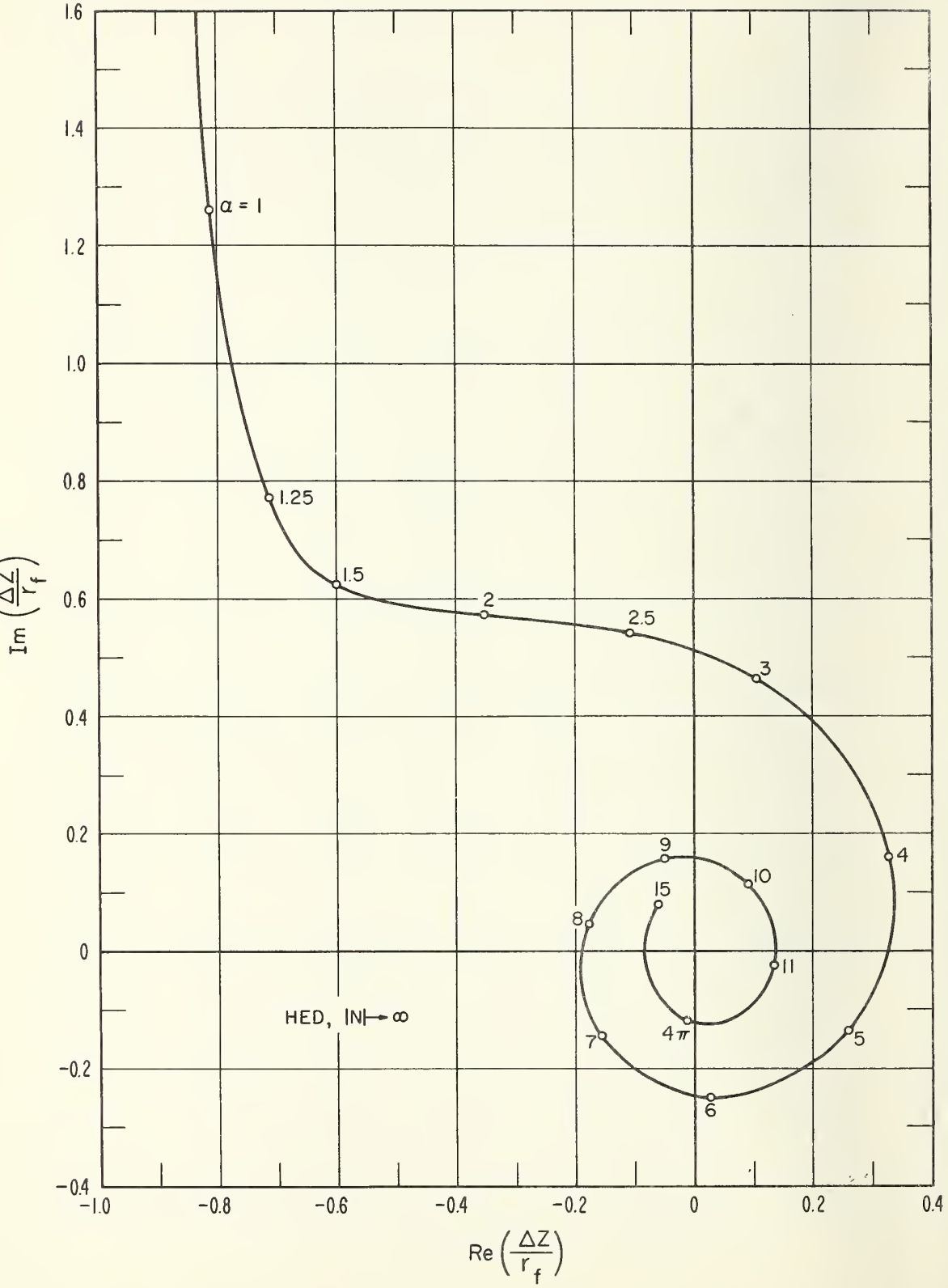

Figure A-46. Normalized input impedance change for HED, $|N| \rightarrow \infty$.

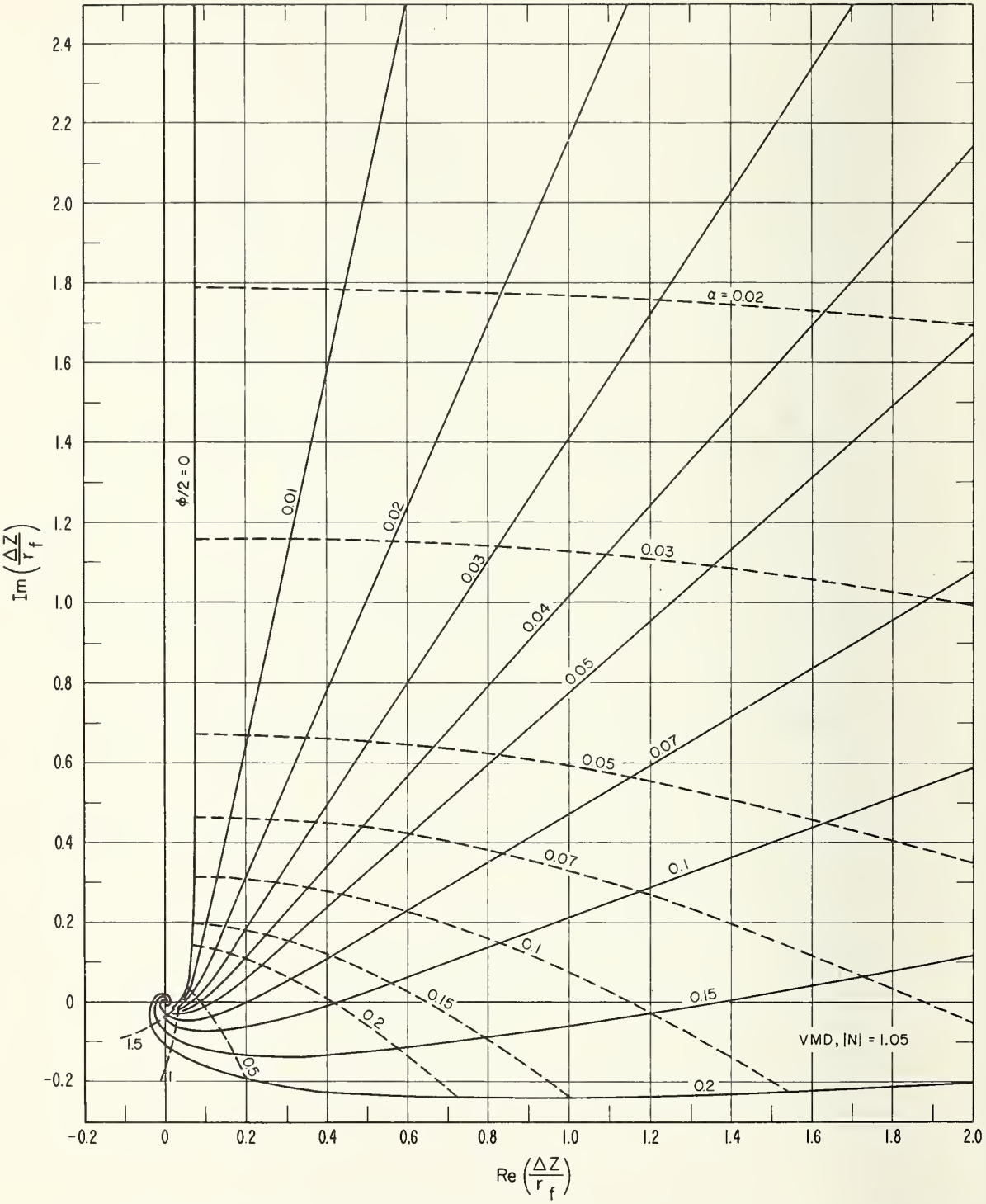

Figure A-47. Normalized input impedance change for VMD, $|N| = 1.05$.

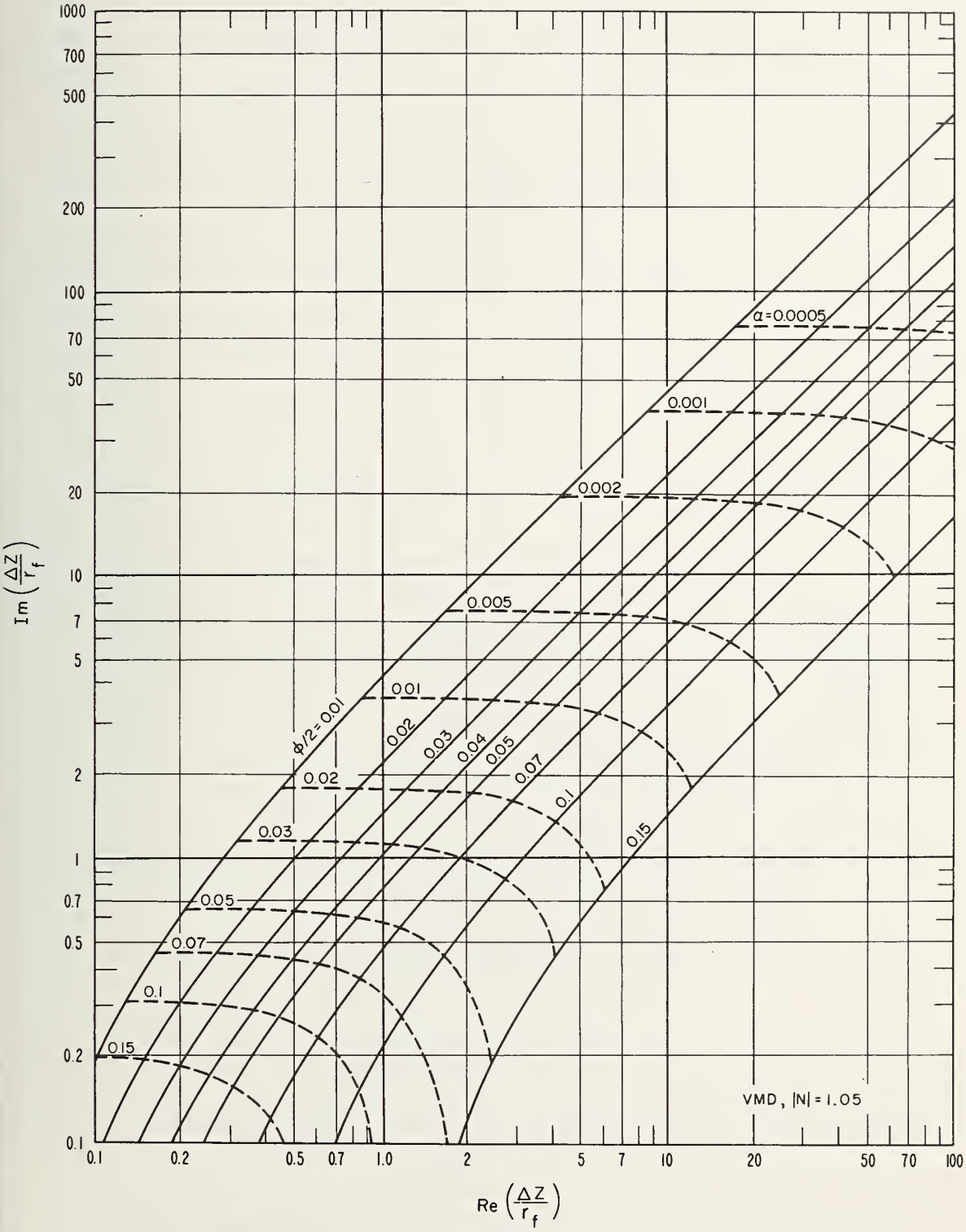

Figure A-48. Normalized input impedance change for VMD, $|N| = 1.05$.

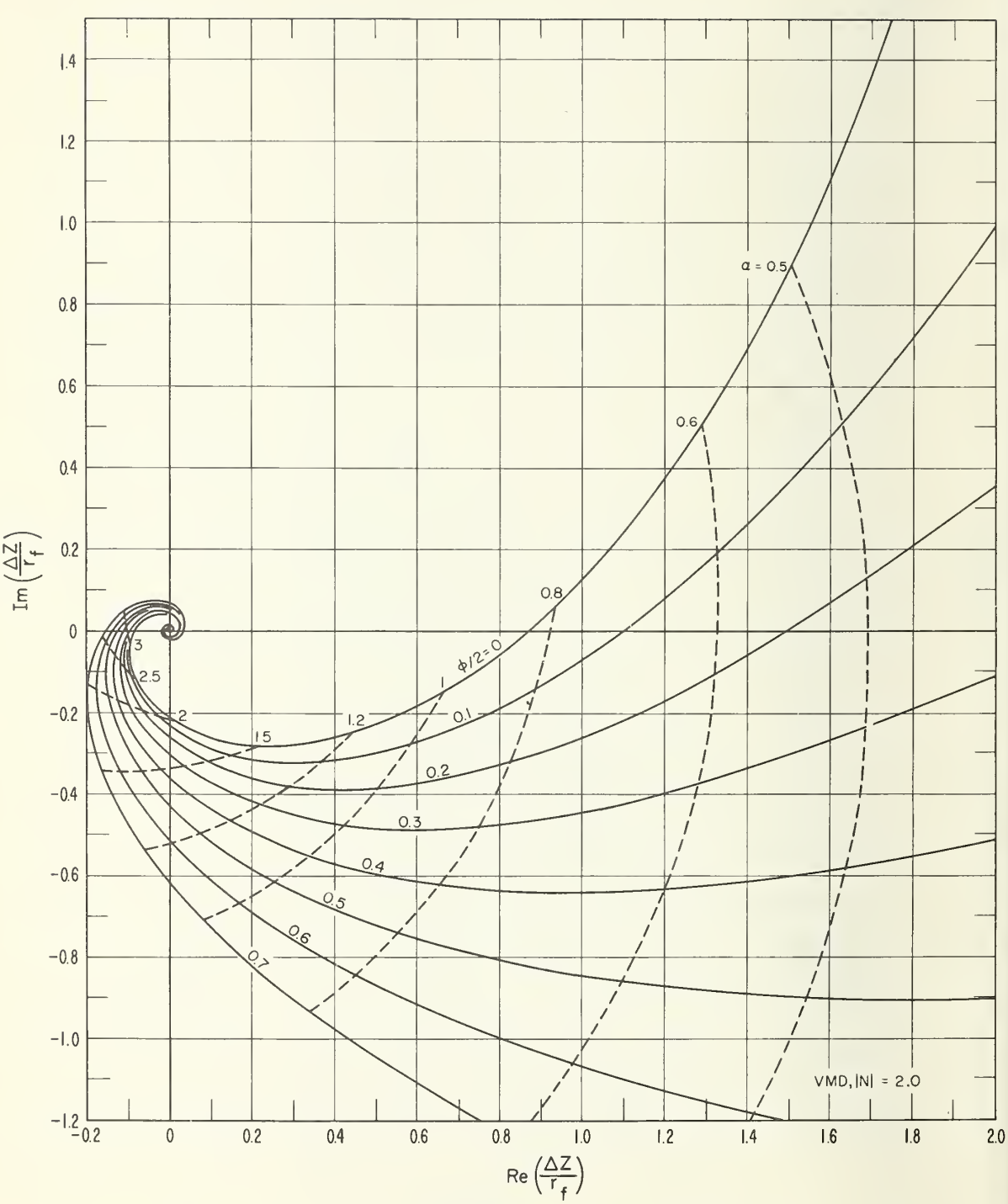

Figure A-49. Normalized input impedance change for VMD, $|N| = 2$.

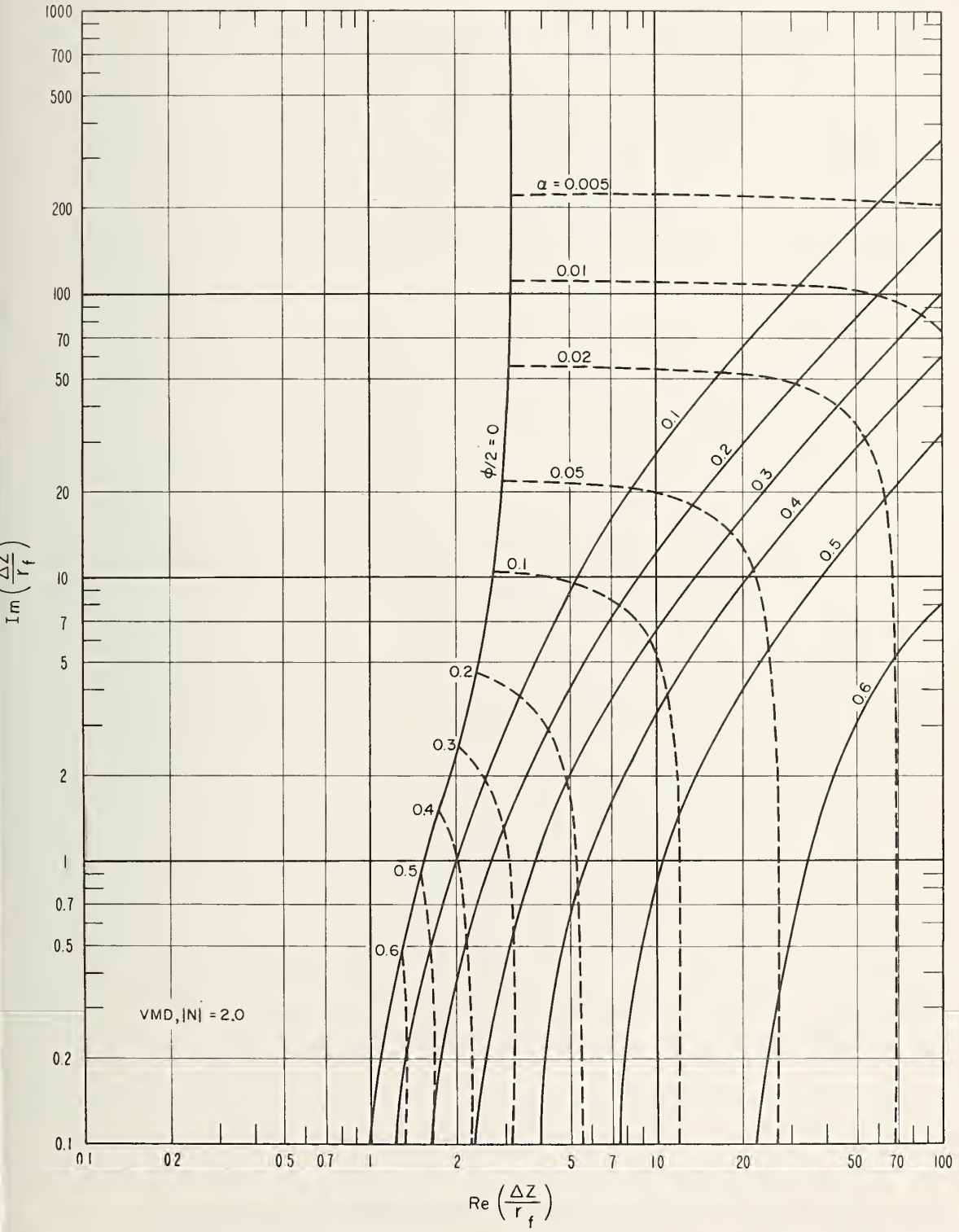

Figure A-50. Normalized input impedance change for VMD, $|N| = 2$.

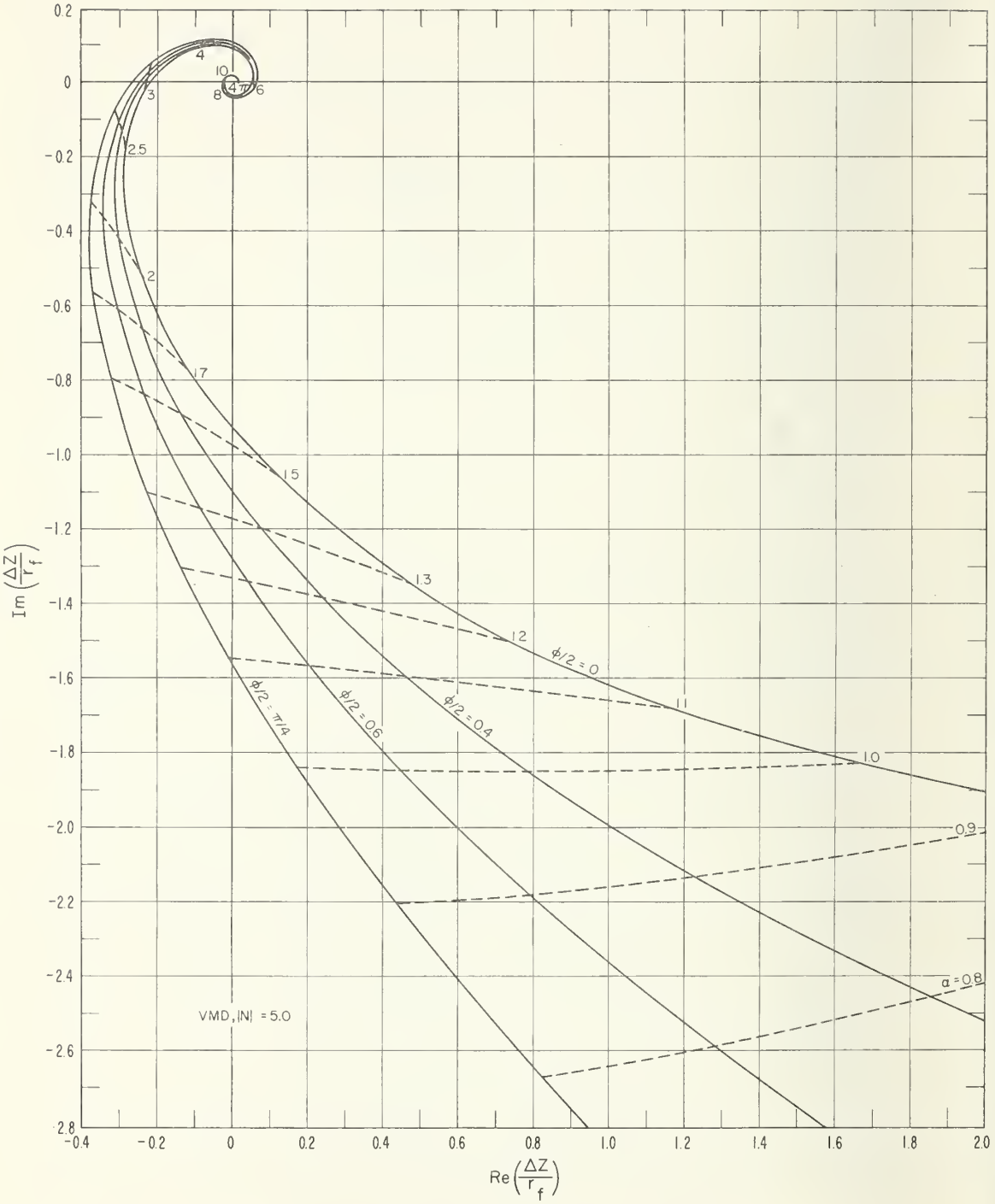

Figure A-51. Normalized input impedance change for VMD, $|N| = 5$.

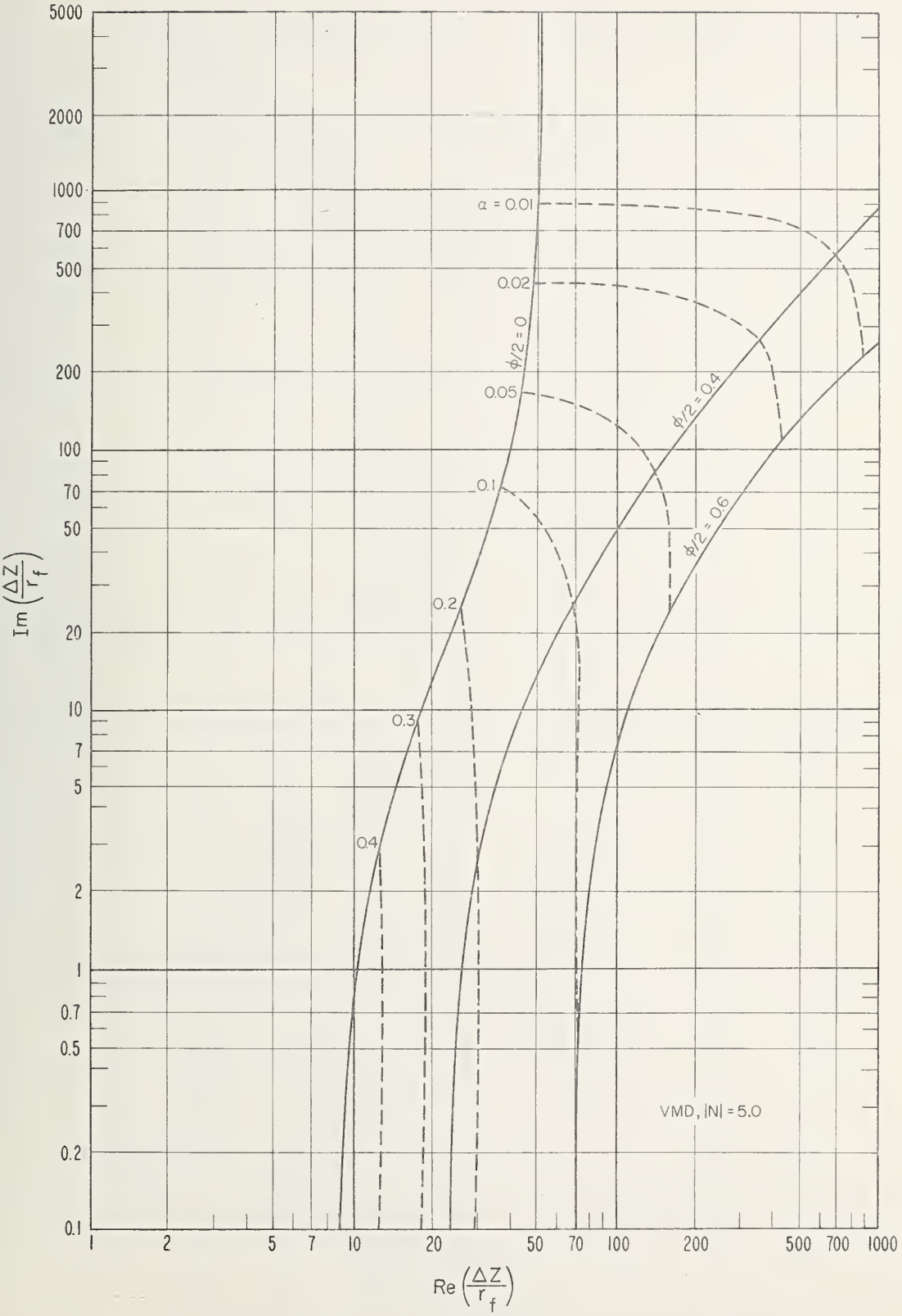

Figure A-52. Normalized input impedance change for VMD, $|N| = 5$.

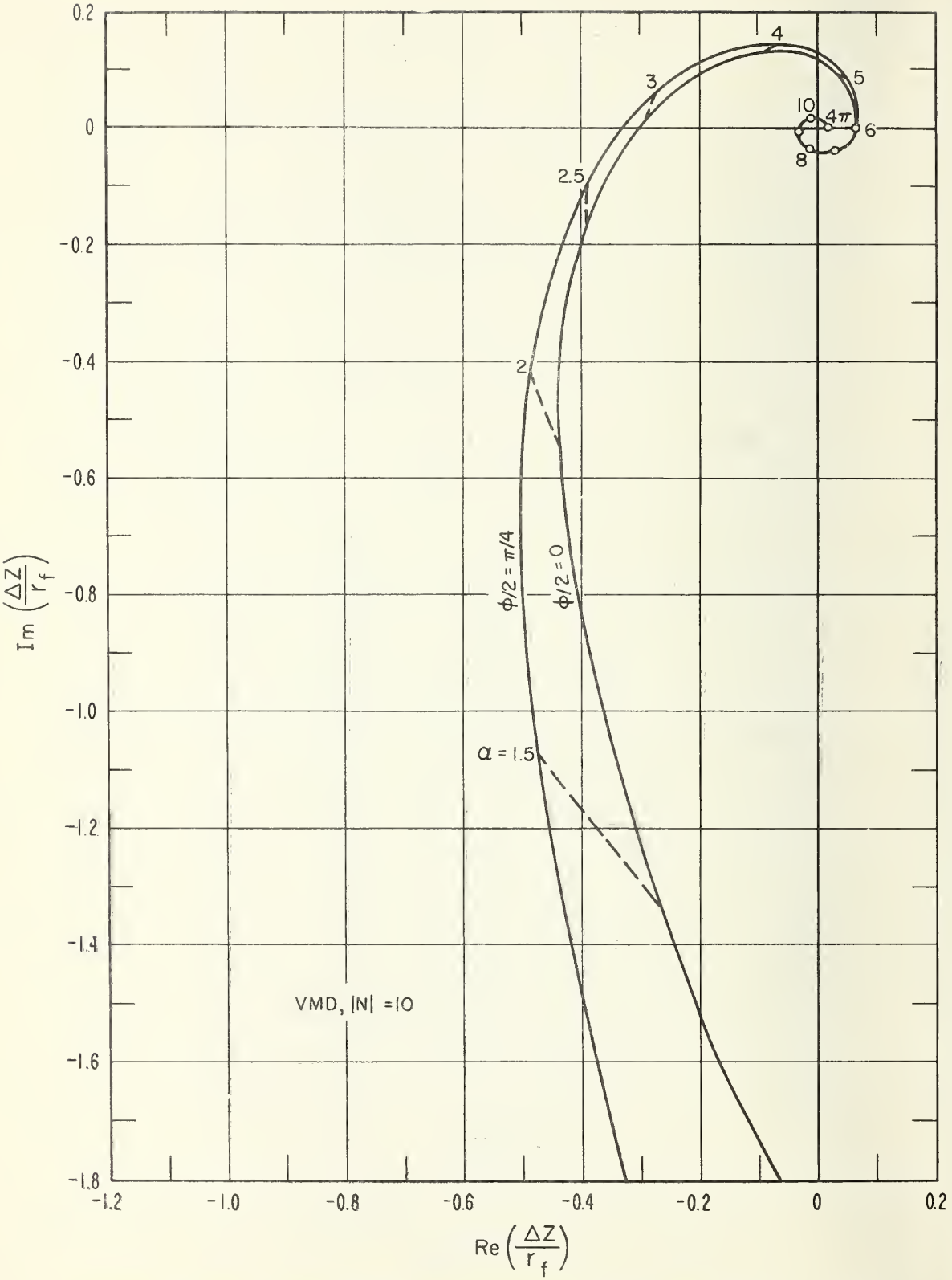

Figure A-53. Normalized input impedance change for VMD, $|N| = 10$.

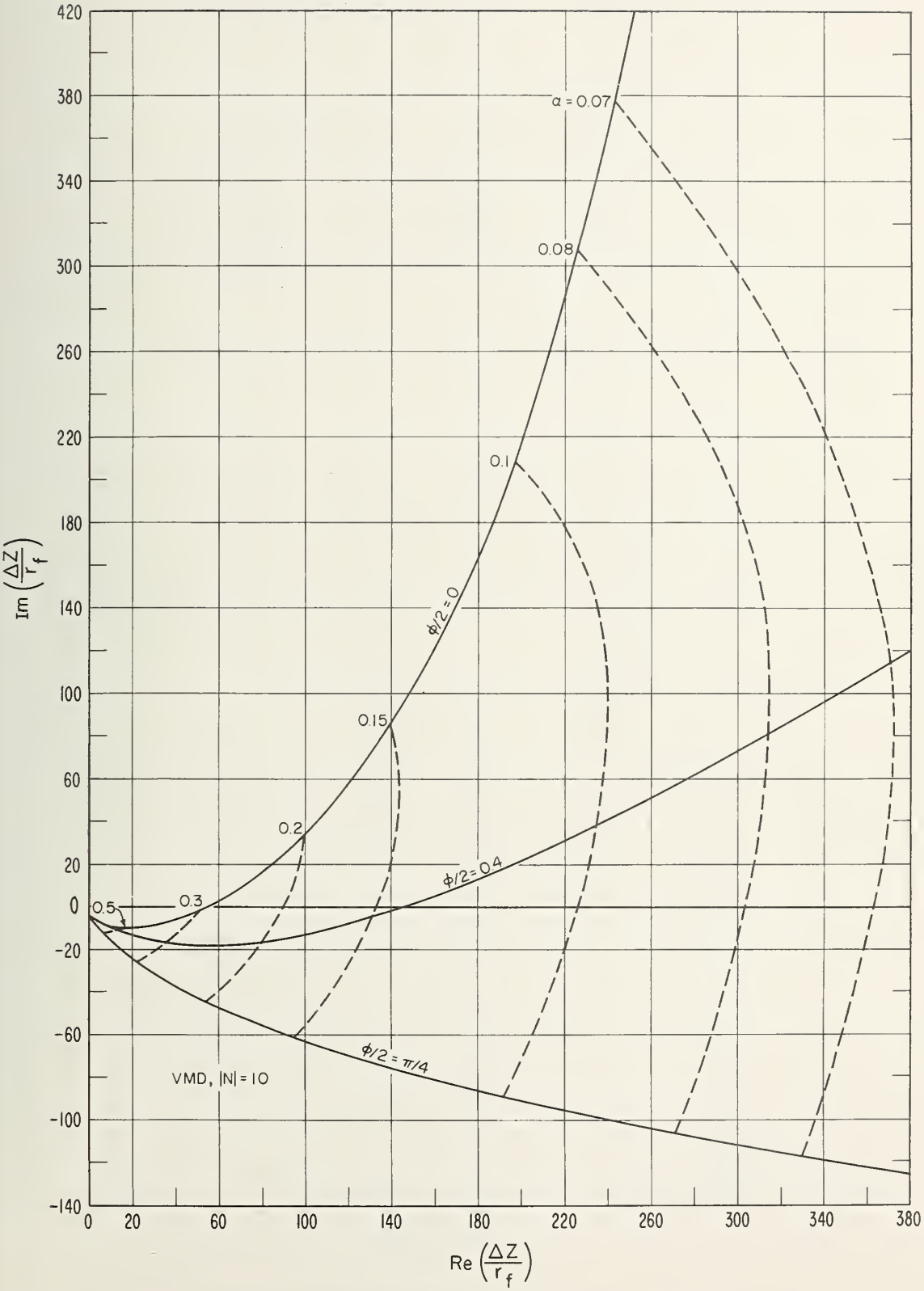

Figure A-54. Normalized input impedance change for VMD, $|N| = 10$.

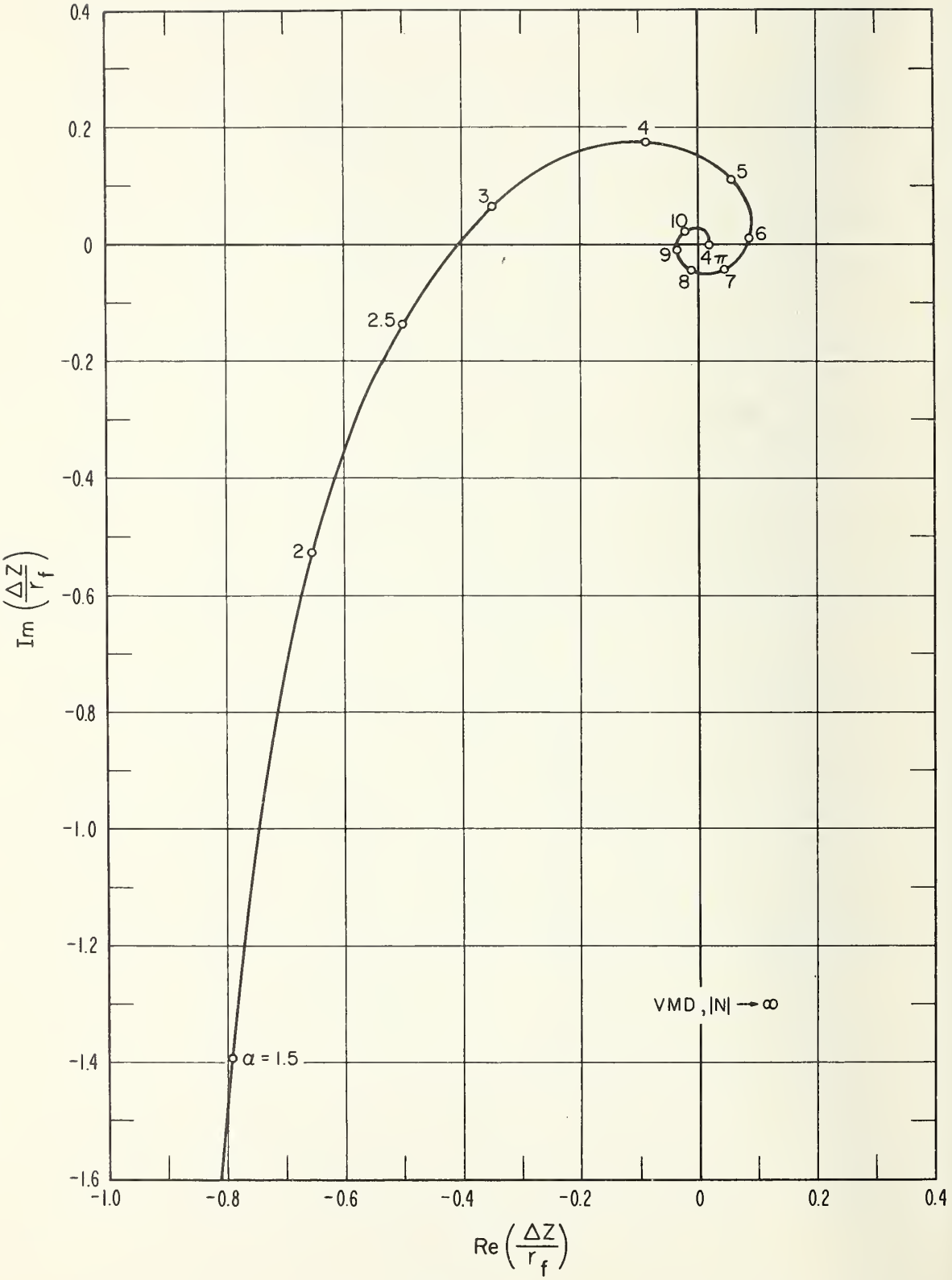

Figure A-55. Normalized input impedance change for VMD, $|N| \to \infty$.

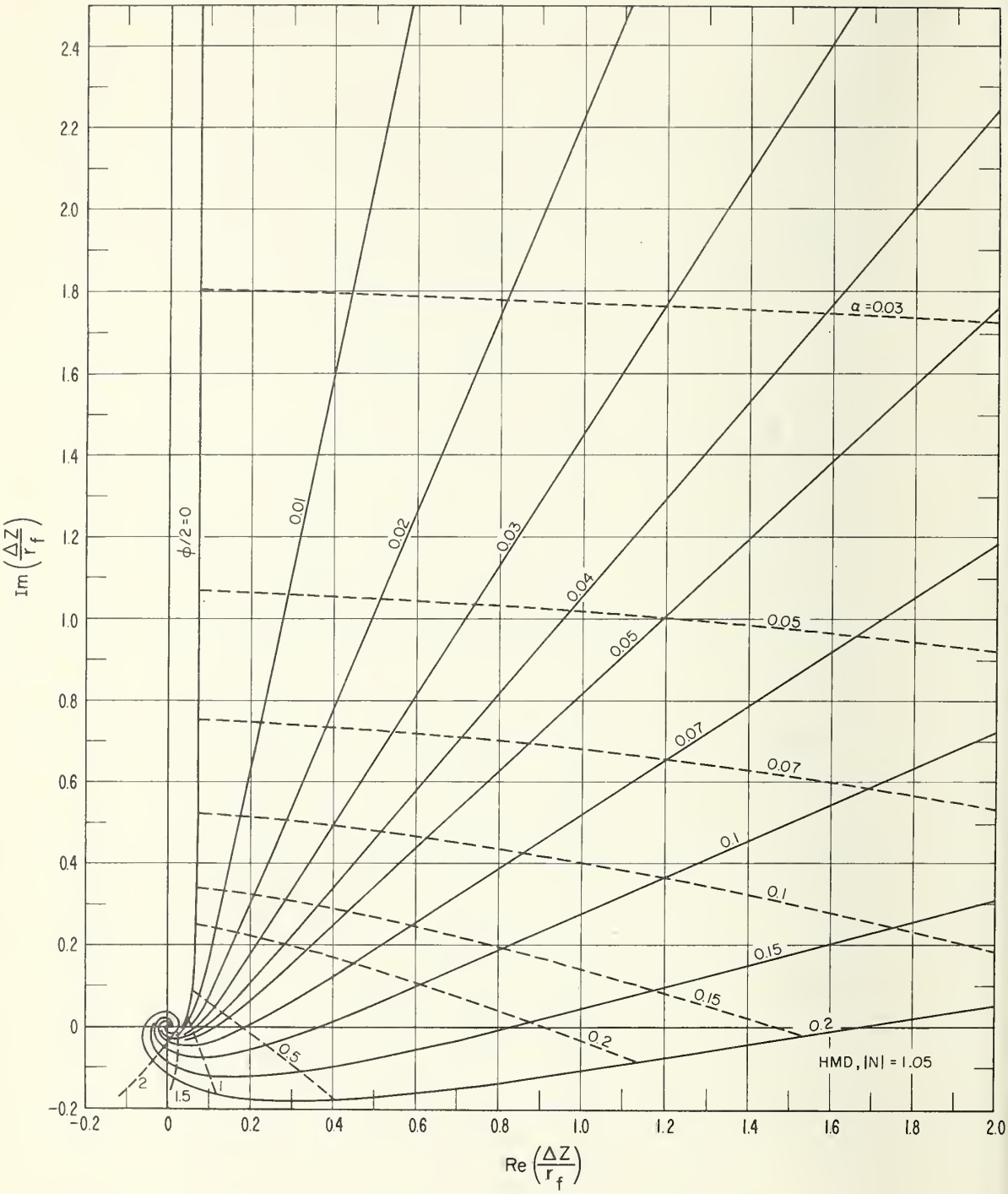

Figure A-56. Normalized input impedance change for HMD, $|N| = 1.05$.

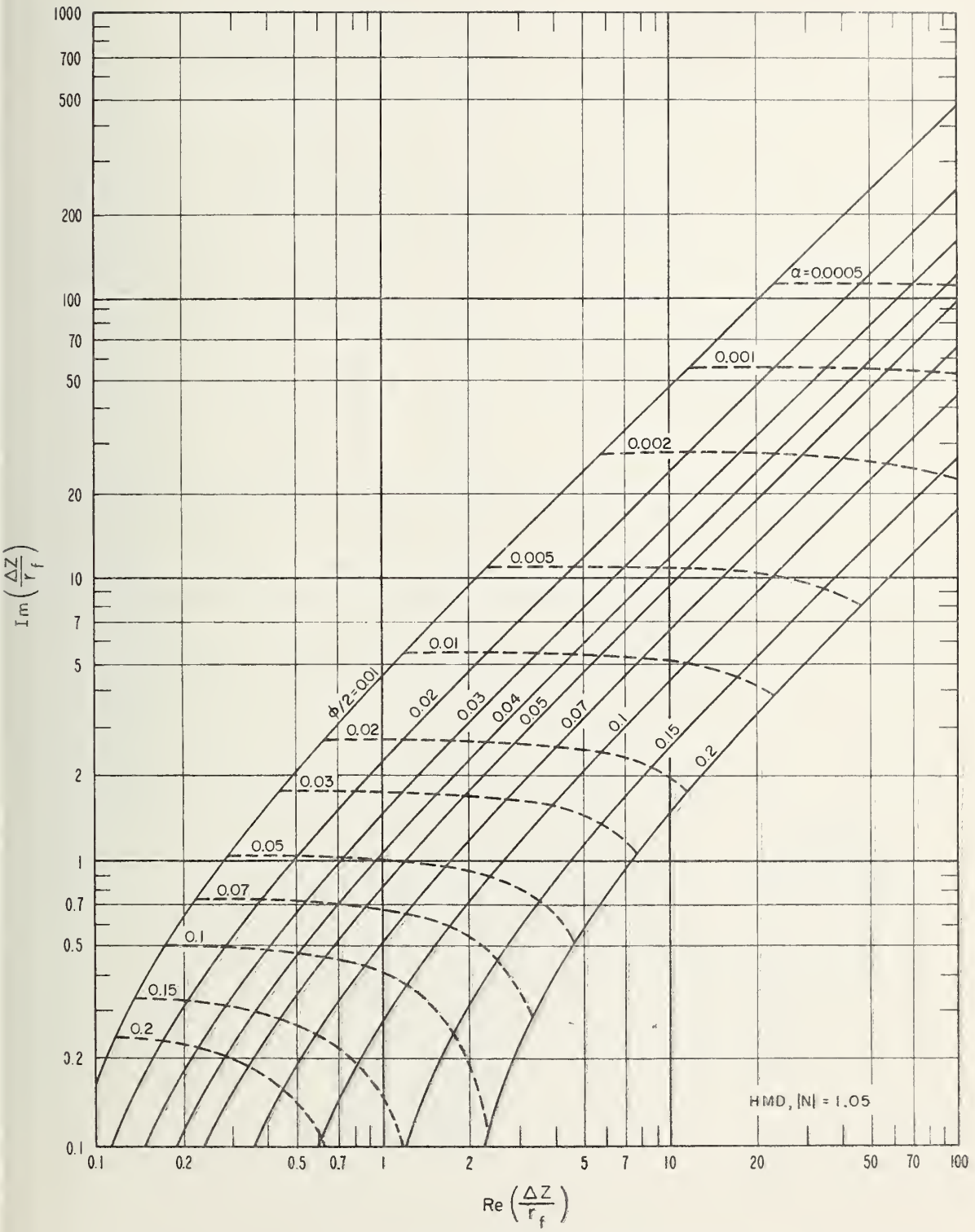

Figure A-57. Normalized input impedance change for HMD, $|N| = 1.05$.

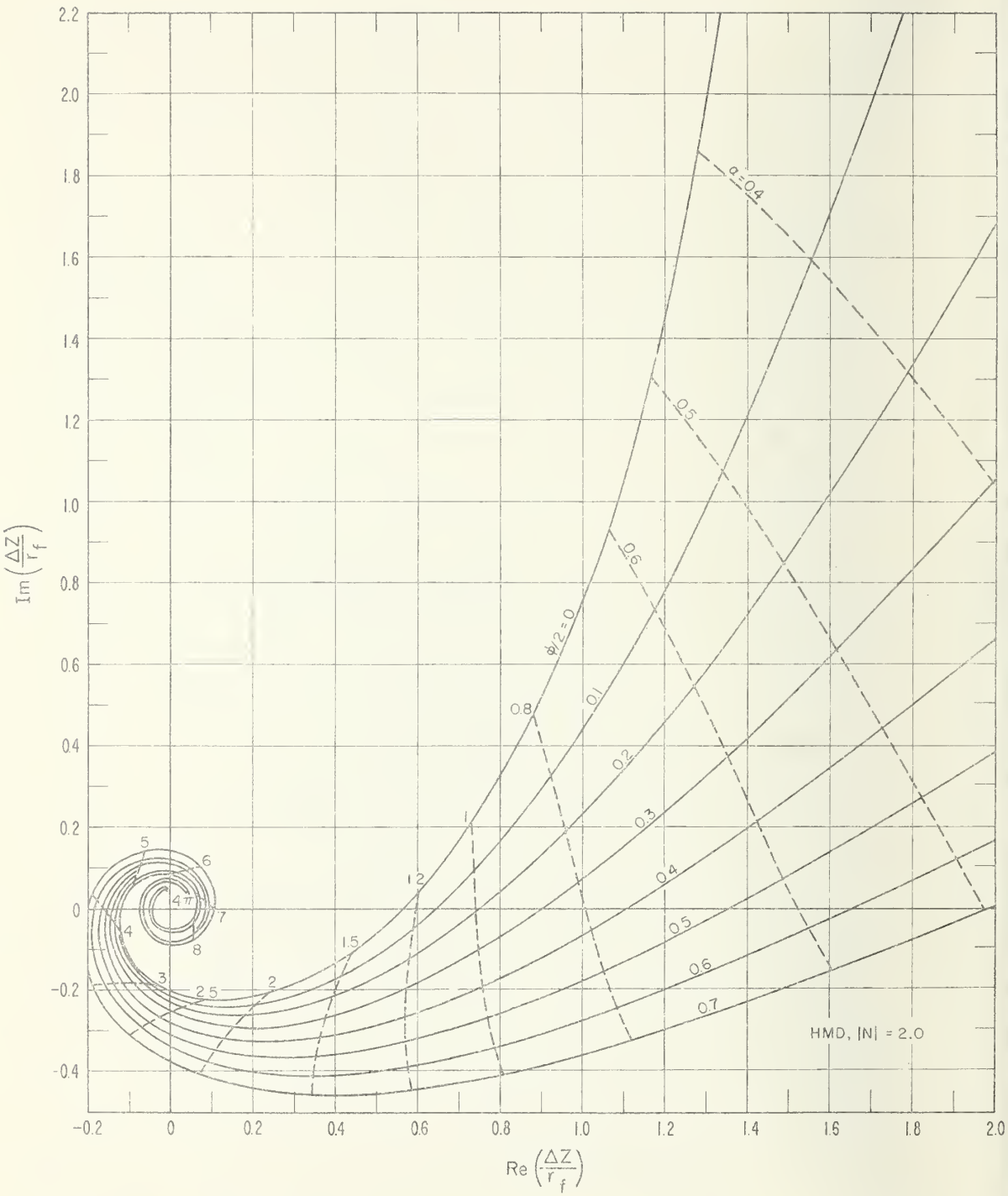

Figure A-58. Normalized input impedance change for HMD, $|N| = 2$.

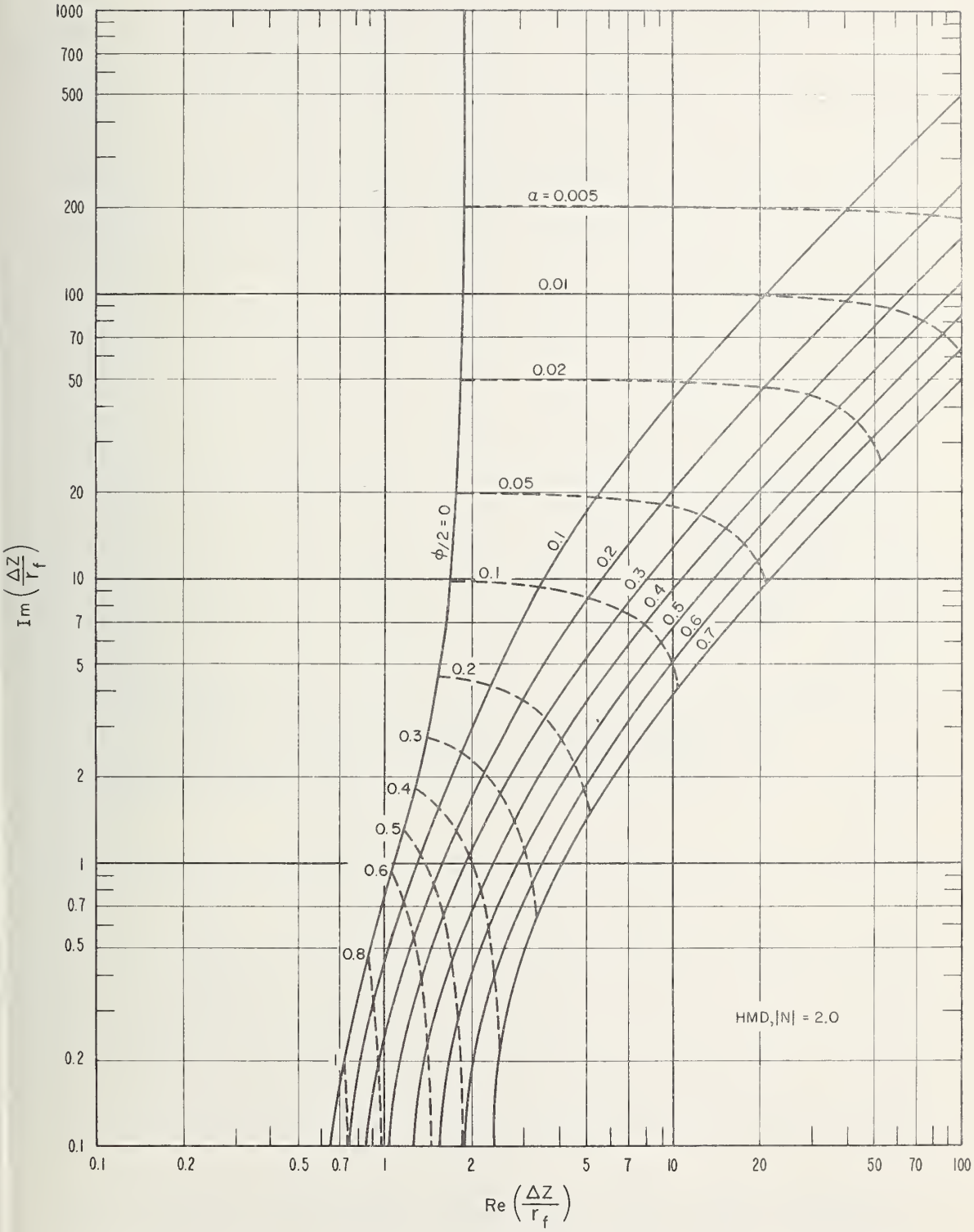

Figure A-59. Normalized input impedance change for HMD, $|N| = 2$.

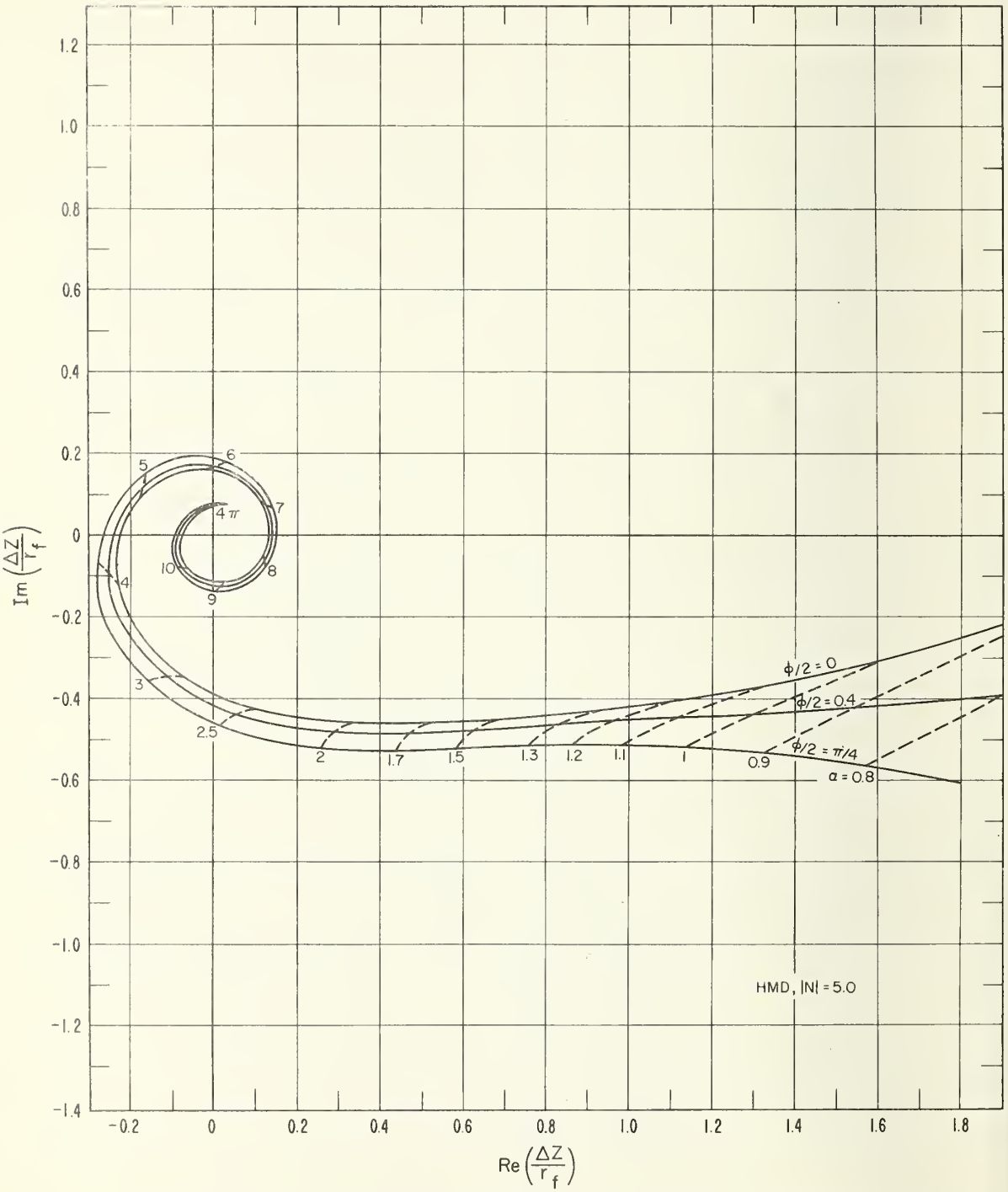

Figure A-60. Normalized input impedance change for HMD, $|N| = 5$.

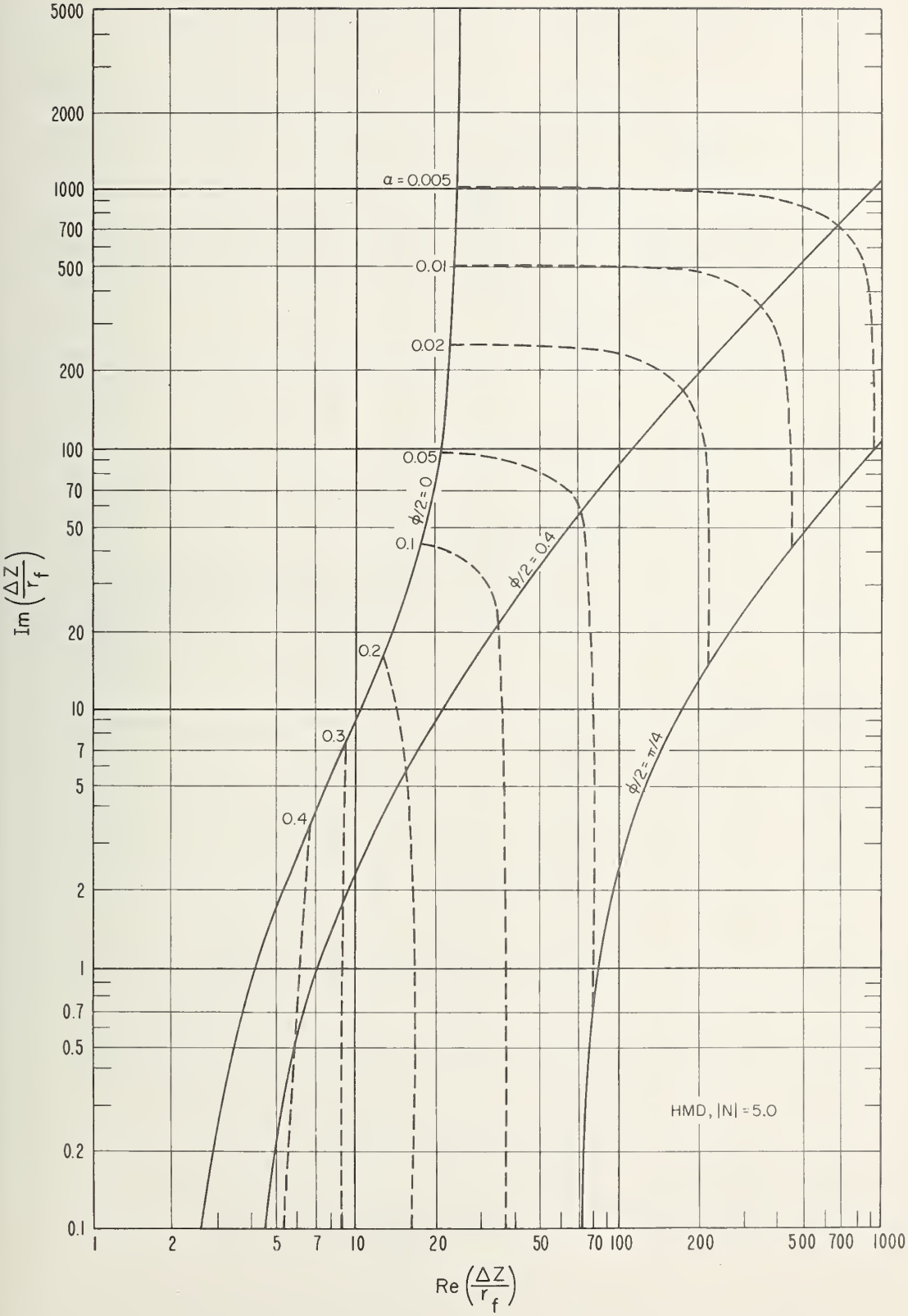

Figure A-61. Normalized input impedance change for HMD, $|N| = 5$.

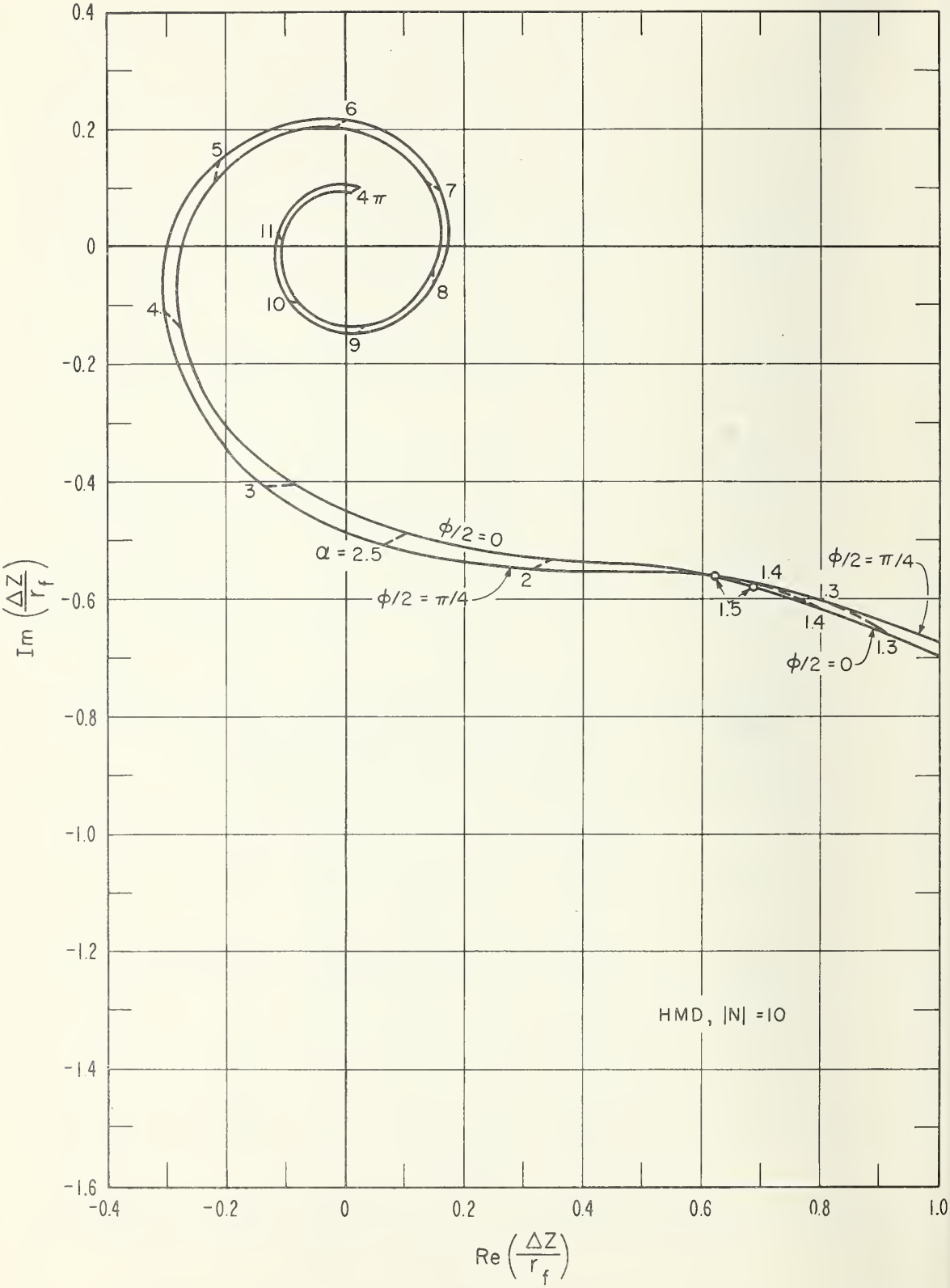

Figure A-62. Normalized input impedance change for HMD, $|N| = 10$.

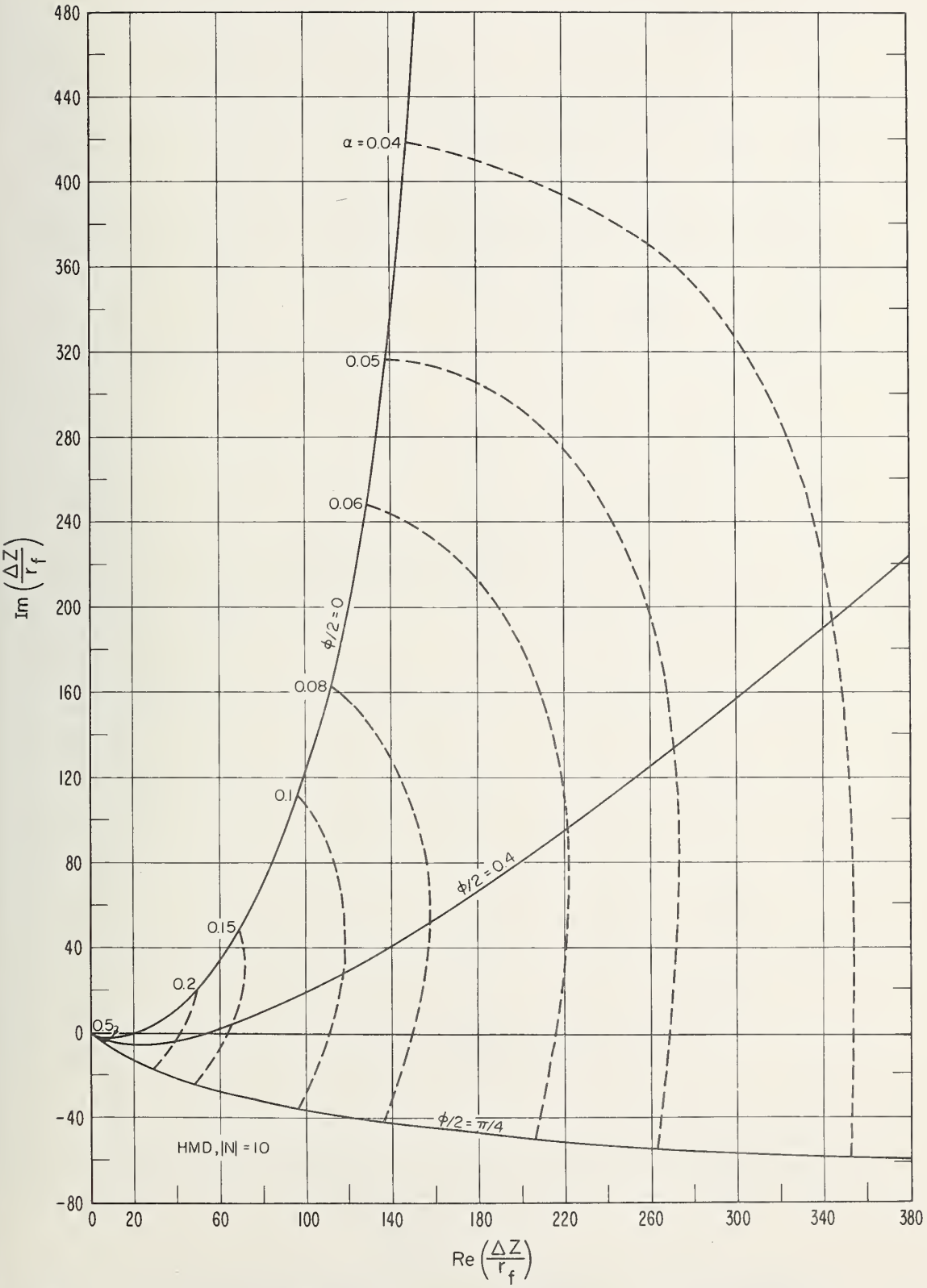

Figure A-63. Normalized input impedance change for HMD, $|N| = 10$.

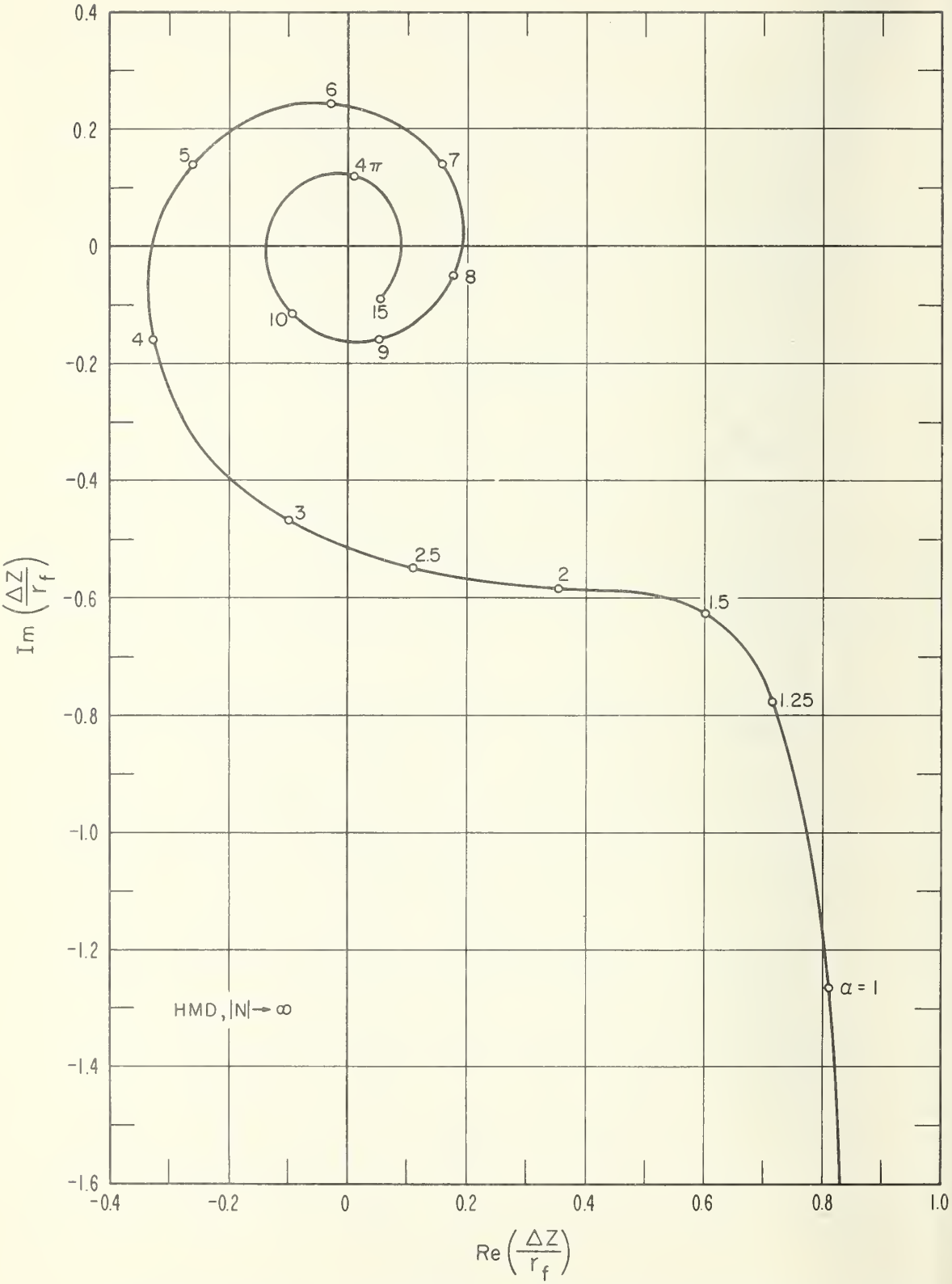

Figure A-64. Normalized input impedance change for HMD, $|N| \rightarrow \infty$.

☆ U. S. GOVERNMENT PRINTING OFFICE : 1964 O - 739-039